CORTICOSPINAL OUTPUT TO HINDLIMB MUSCLES IN THE PRIMATE

by

Heather M Hudson

B.S., University of Kansas, 1999
B.A., University of Kansas, 1999

Submitted to the graduate degree program in Neuroscience
and the Graduate Faculty of the University of Kansas
in partial fulfillment of the requirements for the degree of Doctor of Philosophy

Dissertation Committee:

_____
Paul D. Cheney, Ph.D., Chairman

_____
Thomas J. Imig, Ph.D.

_____
Randolph J. Nudo, Ph.D.

_____
John A. Stanford, Ph.D.

_____
Douglas E. Wright, Ph.D.

Dissertation defended: April 12, 2011

The Dissertation Committee for Heather M Hudson
Certifies that this is the approved version of the following dissertation:

CORTICOSPINAL OUTPUT TO HINDLIMB MUSCLES IN THE PRIMATE

_____
Chairperson Paul D. Cheney, Ph.D.

Date approved: April 12, 2011

ABSTRACT

The overall goal of this study was to investigate the properties of corticospinal output to a wide range of hindlimb muscles in the primate and to map the representation of individual muscles in hindlimb motor cortex. Compared to the forelimb, little is known about cortical control of the hindlimb despite its obvious importance in motor control. We developed two chronic EMG implant methods, arm-mounted and cranial-mounted, that provide stable, long-term EMG recording from large numbers of muscles of the hindlimb in awake behaving monkeys. Using stimulus triggered averaging (15, 30 and 60 μA; 15 Hz) of EMG activity collected from 19 muscles of the hindlimb, we addressed three facets of the cortical control of the hindlimb in the primate. First, we determined the organization of the hindlimb representation of primary motor cortex (M1) in terms of motor output to individual muscles and muscles grouped at different joints. Second, we determined the output properties of hindlimb M1 in terms of sign, latency, magnitude and distribution of effects in comparison to data for the forelimb collected with similar methods. And third, we investigated the differential cortical control of fast and slow muscles of the ankle.

The organization of the hindlimb representation in M1 cortex was similar to that of the forelimb in that there is a core distal representation, surrounded by a peripheral proximal representation separated by a region of proximal-distal cofacilitation. However, there were far fewer poststimulus effects in hindlimb muscles than forelimb muscles. As stimulus intensity increased, both the proximal and distal representations decreased in size. The proximal-distal cofacilitation region, however, increased dramatically in a manner that cannot easily be explained by stimulus-current spread alone. A model of cortical hindlimb organization is presented that includes partial segregation of proximal- and distal-specific corticospinal neurons but also unequal synaptic linkages to proximal and distal motoneurons in the spinal cord.

There were similarities between hindlimb and forelimb output effects but a number of striking differences stand out. Most notable was the vast difference in magnitude of output effects to hindlimb muscles despite ample evidence of corticospinal monosynaptic input to hindlimb motoneurons. The magnitudes of poststimulus facilitation (PStF) effects were twice as strong in the intrinsic hand muscles compared to the intrinsic foot muscles at 15 μA. Magnitude differences were even greater for wrist versus ankle muscles. Interestingly, PStF was more common in the distal muscles of both forelimb and hindlimb but these effects were concentrated in the intrinsic foot muscles of the hindlimb while more evenly distributed among the distal joints of the forelimb. Finally, stimulus triggered averages of hindlimb EMG contained broad, long latency suppression and long latency facilitation components that are not present in forelimb averages.

Conflicting results have been reported in primate and human studies concerning the role of the motor cortex in the control of slow muscles with some studies suggesting that effects on the slow muscle, soleus, are largely inhibitory. Stimulus triggered averaging of EMG activity provided a more sensitive and higher resolution approach to delineating cortical motor output effects than the methods applied in previous studies. We found that PStF was just as common in the slow muscle, soleus, as the fast muscles of the ankle and that there was no difference between the PStF onset latencies and magnitudes of the fast and slow muscles. Based on our results, it is clear that the motor cortex has a powerful excitatory effect on soleus motoneurons although it was also inhibited from more cortical sites than other ankle muscles.

In conclusion, there are important similarities in the organization and properties of hindlimb and forelimb cortical output. Perhaps most notable among them is the basic pattern of cortical map representation of distal and proximal muscles. However, most striking among the differences is the markedly weaker output effects to distal muscles of the hindlimb compared to forelimb. The results suggest a synaptic organization with a much weaker monosynaptic component compared to forelimb muscles. Finally, there is strong evidence of cortical facilitation of the slow muscle, soleus.

TABLE OF CONTENTS

LIST OF TABLES

LIST OF FIGURES

CHAPTER 5

LIST OF ABBREVIATIONS

EMG	…….	Electromyography
EPSP	…….	Excitatory Post Synaptic Potential
ICMS	…….	Intracortical Microstimulation
IPSP	…….	Inhibitory Post Synaptic Potential
M1	…….	Primary Motor Cortex
MRI	…….	Magnetic Resonance Imaging
PPI	…….	Peak Percent Increase
PStE	…….	Poststimulus Effect
PStF	…….	Poststimulus Facilitation
PStS	…….	Poststimulus Suppression
RL-ICMS	……	Repetitive, Long Duration ICMS
TENS	…….	Transcranial Electrical Stimulation
TMS	…….	Transcranial Magnetic Stimulation

CHAPTER 1

INTRODUCTION

The leg is essential for locomotion, posture and balance. Muscle activity is coordinated to flex and extend the leg at different joints using synergies with precise timing to permit the whole leg to function as a unit. Both legs are coordinated in another synergy to maintain balance and motion. The body is positioned to maintain posture and balance. The initiation of walking, the cessation of walking and any perturbation in response to obstacles is also part of the dynamic.

Stroke, brain injury, spinal cord injury and neurological disease can all have deleterious effects on leg function contributing to impairment of locomotion, posture and balance. In order to fully understand dysfunction and develop methods for rehabilitation, a complete understanding of normal organization and function is necessary. Ideally, studying the human motor system would be best. However, a primate model has several advantages. Primate studies can be more invasive than studies using human subjects. Insertion of microelectrodes into the cortex for neural activity recording or stimulation can be performed in awake, behaving primates. Muscles can be chronically implanted with EMG electrodes to record muscle activity assuring consistent electrode placement across time for long studies. Data can be recorded daily and long-term. Environmental factors can be consistently maintained among subjects. In addition, terminal studies and histology can be performed. There are disadvantages to the primate model as well. Musculature is different. The human leg is specifically adapted for bipedal gait, while monkeys are more quadrupedal but with the ability to walk upright. In addition, monkeys have an opposable hallux. Behavioral training is an issue as well. A behavioral task must be implemented that is not only relatively easy for a monkey to learn and perform, but that is also nearly indestructible. Further, primates are expensive to acquire, house and maintain. Despite the disadvantages, the primate model is a useful tool to study cortical motor control.

The investigation of motor control can be approached from different angles. This study focuses on the motor cortex and the cortical control of hindlimb muscles. The motor cortex is located on the precentral gyrus in the frontal lobe of both hemispheres. It can be divided into several areas, each with a different function in the control of movement. The primary motor cortex, also referred to as M1, is

involved in the execution of movement. M1 contains corticospinal neurons that project to the spinal cord where they synapse with α-motoneurons and interneurons associated with the motoneurons. The α-motoneurons innervate muscle fibers. Considering the complexity of movement, there must be a specific organization to this pathway and an organization to M1 in terms of muscle representations. In fact, this general issue has been the subject of study for over a century.

Electrophysiology is the study of the electrical properties of cells, tissues and physiological systems. Stimulation of the cortex, electrical or magnetic, has been used frequently in electrophysiology studies to gain a better understanding of the organization and function of the motor cortex and its role in motor control. As early as 1870, Fritsch and Hitzig were using galvanic currents applied through a pair of blunted platinum wires to stimulate the motor cortex of dogs. They discovered that applying electrical stimulation to the cortex caused muscle contractions in specific parts of the dog. Ferrier developed the first motor map of the monkey cortex in 1875. In 1937, Penfield and Boldrey mapped the human motor cortex using direct stimulation of the cortical surface. They discovered there was an organization of the body represented in the cortex such that stimulation of the most medial areas of the motor cortex evoked a response in the more distal muscles of the body, those nearer the foot. As they moved lateral on the cortex, stimulation evoked movements of more proximal body parts, those nearer the head. In 1958, Woolsey found similar results when mapping the monkey motor cortex. Asanuma and Sakata introduced intracortical microstimulation (ICMS) in 1967. ICMS, as applied by Asanuma and Sakata, consisted of a short train of 10 stimulus pulses delivered at a frequency of 330 Hz. This short duration stimulus train evokes twitch-like movements of body parts. This became a standard electrophysiological technique for studying somatotopic organization of the monkey motor cortex and several other microstimulation techniques have been adapted from it. One of these is repetitive, long duration ICMS (RL- ICMS) which delivers a 500 ms stimulus train at high frequency, generally 200 Hz, to evoke whole limb movements that have a duration more closely matching the duration of natural movements (Graziano et al., 2002). Another variation of ICMS is stimulus triggered averaging of EMG activity, also known as single pulse

ICMS, which delivers a continuous train of microstimuli at a frequency of less than 20 Hz (Cheney and Fetz, 1985). The low frequency used with this method avoids temporal summation of excitatory post synaptic potentials (EPSPs) and limits physiological spread of excitation related to stimulation. This technique does not evoke movement but instead output effects are recorded as transient changes in average EMG activity evoked by the stimulus. More recently, the noninvasive techniques of transcranial electrical stimulation (TENS) and transcranial magnetic stimulation (TMS) have become available. These methods have transformed the study of cortical motor areas in human subjects. TENS was first demonstrated by Merton and Morton in 1980 while Barker and colleagues introduced TMS in 1985. Both are used extensively in human and monkey studies.

The goal of this study is to investigate corticospinal output from primary motor cortex (M1) to hindlimb muscles in the primate using stimulus triggered averaging of EMG activity recorded from 19 hindlimb muscles. With this method, a microelectrode is inserted into layer V of the motor cortex. A low frequency microstimulus (15-60 μA, 15 Hz) is delivered while EMG activity from 19 hindlimb muscles is recorded in reference to the stimulus. This technique is a sensitive and high resolution approach used to characterize the output from corticospinal neurons to hindlimb motoneurons in terms of sign (excitatory or inhibitory), latency and magnitude of effects. Four specific aims are addressed in this study.

Specific Aim 1: Develop new methods to study hindlimb cortical control. A behavioral task that engaged large numbers of proximal and distal hindlimb muscles in a reliable and stereotyped pattern of activation and was relatively easy for a monkey to learn and perform needed to be developed in order to study the cortical control of hindlimb muscles in awake, behaving primates. In addition, a method to chronically implant large numbers of hindlimb muscles for daily recording of EMG activity was also necessary to develop.

Specific Aim 2: Identify the cortical organization of the hindlimb representation of primary motor cortex. Previous mapping studies using ICMS to evoke movement in hindlimb muscles were limited to

describing the representation of the facilitation of groups of muscles. With stimulus triggered averaging, we will identify individual muscle representations, proximal and distal muscle representations, extensor and flexor representations, as well as the representations of muscles grouped at different joints. In addition to muscle representations based on excitatory effects, we will also investigate cortical organization based on inhibitory effects. Changes in hindlimb M1 organization in response to different stimulus intensities will be described. Further, hindlimb M1 organization will be compared to what has previously been documented on forelimb M1 organization (Park et al., 2001).

Specific Aim 3: Delineate the output properties of primary motor cortex to hindlimb muscles. Stimulus triggered averaging of EMG activity will be used to characterize the output from M1 to hindlimb muscles in terms of sign, magnitude and latency of poststimulus effects. Hindlimb output effects will then be compared to previously documented forelimb M1 output effects (Park et al., 2004). Additionally, the effect of different stimulus intensities on output effects will be investigated.

Specific Aim 4: Compare the cortical control of fast and slow muscles of the ankle. The cortical control of slow muscles is a subject of controversy in the motor control field. An excitatory cortical control of fast muscles has been established (Bawa et al., 2002; Brouwer and Ashby, 1990, 1992; Brouwer and Qiao, 1995; Ertekin et al., 1995; Preston and Whitlock, 1963; Uemura and Preston, 1965; Valls-Solé et al., 1994), but conflicting data on the cortical control of the slow muscle, soleus, has been reported. Some studies have found weak or non-existent facilitation of soleus (Ashby and Advani, 1990; Brouwer and Ashby, 1990, 1992; Brouwer and Qiao, 1995; Cowan et al., 1986; Jankowska et al., 1975; Preston and Whitlock, 1963; Uemura and Preston, 1965) while other studies have reported a clear short facilitation of soleus (Bawa et al., 2002; Valls-Solé et al., 1994). Stimulus triggered averaging is a more sensitive and higher resolution technique than was used in the previous studies. We are in a strong position to contribute to the fast and slow muscle debate.

CHAPTER 2

METHODS FOR CHRONIC RECORDING OF EMG ACTIVITY FROM LARGE NUMBERS OF HINDLIMB MUSCLES IN AWAKE RHESUS MACAQUES

The study described in this chapter has been published in the *Journal of Neuroscience Methods*, 2010, volume 189, pages 153-161.

INTRODUCTION

In the field of motor control, chronic recording of EMG activity from large numbers of muscles is highly advantageous. Thus far, the hindlimb has been extensively studied in the cat. A wide range of EMG implant methods have been used, including patch electrodes sutured to muscle surfaces, wire electrodes implanted in muscles and wire electrodes tied or sutured to muscles. These EMG electrodes were tunneled subcutaneously to either back or head connectors. In each study, relatively few muscles were implanted and the length of study ranged from a few weeks to several months (Bretzner and Drew, 2005; Drew, 1988; Hoffer et al., 1987, 1989; Loeb, 1999; Prochazka et al., 1977, 1989). In non-human primates, several studies have described methods of implanting EMG electrodes in muscles of the forelimb (Belhaj-Saïf et al., 1996; Fetz and Cheney, 1980; Miller et al., 1993; Park et al., 2000; Wolpaw et al., 1990). Studies involving chronic EMG implants in the hindlimb of non-human primates are fewer in number and involve a relatively small number of muscles (Courtine et al., 2005; Hodgson et al., 2001; Recktenwald et al., 1999). The goal of this study was to adapt an existing method developed in our laboratory for recording EMG activity from large numbers of chronically implanted forelimb muscles (Park et al., 2000) for use in the hindlimb. The two methods described in this study, the arm-mounted subcutaneous implant and the cranial-mounted subcutaneous implant, have yielded stable recording of EMG activity from 19 muscles of the monkey hindlimb for periods up to 31 months.

MATERIALS AND METHODS

All surgeries were performed in an Association for Assessment and Accreditation of Laboratory Animal Care (AAALAC) accredited facility using full aseptic procedures.

Park et al. (2000) described two EMG implant methods for chronic recording from 24 forelimb muscles simultaneously. We have expanded on these methods and adapted them for chronic recording from 19 muscles of the hindlimb simultaneously. Electrodes were placed both proximally and distally in soleus so the total number of EMG channels was 20. We used two different approaches: (1) an arm-mounted subcutaneous implant method (Fig. 3A) and (2) a cranial-mounted subcutaneous implant method (Fig. 3B). The results described are from one arm-mounted subcutaneous implant performed in one monkey (monkey F) and one cranial-mounted subcutaneous implant performed in a different monkey (monkey C). In both cases, 19 muscles of the hindlimb were implanted including hip muscles: gracilis (GRA), adductor brevis (ADB), gluteus maximus (GMAX) and tensor fascia latae (TFL); knee muscles: biceps femoris (BFL), semimembranosus (SEM), semitendonosus (SET), rectus femoris (RF), vastus lateralis (VL) and vastus medialis (VM); ankle muscles: tibialis anterior (TA), peroneus longus (PERL), medial gastrocnemius (MG), lateral gastrocnemius (LG), proximal soleus (SOLp) and distal soleus (SOLd); digit muscles: flexor digitorum longus (FDL) and extensor digitorum longus (EDL); and intrinsic foot muscles: flexor hallucis brevis (FHB) and extensor digitorum brevis (EDB). Figure 1 illustrates the position of each muscle in cross-sections of the proximal (upper leg) and distal (lower leg) hindlimb.

Figure 2 demonstrates the use of T1- and T2-weighted MRIs in identification of muscle separation by fascial tissue. Magnetic resonance imaging (MRI) was performed using a Siemens Allegra 3T scanner with a custom built transmit/receive Helmholtz radio frequency (RF) coil consisting of two flexible surface loops with diameters of approximately 6 cm. T1-weighted images were acquired using magnetization prepared rapid acquisition of gradient echo (MPRAGE) sequence with parameters as follows: repetition time = 1500 ms, echo time = 2.09 ms, inversion time = 300 ms, slice thickness = 1

mm, field of view = 10 cm, matrix size = 192 x 192, flip angle = 8 degree, number of average = 3. T2-weighted images were acquired using a fast spin echo sequence with the following parameters: repetition time = 3000 ms, echo time = 49 ms, slice thickness = 3 mm, field of view = 7 cm, matrix size = 256 x 256, echo train length = 5, number of average = 2. While bone is easily identifiable with both types of MRI, separation of muscles by identifying fascial boundaries is clearer in the T1-weighted image. Most of the fascial boundaries evident in the section of the upper leg (Figure 1A) are evident in the T1 MRI, although some are less clear. However, the T2 image (lower leg) was much less effective in revealing fascial planes between muscles, at least in this cadaver specimen.

Arm-Mounted Subcutaneous Implant

Connectors

The arm-mounted subcutaneous implant uses single layer connector modules (ITT Canon pin, 031-9540-000; plastic Centi-Loc pin strip, 144-9614-060) that can be affixed to the skin as described in Park et al. (2000). Forty multi-stranded stainless steel wires (Cooner Wire, AS632) were cut to lengths appropriate for the 20 pairs of EMG wires to be implanted. The wires were divided into four modules: proximal one (ADB, TFL, BFL, RF, VL, VM), proximal two (GRA, GMAX, SEM, SET), distal one (MG, LG, SOLp, SOLd, FDL) and distal two (TA, PERL, EDL, FHB, EDB). Connectors were constructed as described in Park et al. (2000).

Surgical Protocol

The monkey was treated with antibiotic (injectable liquid penicillin, 6000 U/kg) one day before surgery, one day post-surgery and three days post-surgery as a prophylactic measure against infection. The monkey was initially tranquilized with ketamine (10 mg/kg) and medetomidine (0.10 mg/kg) before induction of surgical level isoflurane gas anesthesia. Atropine (0.04 mg/kg) was given to reduce secretions and prevent bradycardia. The monkey's forelimb, neck, back, hip, hindlimb and foot were shaved and scrubbed (Betadine: 10% povidone-iodine). The monkey was placed on the surgery table on

his left side and temperature, blood pressure and pulse monitors were applied. The monkey was draped except for the forelimb, back and hindlimb.

The connector modules were first laid on the lateral surface of the proximal forelimb. The tips of each wire were color-coded with permanent marker to ease the identification of each wire after tunneling. Although more costly, Cooner AS632 wire is available in different colors of insulation. Two small incisions (~ 1 cm) were made approximately half way between the shoulder and the elbow on the lateral surface of the proximal forelimb. These incisions functioned as entry points for the wires running subcutaneously to the hindlimb. A vertical incision (~ 4 cm) was made on the back near the midpoint between the shoulder blades. This incision functioned first as the exit point for the subcutaneous tunneling of wires from the forelimb to the hindlimb. A tissue pocket at this incision provided a space to keep extra wire lengths. These loops also served as anchoring points for the wires (arrow 2, Fig. 3A).

Custom designed needles, fabricated from stainless steel rods (Small Parts, 18-8 stainless steel: E-SWX-3035, E-SWX-3043), were used to tunnel the EMG wires. These flexible needles have diameters of 0.035 in. (~ 0.90 mm), 0.045 in. (~ 1.14 mm) and 0.06 in. (~ 1.52 mm) and lengths ranging from 7.5 to 42 cm. Each needle has a sharpened tip with a non-cutting edge and is flattened with 1 to 4 eyes on the other end. The edges of the eyelets were rounded to avoid possible damage to the EMG wire. The wires were threaded through the eyes and folded back for tunneling under the skin. To test the ability of the wire and insulation to withstand the stress of being bent back at the needle eyelet and then tunneled under the skin, we subjected wires to pulling forces after threading them through the eyelets of the tunneling needles. We found that the insulation could withstand forces sufficient to break the wire before becoming compromised. Even after the wire broke, the insulation stretched out but otherwise remained intact.

From the proximal forelimb (arrow 1, Fig. 3A), the four bundles of wires (1 per connector module) were tunneled separately to the back incision (arrow 2, Fig. 3A). A piece of surgical tape was then loosely wrapped around each bundle of wires and marked with a skin marking pen to identify the

bundles later in surgery. Each bundle was then tunneled to a separate, small puncture incision (1-2 mm made with a #11 blade) in the skin above the hip (arrow 3, Fig. 3A). From the most lateral hip incision (1), a pair of wires was tunneled to a small puncture incision in the skin over GMAX. The remaining wires from the most lateral hip incision were tunneled to a small puncture incision on the lateral surface of the proximal hindlimb (arrow 4, Fig. 3A). From here, pairs of wires were tunneled to small puncture incisions in the skin above GRA, SEM and SET. Incision points were staggered to minimize cross-talk between adjacent muscles. In our experience, compared to the forelimb, cross-talk was less problematic. This is probably due to the greater distances between electrode pairs than for the forelimb. From the second hip incision, the bundle of wires was tunneled to a puncture incision in the skin on the lateral surface of the distal hindlimb. From here, pairs of wires were tunneled separately to small puncture incisions in the skin above MG, LG, SOLp, SOLd and FDL. From the third hip incision, the bundle of wires was tunneled to a puncture incision in the skin on the anterior surface of the distal hindlimb. From here, pairs of wires were tunneled separately to small puncture incisions in the skin over TA, PERL, EDL, FHB and EDB. From the most medial hip incision (4), two pairs of wires were tunneled to a puncture incision in the skin on the anterior surface of the proximal hindlimb. From here, one pair of wires was tunneled to a puncture incision in the skin above BFL. A second pair of wires was tunneled to a puncture incision in the skin above VL. A third pair of wires was tunneled from the medial hip incision to a small puncture incision in the skin above TFL. The remaining three pairs of wires were tunneled from hip incision 4 to a puncture incision on the medial surface of the proximal hindlimb. From here, individual pairs of wires were tunneled to small puncture incisions in the skin above RF, VM and ADB. Tunneling to a common puncture incision distal to the target and then tunneling back proximally to sites over individual target muscles helped anchor the EMG wires.

Each wire was pulled through, leaving 8-10 cm of exposed wire at the incision on the back (arrow 2, Fig. 3A). Each wire was cut to length, leaving 6-7 cm exteriorized at the target muscle site. For each wire, 2-3 mm of insulation was removed from the tip. Each wire was then back fed into a 22-gauge

hypodermic needle (type D, beveled to minimize tissue damage) and folded back along the shaft of the needle. The wire was then inserted into the muscle in a proximal direction along the length of the muscle through the same puncture incision in the skin used for tunneling. The wire was then held at its entry point into the skin and the needle was removed leaving the EMG wire with a terminal hook embedded in the muscle belly. The two wires of a pair were inserted into the muscle with a separation of approximately 5 mm.

The wire insertion points for specific muscles were identified on the basis of external landmarks and palpation of muscle bellies. Landmarks and muscle locations were developed from dissection studies in *Macaca mulatta*. A dissected cadaver limb was also available for reference during surgery.

Proper placement of each electrode pair in a muscle was tested by stimulating through the electrodes with brief stimulus trains (biphasic pulse, 0.2 ms each phase, ~ 50 Hz) while observing the evoked movements. Palpating the tendons of implanted muscles during stimulation is another useful technique to confirm proper electrode placement. However, this method is useful only for muscles with easily identifiable tendons such as the ankle and foot muscles. Yet another method to help confirm proper location is to observe movement of the wires with passive movements at joints that will stretch and shorten the implanted muscle. This method is most useful for digit muscles but must be performed carefully with tunneled wires because the exposed loop of wire at the implant site is generally very short. If proper placement was not confirmed, the wires were removed and reinserted.

After implantation and confirmation of the proper location at each muscle, each pair of wires was isolated at the back incision (arrow 2, Fig. 3A) and pulled slowly, avoiding the formation of any kinks, until the wire at the implant site was completely subcutaneous. The hindlimb was then passively moved in all directions, which pulled additional lengths of EMG wire subcutaneously as the muscles lengthened. After all muscles were implanted, each bundle of wires leading to the arm connectors was pulled into the back incision, leaving only 3-4 cm of exposed wire at the connector module on the forelimb (arrow 1, Fig.

3A). At the incision site on the back, a small pocket was created using blunt dissection in the subcutaneous layer. The identifying surgical tape was removed from each bundle. Excess wire was formed into loops and placed in the subcutaneous pocket, thus eliminating all exposed wire. The loops of extra wire served to both accommodate movement of the limb and securely anchor the implant. The incision site was then flushed with saline followed by antibiotic (injectable liquid penicillin) and sutured (3-0 stainless steel). The puncture incisions at the implant sites were sealed with tissue glue (Henry Schein, Nexaband: 893-8109).

The four connectors were affixed to the monkey's proximal forelimb with an elastic medical adhesive tape (Johnson & Johnson Health Care System, Elastikon elastomeric tape: 5174, 2 in. width) as described in Park et al. (2000). To protect the implant, the monkey wore a custom fitted primate jacket (Lomir Biomedical, model PJ05) reinforced with stainless steel mesh (Whiting and Davis, SM5SS) while in its home cage. Implanting 20 pairs of EMG leads in hindlimb muscles with this method required approximately 9 hours of surgery.

Following surgery, the monkey was closely monitored until it was fully awake and able to sit and stand without assistance. Post-operative analgesics (buprenorphine, 0.01 mg/kg) were given for 5 days. Wound edges were inspected daily and treated with Betadine (10% povidone-iodine) and topical antibiotic.

Cranial-Mounted Subcutaneous Implant

Connectors

The cranial-mounted subcutaneous implant uses a high density, miniature circular connector system (Amphenol pin, 220-P03-2-100; Amphenol male connector, 222-11n61), as described in Park et al. (2000). Forty multi-stranded stainless steel wires (Cooner Wire, AS632) were cut to lengths appropriate for the 20 pairs of EMG wires to be implanted and the connector was assembled as described in Park et al. (2000).

Surgical Protocol

The pre-surgical procedures and anesthesia were the same as described for the arm-mounted subcutaneous implant. In an earlier unrelated surgery, a 50 mm diameter chamber for microelectrode recording was attached to the skull using titanium screws and dental acrylic (Park et al., 2000). One month prior to the EMG implant, a preparatory surgery was performed to hollow out the existing dental acrylic on the head, forming a seat for the connector base. At the same time, two channels were made in the acrylic from the base to the edge of the acrylic just above the occipital ridge of the skull. The preparatory procedure and the EMG implant procedure were separate to decrease the individual surgery length.

At the beginning of the EMG implant surgery, the base of the male connector with 40 wires was placed in the seat formed in the dental acrylic. The wires were collected into the channels (proximal muscles in one channel, distal muscles in the second) and directed caudally to the acrylic/skin junction at the occipital ridge (arrow 1, Fig. 3B). Using the custom stainless steel tunneling needles as described above, all wires were passed subcutaneously from the acrylic/skin junction at the occipital ridge to an incision (~ 4 cm) near the midpoint just below the shoulder blades (arrow 2, Fig. 3B). All wires were exteriorized at this incision and separated into four bundles, two proximal and two distal. Wires were tunneled and implanted as described above in the arm-mounted subcutaneous implant method. When all wires were implanted successfully, each was pulled in both directions at the back incision to take up any extra length. Loops of wire 8-10 cm in length remained at the back incision and were tucked into a subcutaneous pocket before suturing. This was important to ensure sufficient extra wire length to accommodate movements of the leg and head that could not be imposed at the time of surgery. The skull connector and wires were then anchored in place with new dental acrylic. Anchoring of wires at the back incision and all subsequent suturing and sealing of incisions were the same as described in the arm-mounted subcutaneous method. Figure 3B illustrates the wiring routes. Implanting 20 pairs of EMG leads in hindlimb muscles with this method required approximately 11 hours of surgery.

Post-surgical care was the same as described above in the arm-mounted subcutaneous implant method.

RESULTS

During surgery, each implanted wire pair was tested for accurate location by sending brief stimulus trains through the wire electrodes and observing evoked movements. These evoked movements were compared to the primary and secondary actions of each muscle as described in Howell and Straus (1971). The target muscle actions and evoked movements during surgery are summarized in Table 1. All muscle responses matched expectations except TFL. However, the evoked movement in TFL was consistent in both monkeys. Stimulus thresholds for evoked movements typically ranged from 0.6V to 10V. The cranial-mounted implant was retested with stimulation several times throughout the life of the implant. Thresholds typically remained below 20V and evoked responses were highly stable.

The push-pull task was designed to engage both proximal and distal hindlimb muscles in reliable and stereotyped patterns of activation. Figure 3C shows the activation of each implanted muscle with respect to the action of the hindlimb at different phases of the task. The graph of joint angles throughout the push-pull task shows the greatest change in angle at the knee and the least change in angle at the hip. This may explain the broad activation of some hip muscles while the knee muscles were more phasic. Extensor and flexor muscles showed reciprocal patterns of activation, with extensors primarily active during the extension phase of the task and flexors primarily active during the flexion phase of the task. VM, while expected to show EMG activity during the extension phase based upon muscle anatomy, was primarily active during the flexion phase. This may have been due to task design and was consistent in both monkeys and over time. BFL, while primarily a knee flexor, has a secondary action of hip extension and was most active in the extension phase of the task. The digit and intrinsic foot muscles showed broad activation throughout the task.

Cross-talk is more likely to occur between muscles that are adjacent to each other. With the larger size of the hindlimb (compared to the forelimb), we were able to achieve greater separation between electrode pairs. When implanting in adjacent muscles, we made an effort to stagger electrode

placement so electrode pairs were not directly adjacent to each other. In the two implants described in this paper, cross-talk was absent in almost all cases. Monkey C showed some cross-talk between LG and SOL, but the magnitude was less than the criterion for rejection.

The arm-mounted subcutaneous implant was used in monkey F. This implant remained fully viable at 31 months, at which point data collection ended. At regular intervals (approximately every two weeks), the monkey was tranquilized to remove the old elastomeric tape, shave the forelimb of hair and affix new tape to the external connectors. Figure 4 shows samples of EMG activity from all 19 muscles obtained with this method at 1 month (4A) and 18 months (4B) following implantation. The left column shows a sample of raw EMG from each muscle during two consecutive trials of the push-pull task. The right column shows EMG activity from each muscle averaged over a number of trials. After 18 months, all EMG electrodes were functional. Comparison of the 1 month and 18 month records shows a very consistent pattern of activation across all muscles during performance of the push-pull task.

The cranial-mounted subcutaneous implant was used in monkey C. This implant remained viable for 12 months. Figure 5 shows samples of EMG activity from all 19 muscles four months after implantation. EMG activity patterns were consistent with those obtained with the arm-mounted subcutaneous implant. Four muscles were lost when a small ulceration of the skin developed over a site where several EMG wires were tunneled on the lateral aspect of the distal hindlimb. The ulceration allowed the monkey access to the wires, thus compromising this section of the implant.

Both implant methods were relatively non-traumatic. Each monkey recovered quickly from the surgical procedure and was able to perform the behavioral task a few days after surgery.

DISCUSSION

This paper presents two chronic EMG implant methods that are minimally invasive, relatively non-traumatic and capable of recording from 19 muscles of the hindlimb in awake behaving monkeys for periods up to 31 months. Several advantages are common to both methods. The procedure of tunneling the wires subcutaneously adds stability to the implant as the fascia bonds well to the wires' insulation. Tunneling to a point beyond the target muscle and then back proximally to insert wires in the muscle also aids in anchoring the wire in the fascia. The creation of a hook at the tip of the wire, which is then implanted in the muscle belly, increases the stability of the EMG wire in the muscle. The placement of loops of wire in the pocket on the back along with the lengthening of the hindlimb after implantation ensures that the full range of motion was accommodated. Risk of infection and edema is minimized by the very small incision sizes and flushing of the wire pocket on the back with antibiotic (injectable liquid penicillin). Trauma was minimized as well. The monkeys were able to perform behavioral tasks within a few days of the surgery. At necropsy, efforts were made to forcibly remove the implant but there was no give, particularly at the loop on the back, demonstrating how firmly embedded the wires had become. Dissection along the course of the wires showed no evidence of inflammation.

There are advantages and disadvantages to both implant methods. A major benefit of the arm-mounted implant is its modular division and lack of permanence. Parts of the connector can be removed and re-implanted if necessary. The implant is not one unit but rather divided into four individual units. If a problem occurs with a single connector, that connector can be removed and re-implanted rather than the entire EMG implant. The arm-mounted subcutaneous implant is also a shorter surgery than the cranial-mounted subcutaneous implant. The major disadvantage is that the stability of the implant depends upon anchoring the modular connectors to the forelimb with elastomeric tape. With time and hair growth, the adhesiveness of the tape deteriorates. This increases the possibility of the implanted wires becoming dislodged. The tape must be replaced and the forelimb shaved on a regular basis. The jacket, while

effective as a protective barrier for the modular connectors, is expensive and requires a significant amount of maintenance due to constant probing and manipulation by the monkey.

The cranial-mounted subcutaneous implant also has advantages and disadvantages. The implant is completely subcutaneous. The head connector is durable and non-removable. The monkey has no access to the implant (barring any unforeseen circumstances such as the skin ulceration described in the methods). Another major advantage is that re-taping the forelimb and the use of a protective jacket are unnecessary. One disadvantage is the possibility of infection at the acrylic/skin junction on the back of the head where the wires first become subcutaneous. Several strategies were implemented to reduce the possibility of infection at the skin edge near the cortical chamber. 1) Ample time was allowed following the cortical chamber implant surgery for the skin edge to heal. This usually requires at least one and a half months. 2) The bundle of wires leading from the cranial connector was split into two bundles decreasing the size of the skin opening at the edge of the cranial implant. 3) The wires were tunneled deep and close to the skull at the skin–acrylic interface to minimize the chances that any infectious superficial debris was able to enter the subcutaneous wire tunnel. 4) Antibiotics were given until the skin edge healed. 5) Care was taken to avoid disturbing the surface of the skin edge allowing the skin to create its own natural defenses against infection (e.g. scabbing). The length of the implant surgery is another disadvantage. However, by dividing the head connector into two modules, this implant can be accomplished in two much shorter surgeries. This method is also less flexible than the arm-mounted subcutaneous implant method in terms of re-implantation. If there is electrode failure resulting in loss of a viable EMG signal from a muscle or muscles, they cannot be easily recovered using this implant method.

In summary, this paper reports two chronic EMG implant methods, the arm-mounted subcutaneous implant and the cranial-mounted subcutaneous implant. Both methods have individual advantages and disadvantages. However, both methods have been shown to have minimal risk of

infection, are relatively non-traumatic and provide stable, long-term EMG recording from large numbers of muscles of the hindlimb in awake behaving monkeys.

MANUFACTURERS AND SUPPLIERS

A list of manufacturers and suppliers can be found in Park et al. (2000). The following represents any updates or changes.

Stainless steel mesh

Whiting and Davis

200 John Dietsch Boulevard

Attleboro Falls, MA 02763

(508) 699-4412

Table 1. Actions of recorded muscles and stimlus evoked responses.

Muscle	Joint	Primary action#	Secondary action#	Stimulus evoked response
GRA	**hip** knee*	hip adduction	knee flexion medial rotation	knee flexion medial rotation
ADB	**hip**	hip adduction	lateral rotation	hip adduction
GMAX	**hip** knee*	hip extension	hip abduction knee flexion	hip extension
TFL	**hip**	hip abduction		hip flexion
BFL	**hip** knee*	knee flexion	hip extension lateral rotation hip abduction	hip extension knee flexion
SEM	**knee** hip*	knee flexion	hip extension medial rotation	knee flexion medial rotation
SET	**knee** hip*	knee flexion	hip extension medial rotation	knee flexion medial rotation
RF	**knee** hip*	knee extension	hip flexion	knee extension
VL	**knee**	knee extension		knee extension
VM	**knee**	knee extension		knee extension
TA	**ankle**	ankle flexion	foot inversion	ankle flexion
PERL	**ankle**	foot eversion	ankle extention	foot eversion
MG	**ankle**	ankle extention		ankle extention (fast)
LG	**ankle**	ankle extention		ankle extention (fast)
SOLp	**ankle**	ankle extention		ankle extention (slow)
SOLd	**ankle**	ankle extention		ankle extention (slow)
FDL	**digits** ankle*	digit flexion	foot adduction	digit 2-5 flexion
EDL	**digits** ankle*	digit extention	ankle flexion	digit 4-5 extention
FHB	**intrinsic foot**	hallux flexion		hallux flexion
EDB	**intrinsic foot**	digit 2-5 extention	digit abduction	digit 3-4 extention

Primary and secondary actions as listed in Howell and Strauss (1971)
* Biarticulate, primary joint listed in bold

Figure 1. Cross-section of muscle anatomy in the lower leg (A) and upper leg (B). A cadaver hindlimb was frozen and sectioned using a 19 tooth/inch, bi-metal band saw blade (L.S. Starret Co.). Photographs were taken of each cross-section and the boundaries between muscles were traced directly from the sections. Where separation of muscles was difficult to discern, macroscopic ultraviolet epifluorescence was used to identify fascial boundaries. Identification of muscles was confirmed by cross-referencing to a dissected cadaver limb with muscles intact. Medial (M) and lateral (L) aspects of the hindlimb are marked on the photographs in A and B.

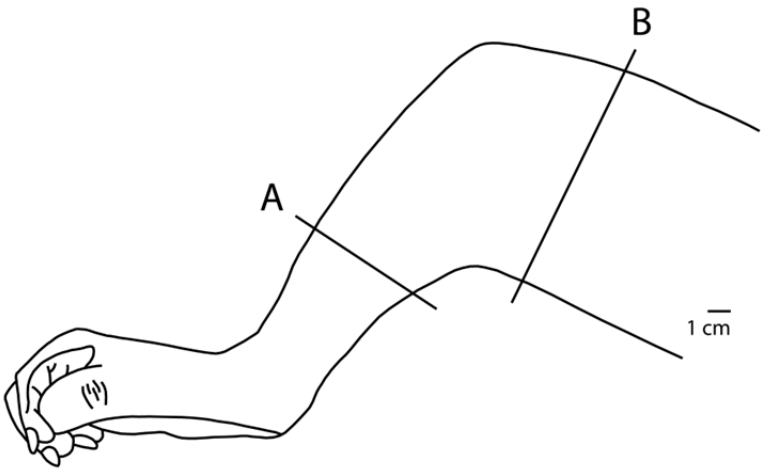
B
A
1 cm

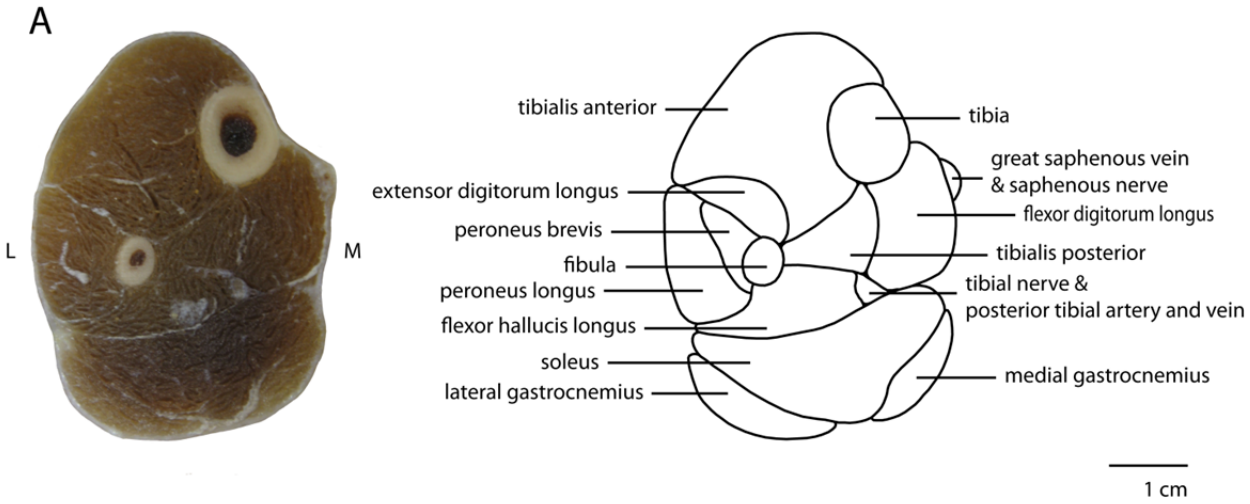
A
L
M
tibialis anterior
tibia
great saphenous vein
& saphenous nerve
extensor digitorum longus
flexor digitorum longus
peroneus brevis
tibialis posterior
fibula
tibial nerve &
posterior tibial artery and vein
peroneus longus
flexor hallucis longus
soleus
medial gastrocnemius
lateral gastrocnemius
1 cm

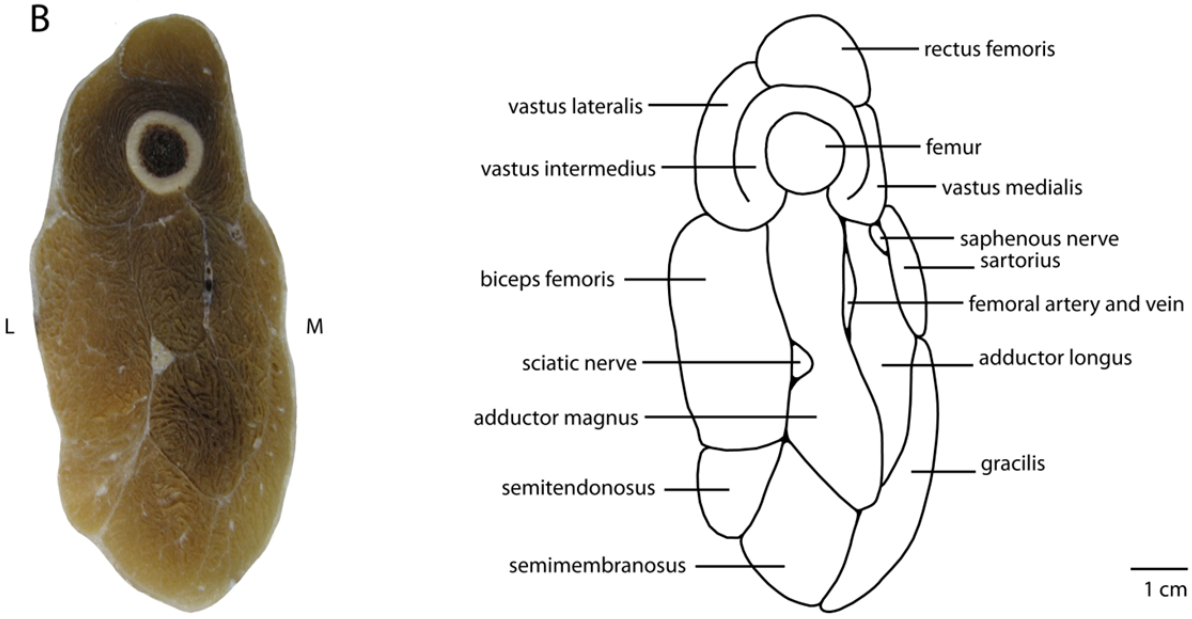
B
L
M
rectus femoris
vastus lateralis
femur
vastus intermedius
vastus medialis
saphenous nerve
sartorius
biceps femoris
femoral artery and vein
sciatic nerve
adductor longus
adductor magnus
gracilis
semitendonosus
semimembranosus
1 cm

Figure 2. T1- and T2-weighted MRIs of the upper and lower hindlimb in a cadaver rhesus monkey leg. Bone is easily identifiable with both types of imaging. Fascial boundaries separating muscles are more pronounced in the T1-weighted image. Bright spots on the periphery of the T1-weighted image are due to placement of the Helmholtz RF coil loop relative to the leg.

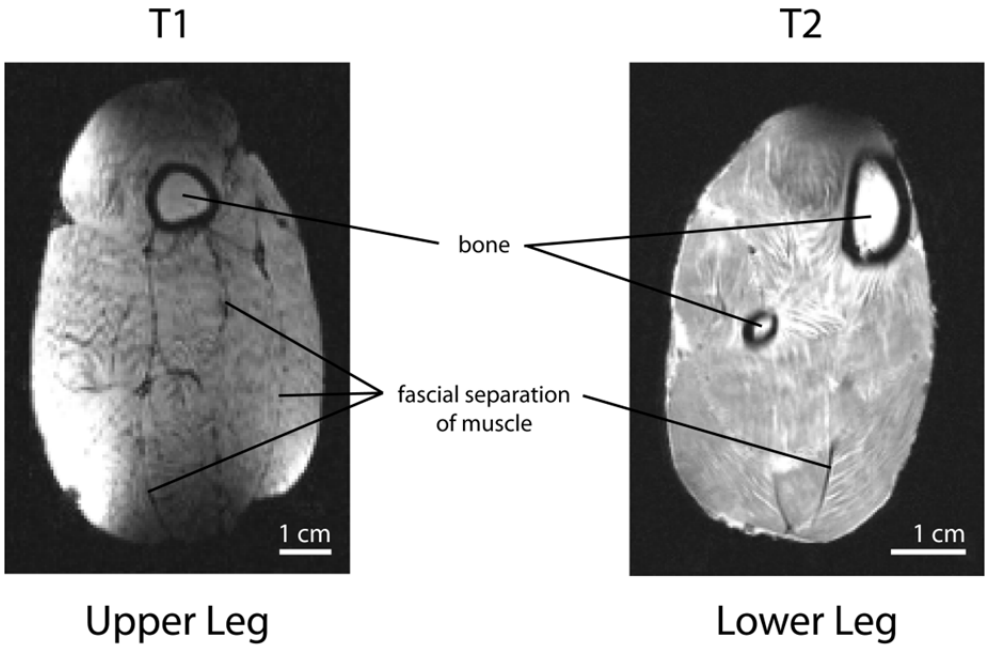
T1
T2
bone
fascial separation
of muscle
1 cm
1 cm
Upper Leg
Lower Leg

Figure 3. (A) Arm-mounted subcutaneous implant. Orange rectangles on forelimb: exteriorized connectors that allow connection of EMG wires to amplifiers. Short black lines: exterior wires leading to connectors. Red lines: subcutaneous paths of EMG wires to individual target muscles, wires continuing onto medial side of hindlimb go to target muscles. Light blue circles: sites of small incisions during tunneling. Long light blue line: back pocket where wire loop is seated. Black arrows: 1 - exterior arm connectors and entry point of EMG wires, 2 - back incision, 3 - puncture incisions on the hip, 4 – puncture incision on lateral hindlimb for wires tunneled from hip incision 1. Hip incisions (arrow 3) are numbered 1-4 from most lateral to most medial. (B) Cranial-mounted subcutaneous implant. Red lines, light blue circles and light blue line as described above. Green circle: EMG connector, affixed to skull with dental acrylic, connects to amplifiers. Black arrows: 1 - cranial connector and entry point of EMG wires, 2 - back incision, 3 - puncture incisions on the hip, 4 – puncture incision on lateral hindlimb for wires tunneled from hip incision 1. Hip incisions (arrow 3) are numbered 1-4 from most lateral to most medial. (C) EMG records and joint angle during two cycles of the hindlimb push-pull task. Angle measurement at each joint is described in graph legend and also depicted in (A) and (B).

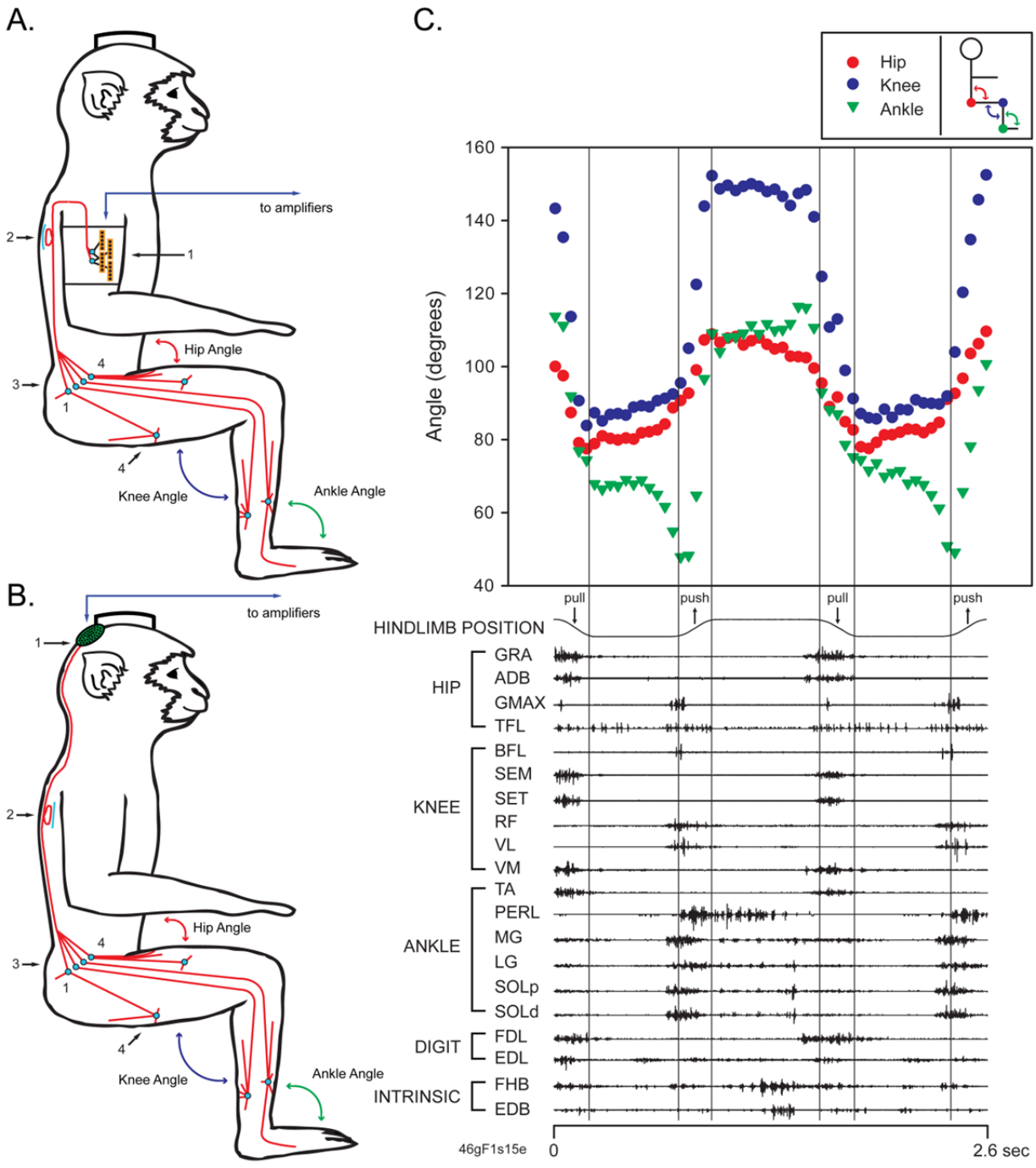
A.
to amplifiers
2
1
Hip Angle
3
4
1
4
Knee Angle
Ankle Angle
B.
to amplifiers
1
2
Hip Angle
3
4
1
4
Knee Angle
Ankle Angle
C.
Hip
Knee
Ankle
160
140
120
100
80
60
40
Angle (degrees)
pull
push
pull
push
HINDLIMB POSITION
HIP
GRA
ADB
GMAX
TFL
KNEE
BFL
SEM
SET
RF
VL
VM
ANKLE
TA
PERL
MG
LG
SOLp
SOLd
DIGIT
FDL
EDL
INTRINSIC
FHB
EDB
46gF1s15e
0
2.6 sec

Figure 4. EMG signals (left) and response averages (right) from 20 pairs of EMG wires implanted in hindlimb muscles at 1 month (A) and 18 months (B) following the arm-mounted subcutaneous implant in monkey F. The records shown are from two consecutive trials of the push-pull task. Different channels of EMG activity were amplified from 5-200 K. Filtering was generally 30 Hz to 3 kHz. All channels were digitized at 4 kHz. Muscle abbreviations are given in Materials and Methods. PP: push-pull task. Shaded area indicates extension position zone. Calibration bar to the left of the task signal indicates linear distance of foot movement during the push-pull task.

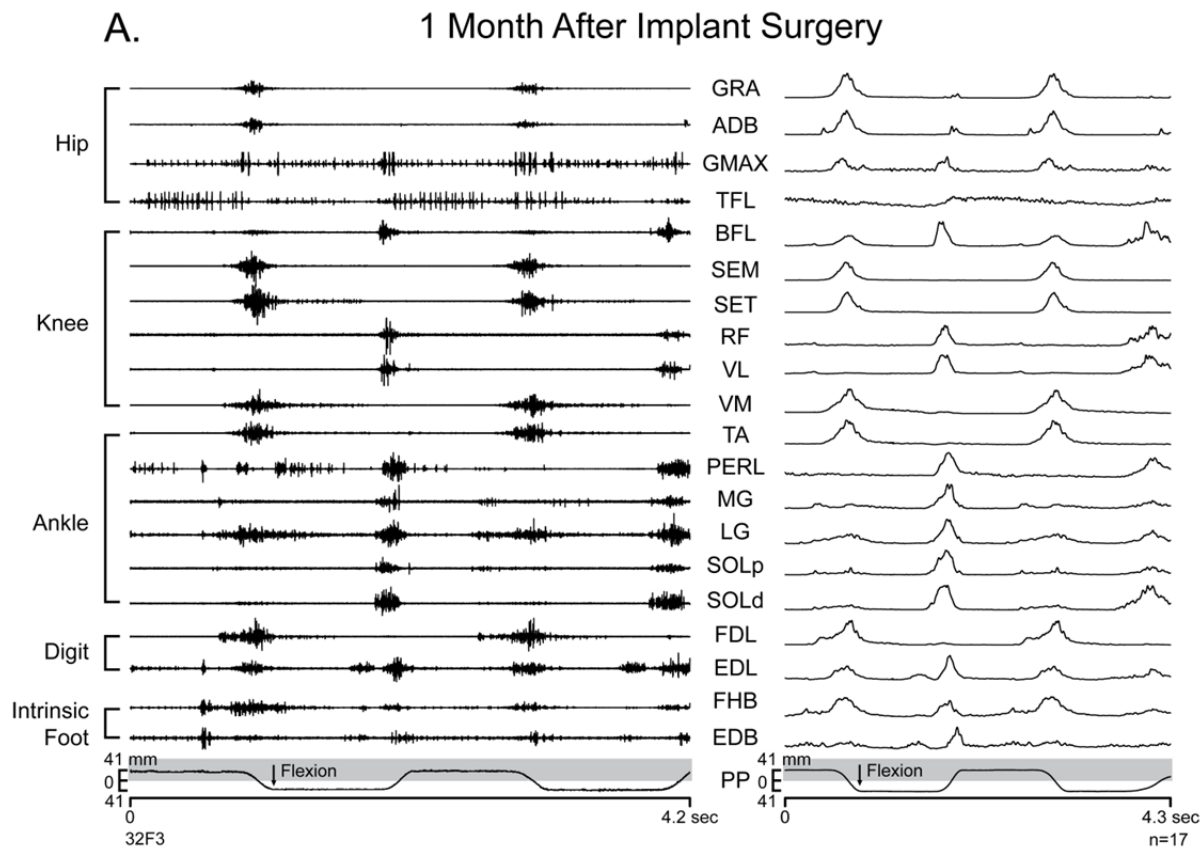
A.
1 Month After Implant Surgery
Hip
Knee
Ankle
Digit
Intrinsic Foot
GRA
ADB
GMAX
TFL
BFL
SEM
SET
RF
VL
VM
TA
PERL
MG
LG
SOLp
SOLd
FDL
EDL
FHB
EDB
41 mm
0
41
Flexion
0
4.2 sec
32F3
PP
0
4.3 sec
n=17

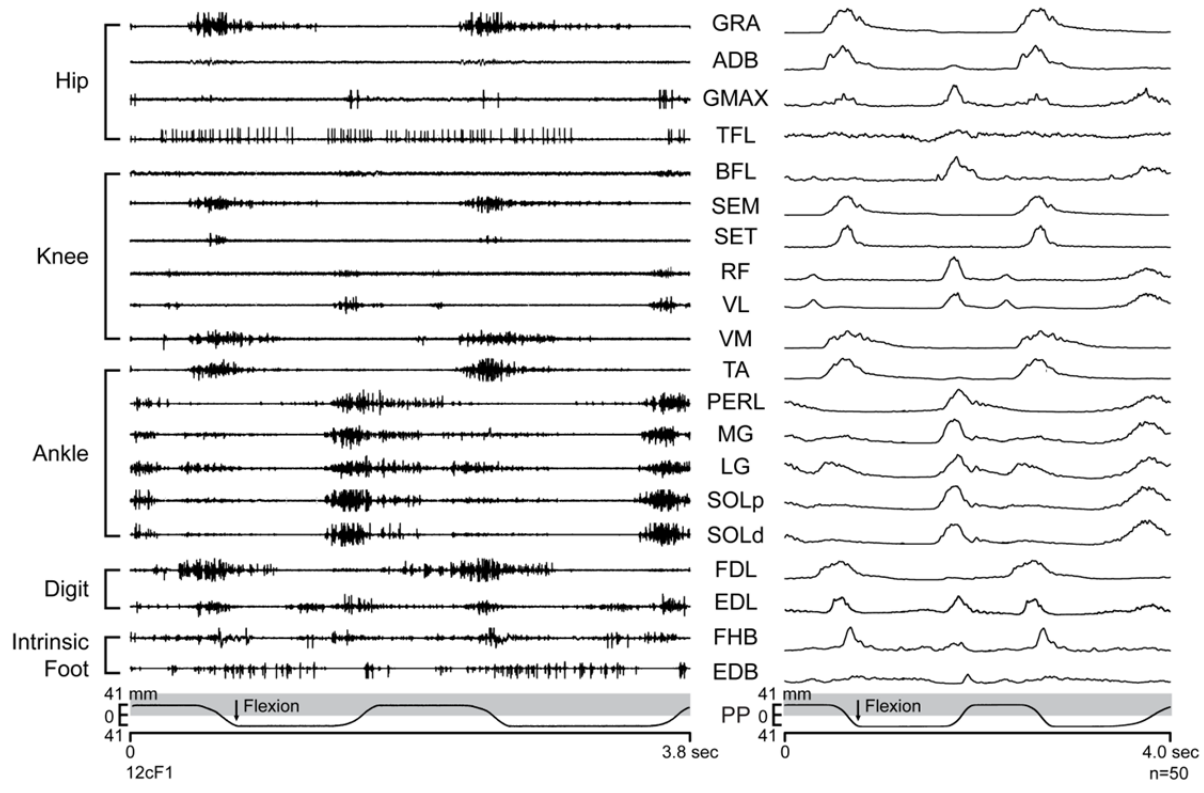
B.
18 Months After Implant Surgery
Hip
Knee
Ankle
Digit
Intrinsic Foot
GRA
ADB
GMAX
TFL
BFL
SEM
SET
RF
VL
VM
TA
PERL
MG
LG
SOLp
SOLd
FDL
EDL
FHB
EDB
41 mm
0
41
Flexion
0
3.8 sec
12cF1
PP
0
4.0 sec
n=50

Figure 5. EMG signals (left) and response averages (right) from 20 pairs of EMG wires implanted in hindlimb muscles at 4 months following the cranial-mounted subcutaneous implant in monkey C. The records shown are from two consecutive trials of the push-pull task. Different channels of EMG activity were amplified from 5-200 K. Filtering was generally 30 Hz to 3 kHz. All channels were digitized at 4 kHz. Muscle abbreviations are given in Materials and Methods. PP: push-pull task. Shaded area indicates extension position zone. Calibration bar to the left of the task signal indicates linear distance of foot movement during the push-pull task.

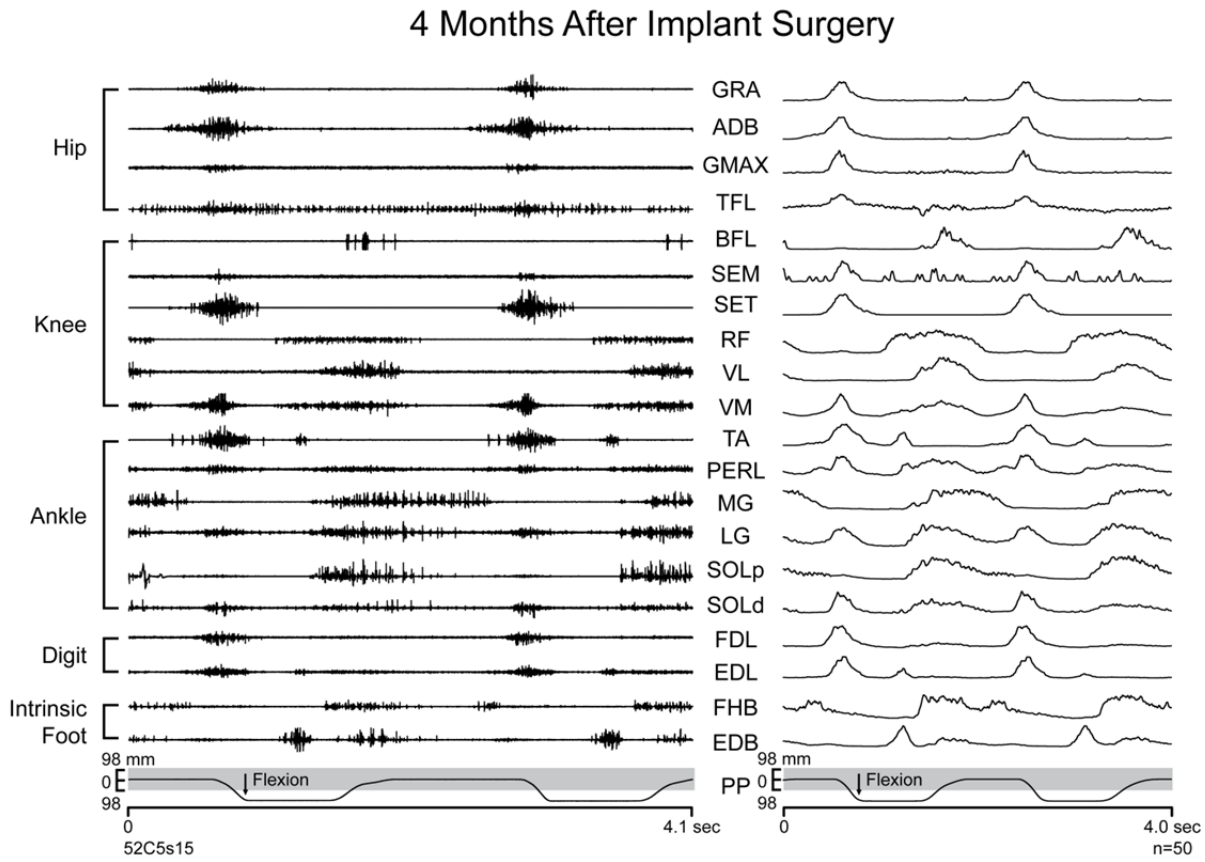
4 Months After Implant Surgery
Hip
Knee
Ankle
Digit
Intrinsic
Foot
GRA
ADB
GMAX
TFL
BFL
SEM
SET
RF
VL
VM
TA
PERL
MG
LG
SOLp
SOLd
FDL
EDL
FHB
EDB
PP
98 mm
0
98
Flexion
0
4.1 sec
52C5s15
98 mm
0
98
Flexion
0
4.0 sec
n=50

CHAPTER 3

REPRESENTATION OF HINDLIMB MUSCLES IN PRIMARY MOTOR CORTEX

INTRODUCTION

The organization of forelimb primary motor cortex (M1) has been studied extensively using a variety of techniques such as high frequency intracortical microstimulation (ICMS), spike triggered averaging (SpTA), stimulus triggered averaging (StTA) and retrograde tracers (Baker et al., 1998; He et al., 1993; Kwan et al., 1978; McKiernan et al., 1998; Park et al., 2001; Rathelot and Strick, 2006; Schieber and Rivlis, 2005; Stepniewska et al., 1993). Consistent features of the forelimb output maps included a core distal muscle representation, largely in the bank of the central sulcus, surrounded by a proximal muscle representation. Using stimulus triggered averaging of electromyographic (EMG) activity from 24 muscles of the forelimb, Park et al. (2001) not only identified a core distal representation surrounded by a horseshoe shaped proximal muscle representation that closely resembled the anatomical maps of He et al. (1993), but also the existence of a large output zone producing cofacilitation of both proximal and distal muscles. This zone separated the core distal muscle representation from the surrounding proximal muscle representation. Forelimb M1 was shown to have a lateral border with the face representation and a medial border with the trunk representation. Anteriorly, the forelimb representation bordered a zone producing no effects with StTA (30 μA) or repetitive ICMS (30 μA).

In comparison to forelimb M1, few studies have focused on the organization of hindlimb M1. Using retrograde tracers injected into the lower lumbosacral spinal cord of pig-tailed macaques, He et al. (1993) found hindlimb corticospinal neurons located in the precentral gyrus medial to forelimb neurons, extending into the medial wall of the interhemispheric fissure and caudally into the anterior bank of the central sulcus. Using ICMS to evoke movements, Hatanaka et al. (2001) showed a distal muscle representation surrounded by a proximal muscle representation in hindlimb M1 of Japanese macaques. The hindlimb representation extended into the medial wall of the hemisphere where it bordered on the tail representation. The trunk representation bordered the hindlimb representation laterally (Hatanaka et al., 2001; Luppino et al., 1991; Wise and Tanji, 1981). Neafsey (1980), using single unit recording, reported that neurons in hindlimb M1 related to extension and flexion were spatially separated.

In this study, we investigated the organization of motor output to proximal and distal as well as extensor and flexor muscles of the hindlimb by systematically mapping the hindlimb area of M1. Using methods similar to Park et al. (2001), we computed stimulus triggered averages of EMG activity for 19 muscles of the hindlimb while the monkey performed a push-pull task (Hudson et al., 2010). The sign, latency and magnitude of poststimulus output effects were determined for each M1 site stimulated and used to construct motor output maps for all 19 muscles tested. These maps were then compared to previous hindlimb maps based on stimulus evoked movements and to forelimb M1 motor output maps derived from stimulus triggered averaging.

MATERIALS AND METHODS

Behavioral task

Two male rhesus macaques (*Macaca mulatta*, ~10 kg, 6-7 years old) were trained to perform a hindlimb push-pull task that engaged both distal and proximal muscles in reliable and stereotyped patterns of activation (Figure 1 and Hudson et al., 2010). Inside a sound-attenuating chamber, the monkey was seated in a custom-designed primate chair equipped with a push-pull device used by the right hindlimb. The push-pull device consisted of an external manipulandum attached to internal linear bearings housed in a lexan exterior. A linear potentiometer was attached to the linear bearings to measure displacement (leg movement). Both arms and the left leg were restrained. With the right foot, the monkey gripped the manipulandum (horizontal post) and extended the leg until the target zone was achieved. After a hold period of 500 ms in the target zone, the monkey flexed the leg pulling the manipulandum to a second target zone which also required a hold period of 500 ms. After each successful push-pull trial, the monkey was given an applesauce reward. The behavioral task was guided by visual and auditory cues.

Surgical procedures

Upon completion of training, both monkeys were implanted with a cortical recording chamber (titanium, 30 mm inside diameter). The recording chambers were centered at anterior 13.5 mm, lateral 0 mm and 0° angle to the midsagittal plane (Paxinos et al. 2000).

EMG activity was recorded from 19 muscles of the hindlimb using pairs of insulated, multi-stranded stainless steel wire (Cooner Wire, AS632) implanted during an aseptic surgical procedure. One monkey (monkey F) was implanted using an arm-mounted subcutaneous implant technique and the other (monkey C) was implanted using a cranial-mounted subcutaneous implant technique (Hudson et. al, 2010). Briefly, pairs of wires were tunneled subcutaneously to their target muscles from either four external connector modules (ITT Canon) affixed to the upper arm with elastic medical adhesive tape

(arm-mounted subcutaneous implant) or an external circular connector (Amphenol) affixed to the skull using dental acrylic (cranial-mounted subcutaneous implant). Proper placement of electrode pairs in each muscle was tested by stimulating through the electrodes with brief stimulus trains (biphasic pulse, 0.2 ms/phase, ~50 Hz) while observing the evoked movements. If proper placement was not confirmed, wires were removed and reinserted.

EMGs were recorded from four hip muscles: gracilis (GRA), adductor brevis (ADB), gluteus maximus (GMAX) and tensor fascia latae (TFL); six knee muscles: biceps femoris (BFL), semimembranosus (SEM), semitendonosus (SET), rectus femoris (RF), vastus lateralis (VL) and vastus medialis (VM); five ankle muscles: tibialis anterior (TA), peroneus longus (PERL), medial gastrocnemius (MG), lateral gastrocnemius (LG) and soleus (SOL); two digit muscles: flexor digitorum longus (FDL) and extensor digitorum longus (EDL); and two intrinsic foot muscles: flexor hallucis brevis (FHB) and extensor digitorum brevis (EDB). In monkey C, the EMG leads to PERL were compromised shortly after the implant. As a result, PERL was not included in the data set for monkey C.

All surgeries were performed in an Association for Assessment and Accreditation of Laboratory Animal Care (AAALAC) accredited facility using full aseptic procedures. Postoperative analgesics (buprenorphine, 0.01 mg/kg) were given for 5 days. Wound edges were inspected daily and treated with Betadine (10% povidone-iodine) and topical antibiotic. All procedures were in accordance with the standards outlined by the *Guide for the Care and Use of Laboratory Animals* published by the U.S. Department of Health and Human Services and the National Institutes of Health.

Data collection

Cortical activity, EMG activity and task-related signals were simultaneously monitored. Glass and mylar-insulated platinum-iridium electrodes (Frederick Haer) with impedances of 0.5-1.5 MΩ were used to record cortical unit activity and for stimulation. The electrode was positioned in the recording chamber using a custom-built x-y positioner and advanced using a manual hydraulic microdrive

(Frederick Haer). Electrode penetrations were systematically made at 1 mm intervals in the precentral cortex of the left hemisphere. Data were collected from sites in layer V of the cortex, as determined by depth from first cortical activity and size and nature of neuronal spikes. Within each electrode track in the banks of the medial wall and central sulcus, data were collected from sites in layer V at 0.5 mm intervals over the extent of the electrode track.

At each layer V site, StTAs (15, 30 and 60 μA at 15 Hz) of EMG activity were computed for 19 muscles of the hindlimb as the monkey performed the push-pull task. Individual stimuli were symmetrical biphasic pulses, 0.2 ms negative pulse followed by a 0.2 ms positive pulse, applied throughout all phases of the task. EMGs were generally filtered at 30 Hz to 1 kHz, digitized at 4 kHz and full-wave rectified. StTAs were compiled over an 80 ms epoch, 20 ms pre-trigger and 60 ms post-trigger, and consisted of at least 500 trigger events. To prevent averaging periods where EMG activity was minimal or non-existent, segments of EMG activity associated with each stimulus were evaluated and accepted for averaging only when the average of all EMG data points over the entire 80 ms epoch was ≥ 5% of full-scale input (McKiernan et al., 1998).

When no poststimulus effects (PStEs) were detected at 60 μA, repetitive long duration ICMS (RL-ICMS, 15-60 μA, 200 Hz, 500 ms), as described by Graziano et al. (2002), was performed to determine the motor output representation for that site. Evoked movements and muscle twitches were noted. Sensory areas were identified by spike activity in response to light touch to the hair and skin and joint manipulation (Widener and Cheney, 1997).

Cross-talk between muscles was tested by computing EMG-triggered averages (Cheney and Fetz, 1980). Averages of EMG activity were compiled for each muscle using one muscle's EMG activity as a trigger. This process was repeated using all 19 muscles as triggers. A muscle was considered to have an unacceptable level of cross-talk if the ratio between the test and trigger muscles exceeded the ratio of their

cross-talk peaks by a factor of 2 or more (Buys et al., 1986). No muscle in this study showed significant cross-talk.

Data analysis

At each stimulation site, averages were obtained from all 19 muscles. Post stimulus facilitation (PStF) and suppression (PStS) effects were computer measured as described by Mewes and Cheney (1991). Each average consisted of an 80 ms epoch, 20 ms pre-trigger and 60 ms post-trigger. A PStE was defined as a peak or trough of EMG activity that rose or fell from baseline EMG activity and maintained a level of activity exceeding two standard deviations of baseline for a period equal to or greater than 0.75 ms. Baseline EMG activity was measured as the 12 ms period preceding the onset of the effect determined initially by visual inspection. Baseline statistics were then used to determine the onset of the effect as the point where the envelope of the record exceeded two standard deviations of baseline. The magnitude of PStEs was expressed as the peak percentage increase (+ppi) or peak percentage decrease (-ppi) in EMG activity above (PStF) or below (PStS) baseline. To ensure PStEs were significant, only PStF effects with a ppi $\geq$ 15 and PStS effects with a ppi $\leq$ -15 were included in data analysis (Figure 2).

MRI

Prior to recording chamber implant surgery, structural MRIs were obtained using a Siemens Allegra 3T system. The monkey's head was placed in an MRI-compatible stereotaxic apparatus and structural MRIs in the sagittal, coronal and horizontal planes were acquired. Using CARET software (Computerized Anatomical Reconstruction and Editing Tool Kit), a 3-dimensional reconstruction of each monkey's brain was produced.

Unfolding the cortex

A two-dimensional representation of cortical layer V of the cortex in the anterior bank of the central sulcus, the medial wall of the hemisphere and the surface cortex required flattening and unfolding the curvature of the cortex. This process has been described in detail by Park et al. (2001). Briefly, the cortex was unfolded and 2-dimensional maps were generated based on electrode track x-y coordinates, electrode penetration depth, MRI images, properties of recorded neurons, known architectural landmarks and observations during the cortical chamber implant surgery.

RESULTS

Dataset used for mapping

Data were collected from the left M1 in two rhesus macaques (Table 1). A total of 312 electrode penetrations were made, 170 in monkey F and 142 in monkey C (Figure 3). RL-ICMS was performed at 133 sites to identify output effects (movements or EMG responses) when no effects were obtained with StTAing. The presence or absence of sensory responses was tested at 65 sites primarily to aid in identifying the border of somatosensory cortex. At 15 μA, stimulus triggered averaging of EMG activity from 19 muscles of the hindlimb was performed at 259 layer V sites (292 sites at 30 μA and 317 sites at 60 μA). Seventy-four layer V sites yielded PStEs at 15 μA, 143 at 30 μA and 205 at 60 μA. Overall, PStF effects greatly outnumbered PStS effects at all stimulus intensities.

Boundaries of the M1 hindlimb representation

Sites yielding no poststimulus effects at 60 μA defined the boundaries of the hindlimb representation. At its most lateral extent, the hindlimb representation of primary motor cortex extended 4-6 mm anterior from the central sulcus (Figure 3). Closer to the midline, the central sulcus became shallow or non-existent. Here the hindlimb representation extended 10-11 mm anteriorly from the border with somatosensory cortex. From the midline, the hindlimb representation extended 8-10 mm laterally and 0-2 mm down the bank of the medial wall. Closer to the midline, where the central sulcus was shallow or non-existent, an area lacking poststimulus effects at 60 μA defined the border. RL-ICMS evoked tail and trunk movements along the anterior-medial border, trunk and forelimb movements along the lateral border.

Comparing the motor output maps of PStF for the two monkeys, a substantial difference in the number of sites yielding effects was apparent, especially at 15 μA (Figure 3). Nevertheless, several consistent features emerged from the maps. At 15 μA, there was a core distal muscle representation

(blue) on the surface of the cortex that extended into the central sulcus. Ankle, digit and intrinsic foot muscles were considered distal. The core distal representation was surrounded by a peripheral proximal muscle representation (red). Hip and knee muscles were considered proximal. A small area representing cofacilitation of proximal and distal muscles (purple) was located at the boundary of the distal only representation and was present in both monkeys, although in monkey F it was only one cortical site at 15 μA. At 30 μA, the number of sites with PStF of only proximal muscles increased but the size of the proximal representation, as a percentage of the total hindlimb cortical area, slightly decreased or remained the same (Table 2). The number of distal only sites at 30 μA compared to 15 μA also increased in one monkey but decreased slightly in the second monkey. However, the distal only muscle representation expressed as a percent of total hindlimb area decreased substantially although it remained at the central core of the hindlimb representation in both monkeys. At 30 μA compared to 15 μA, the proximal-distal muscle cofacilitation region increased in size in both monkeys and in monkey C occupied an intermediate zone separating the specific proximal and distal muscle areas. At 60 μA, the proximal-distal cofacilitation area increased substantially in both monkeys, occupying most of the hindlimb representation (Table 2). The proximal representation, while smaller than at 30 μA, remained at the periphery in both monkeys. The distal representation also decreased in size in both monkeys leaving only isolated pockets of representation. In monkey F, the proximal-distal cofacilitation zone more clearly separated the distal and proximal representations at 60 μA.

Muscle representation by joint

Figures 4, 5 and 6 show maps of individual muscle representations for each monkey at 15 μA, 30 μA and 60 μA, respectively, color coded for the magnitude of PStF. Note that due to large differences in the magnitude of effects in muscles at different joints, particularly the intrinsic muscles, the scales at different joints are different. As expected, the area of representation for a particular muscle increases with stimulus intensity. The representations for individual proximal muscles were highly overlapping,

particularly for muscles at the same joint. The same was true of distal muscles. Looking across the maps at all intensities, what is most evident is the presence of noncontiguous hot spots of representation. In some cases, two primary hot spots are present forming a dual representation (for example, VL) while in other cases three or more peaks of representation are evident. In fact, many of the hip and knee muscles in both monkeys showed two widely separated regions of representation – one in the central sulcus and one near the midline. This is most evident at 30 μA and clearer in monkey C than monkey F.

Representation of flexor and extensor muscles

While there were extensor only and flexor only sites in hindlimb M1, cofacilitation of extensor and flexor muscles was the most common effect at all stimulus intensities (Figure 7). Figure 8 shows maps of flexors and extensor muscles at each joint color coded for magnitude. At 15 and 30 μA, the hip flexors tended to be represented in two locations with one site near the central sulcus and the other near the midline. For unknown reasons, there was very little representation of the hip extensors in monkey C. In monkey F, the hip extensor representation was stronger but still considerably less than the hip flexors. There was little cofacilitation of extensors and flexors at the hip at any stimulus intensity. Both the knee extensors and knee flexors showed a dual representation with foci at both the central sulcus and the midline. These sites strengthened as stimulus intensity increased. Again, the dual representations could still be seen at 60 μA when looking at sites with strong average magnitude of PStF. There was little cofacilitation of extensors and flexors of the knee at the lower stimulus intensities, however, at 60 μA, cofacilitation increased (Figure 8). The ankle, digit and intrinsic foot muscles showed similar organizations with a core of extensor-flexor cofacilitation at 30 and 60 μA surrounded by flexor and extensor representations (Figure 8).

Map organization of M1 inhibitory output

Motor output maps of suppression effects (PStS) revealed an aspect of hindlimb M1 organization of proximal and distal muscles paralleling the representation of facilitation effects (Figure 9). For this

analysis we only included pure PStS effects; biphasic effects (PStF followed by apparent PStS) were excluded. In both monkeys, there were far fewer PStS effects than PStF effects at all stimulus intensities. Interestingly, the map of suppression was essentially the reverse of the facilitation map. Unlike facilitation, suppression maps tended to have a core proximal muscle representation surrounded by a peripheral distal muscle representation. Distal muscles dominated the central sulcus and medial wall. The proximal-distal co-suppression representation was small in comparison to the proximal muscle and distal muscle representations. At 60 μA, the proximal-distal co-suppression area separated the proximal muscle area and the distal muscle area in monkey C but was less clear in monkey F.

DISCUSSION

Hindlimb M1 compared to forelimb M1

Our approach in this study paralleled a previous study from our laboratory in which stimulus triggered averaging of EMG activity was used to map 24 forelimb muscles in rhesus monkeys (Park et al., 2001). Forelimb motor output maps constructed from PStF effects (15 μA) show a clear intra-areal somatotopic organization with a core distal muscle representation (blue) surrounded by a horseshoe-shaped proximal muscle representation (red) (Figure 10). Separating the distal only and the proximal only representations was a substantial region where sites activated combinations of proximal and distal muscles. A similar pattern of representation is evident in the maps of hindlimb muscle organization at 15 μA. Although there were fewer effective sites in the hindlimb maps at 15 μA than the forelimb, a similar pattern of representation is evident with a core distal representation surrounded by proximal sites at the periphery. At 15 μA the proximal-distal representation is very limited and the distal representation dominates the maps. At 30 μA the core distal representation is still clear with proximal muscles represented at the periphery but now the proximal-distal cofacilitation zone dominates the map in monkey C and is becoming more prominent in monkey F. At 60 μA the proximal-distal cofacilitation zone dominates the hindlimb map in both monkeys. Only fragmentary remnants remain of the core distal and peripheral proximal representations. We wondered how the map of forelimb muscles would change in going from 15 to 60 μA. Although the forelimb data was only collected at 15 μA, we extrapolated this data to create maps at 60 μA (Figure 10). The extrapolation was based on estimates of physical current spread using the expression $r = \sqrt{i/k}$ where *r* is the radius of activation, *i* is current intensity and *k* is a proportionality constant (Cheney and Fetz, 1980). For the extrapolation, we used $k = 250$ μA/mm which is near the low end of the range of possible *k* values and would have produced greater overlap of output zones compared to larger *k* values. In both monkeys D and M, the area representing proximal-distal cofacilitation (purple) increased in size and occupied areas that at 15 μA were proximal only or distal

only. However, in the extrapolated maps at 60 μA the fundamental pattern of intra-areal representation remained clear, namely, core distal and peripheral proximal representations separated by a proximal-distal cofacilitation zone. Although in going from 15 μA to 60 μA, the proximal-distal cofacilitation zone substantially increased in both the forelimb and hindlimb maps, the increase was greatest for the hindlimb This might suggest real differences in underlying organization with greater emphasis on linkages between distal and proximal muscles. Alternatively, it might be due to the fact that our extrapolation of the forearm maps to 60 μA took into account physical spread of excitatory current but not physiological spread.

Somatotopic organization of hindlimb M1

Using ICMS (high frequency stimulus trains) in hindlimb M1 to map evoked movements in the rhesus macaque, Wise and Tanji (1981) found a core distal muscle representation, extending into the medial wall, surrounded by a proximal muscle representation. Hatanaka et al. (2001) showed this same nested distal-proximal organization using ICMS in the Japanese macaque, but with a proximal hindlimb muscle representation in the medial wall. Both studies found tail and trunk representations in the medial wall as well. Both Mitz and Wise (1987), using ICMS in pig-tailed macaques, and Luppino et al. (1991), using crab-eating macaques, found both proximal and distal hindlimb muscle representations in the medial wall, along with tail and trunk representations. The trunk representation bordered hindlimb M1 laterally (Hatanaka et al., 2001; Luppino et al., 1991; Wise and Tanji, 1981). Using stimulus triggered averaging of EMG activity from 19 muscles of the hindlimb, we found a similar organization. In the medial wall, there were proximal only, distal only and proximal-distal cofacilitation regions. Consistent with previous studies, trunk and tail representations were present in the medial wall and a trunk area bordered hindlimb M1 laterally.

Interpretation of map changes with stimulus intensity

As noted above, the size of the proximal-distal cofacilitation zone increased dramatically in the hindlimb maps with increased stimulus intensity, while the size of the proximal only and distal only zones either stayed the same or decreased in size. What could account for these changes? One simple explanation is that there might be separate proximal only and distal only output zones with a relatively sharp boundary and as stimulus intensity increases physical spread across the boundary results in activation of cells in both distal and proximal zones creating the appearance of a separate proximal-distal cofacilitation (PDC) zone. However, this possibility can be rejected because physical spread of excitatory current across an otherwise relatively sharp border is too limited to account for the size of the proximal-distal representation.

Other possibilities are illustrated in Figure 11. Multiple factors can influence the changes in map organization as a function of stimulus intensity. One is the presence of different types of corticospinal neurons based on their target muscles (proximal only, distal only, proximal + distal) and how they are arranged in the cortex. Another factor is the synaptic linkage these neurons make with motoneurons. The more indirect the linkage to motoneurons, the greater the stimulus intensity that might be needed to achieve transmission to motoneurons. How these factors could combine in different ways to affect the results is illustrated in Figure 11. One possible organization would be a segregated arrangement of distal only, proximal only and proximal + distal neurons all of which make monosynaptic connections to motoneurons (Figure 11A). In this model, the map at low stimulus intensity should consist of separate proximal only, distal only and PDC regions with only a narrow band of proximal-distal cofacilitation between the proximal only and the distal only regions. At higher stimulus intensities, the physical spread of the current will modestly increase the size of the PDC region but the overall map organization should remain relatively intact, as seen with the extrapolated forelimb maps (Figure 10). This is not what we see in hindlimb M1. The expansion of the PDC region is much greater than what can be accounted for by physical spread of the stimulus alone.

Another possibility is that the different types of corticospinal neurons have monosynaptic connections to motoneurons but unlike A, they are completely intermixed in the cortex (Figure 11B). In this case, the entire map would appear as a proximal-distal cofacilitation zone regardless of stimulus intensity. Again, this is not what we observed in the hindlimb M1 map. At lower stimulus intensities, there were clear proximal only, distal only and PDC regions. A variation of this mixed model excludes proximal + distal neurons and varies the synaptic linkage such that proximal only cells have a non-monosynaptic linkage to motoneurons and distal only cells have a monosynaptic linkage (Figure 11C). In this case, at low (threshold) stimulus intensities, the entire hindlimb representation would consist of a large distal only region. There would be no proximal only regions as transmission through the non-monosynaptic pathway would be less robust. However, at higher stimulus intensities, the reliability of discharging the interneurons would increase, proximal muscles would be recruited, and the entire map would transition to a proximal-distal cofacilitation representation. Again, this is not what we observed in the maps of hindlimb M1 representation. At lower stimulus intensities, there are clear proximal only, distal only and a small proximal + distal representation. At higher stimulus intensities, the proximal + distal representation dramatically increases in size, but there remain clear proximal only and distal only representations.

A variation of Model C would be the existence of predominately proximal and distal zones but with some mixing of the two cells types throughout out each representation. Additionally, each representation would have some cells with monosynaptic connections to motoneurons. In this case, the fact that each cell type has at least some monosynaptic component to its linkage with motoneurons suggests that all sites should yield facilitation in both distal and proximal muscles, even at low intensities assuming sufficient numbers of sweeps are taken. This is not what was observed.

A fourth possibility combines elements of models A-C. In this model there is partial segregation of corticospinal neurons, some projecting monosynaptically to proximal motoneurons (red), some projecting monosynaptically to distal motoneurons (blue) and some projecting monosynaptically to distal

motoneurons but non-monosynaptically to proximal motoneurons (yellow) (Figure 11D). At low (threshold) stimulus intensity, the map would consist of a large distal only region, a small proximal only region and a small proximal-distal cofacilitation zone depending on the amount of overlap of different types of cells. As in model 13C, at higher stimulus intensities, the reliability of transmission through the circuit would increase and output effects would reflect not only the monosynaptic linkages but also the less direct linkages. Accordingly, at higher stimulus intensities the size of the proximal + distal representation would substantially increase but small zones of proximal only and distal only representation should remain. The predicted output from this model is most consistent with the changes in map organization we observed for hindlimb M1. It is also possible that the model represented in Figure 11D applies to forelimb M1 maps. This is supported by recent evidence suggesting that the linkage to motoneurons from corticospinal cells on the surface of the precentral gyrus (mostly proximal muscle representation) is predominantly non-monosynaptic while the linkage from cells in the bank of the gyrus is predominantly monosynaptic (Rathelot and Strick, 2009).

Table 1. Summary of data collected

	Monkey F			Monkey C			Total		
Electrode tracks	170			142			312		
RL-ICMS sites*	83			50			133		
Sensory test	24			41			65		
	15 µA	30 µA	60 µA	15 µA	30 µA	60 µA	15 µA	30 µA	60 µA
Sites stimulated	130	163	180	152	152	164	282	315	344
StTA records (all)	2470	3097	3420	2692	2692	2908	5162	5789	6328
Layer V sites	117	150	167	142	142	150	259	292	317
StTA records (layer V)	2223	2850	3173	2524	2524	2670	4747	5374	5843
Sites yielding PStEs	23	54	101	51	89	104	74	143	205
Sites yielding PStF	19	50	93	46	83	101	65	133	194
Sites yielding PStS	4	14	51	17	38	55	21	52	106
PStEs obtained	35	146	521	136	388	790	171	534	1311
PStF effects	31	127	445	113	331	691	144	458	1136
PStS effects	4	19	76	23	57	99	27	76	175

* 500 ms train, 200 Hz, 15-60 µA. For testing sites outside the hindlimb representation

Table 2. Areas of PStF regions as percentages of total hindlimb M1

		Stimulus intensity		
		15 μA	30 μA	60 μA
Monkey F	P	30%	28%	26%
	D	64%	49%	17%
	PDC	6%	23%	57%
Monkey C	P	27%	27%	13%
	D	59%	25%	10%
	PDC	14%	48%	77%

Total area = (# surface sites) + (# deep sites/2). Areas of each region were converted into a percentage of total hindlimb area for each stimulus intensity.

Figure 1. Hindlimb push-pull task. The monkey is seated in a custom-built primate chair with both arms and the left leg restrained. The monkey gripped the push-pull device's manipulandum (horizontal post) with the right foot and pushed it to a target zone. After a hold period of 500 ms in the target zone, the monkey pulled the manipulandum to a second target zone and held for 500 ms. Upon successful completion of each push-pull trial, the monkey was given an applesauce reward. The behavioral task was guided by visual and auditory cues.

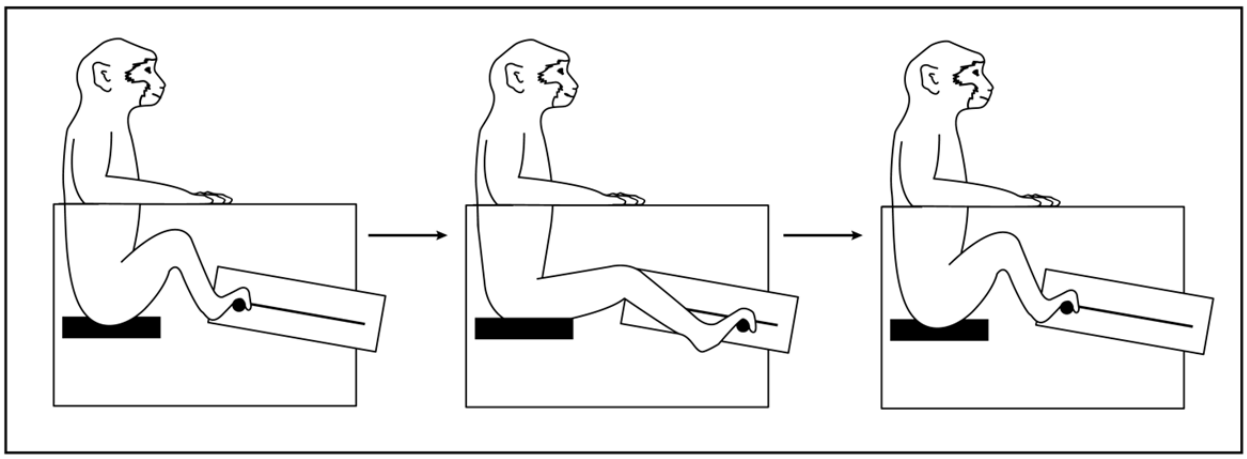

Figure 2. Types of poststimulus effects obtained with stimulus triggered averaging of EMG activity (60 μA at 15 Hz). Zero time corresponds to stimulus delivery. Numbers of trigger events (stimuli) are given in parentheses. The magnitude of each effect is measured as the peak percent increase (ppi) from baseline EMG. Only PStF effects with a ppi $\geq$ 15 and PStS effects with a ppi $\leq$ -15 were included in data analysis. EDB, extensor digitorum brevis; MG, medial gastrocnemius; LG, lateral gastrocnemius.

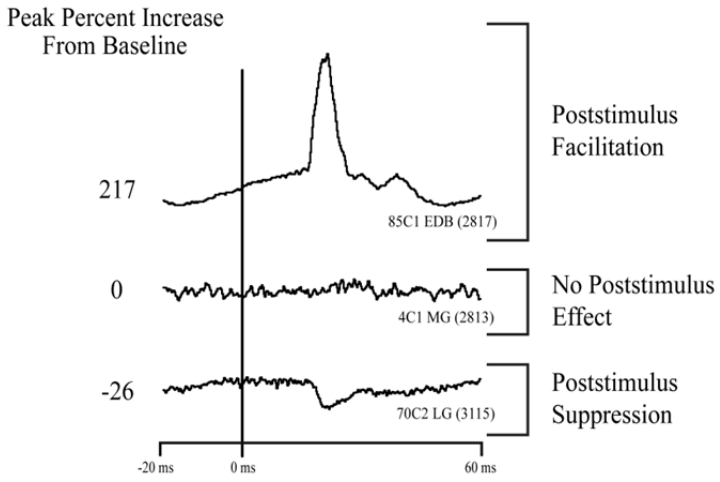
Peak Percent Increase
From Baseline
217
0
-26
85C1 EDB (2817)
4C1 MG (2813)
70C2 LG (3115)
-20 ms
0 ms
60 ms
Poststimulus
Facilitation
No Poststimulus
Effect
Poststimulus
Suppression

Figure 3. Maps of hindlimb primary motor cortex organization in two monkeys (F and C), represented in two dimensions after unfolding the medial wall and central sulcus. Maps of hindlimb muscles were based on PStF effects at 15, 30 and 60 μA. If no effects were obtained with stimulus triggered averaging at 60 μA, RL-ICMS was used to evoke movements at joints whose muscles were not implanted with EMG electrodes. RL-ICMS was performed at 15, 30 and 60 μA and for clarity evoked movements for all stimulus intensities are shown only in the 60 μA maps. Cutaneous responses of cortical neurons were used to identify boundaries with sensory areas. Cortical areas producing only proximal muscle facilitation, distal muscle facilitation or proximal-distal muscle cofacilitation are distinguished by color (red, blue, purple respectively). Black dots are sites that produced a poststimulus effect; open circles are sites that did not produce poststimulus effects in the hindlimb muscles tested but were tested with RL-ICMS. For mapping, an effect in only one muscle was considered sufficient to identify the site as distal or proximal. To be categorized as proximal-distal cofacilitation an effect had to be present in at least one distal muscle and one proximal muscle. Light blue line: midline, above the light blue line represents the bank of the medial wall of the hemisphere. Solid black curved line: central sulcus. Dotted black curved line: fundus of the central sulcus. A: anterior. P: posterior. M: medial. L: lateral.

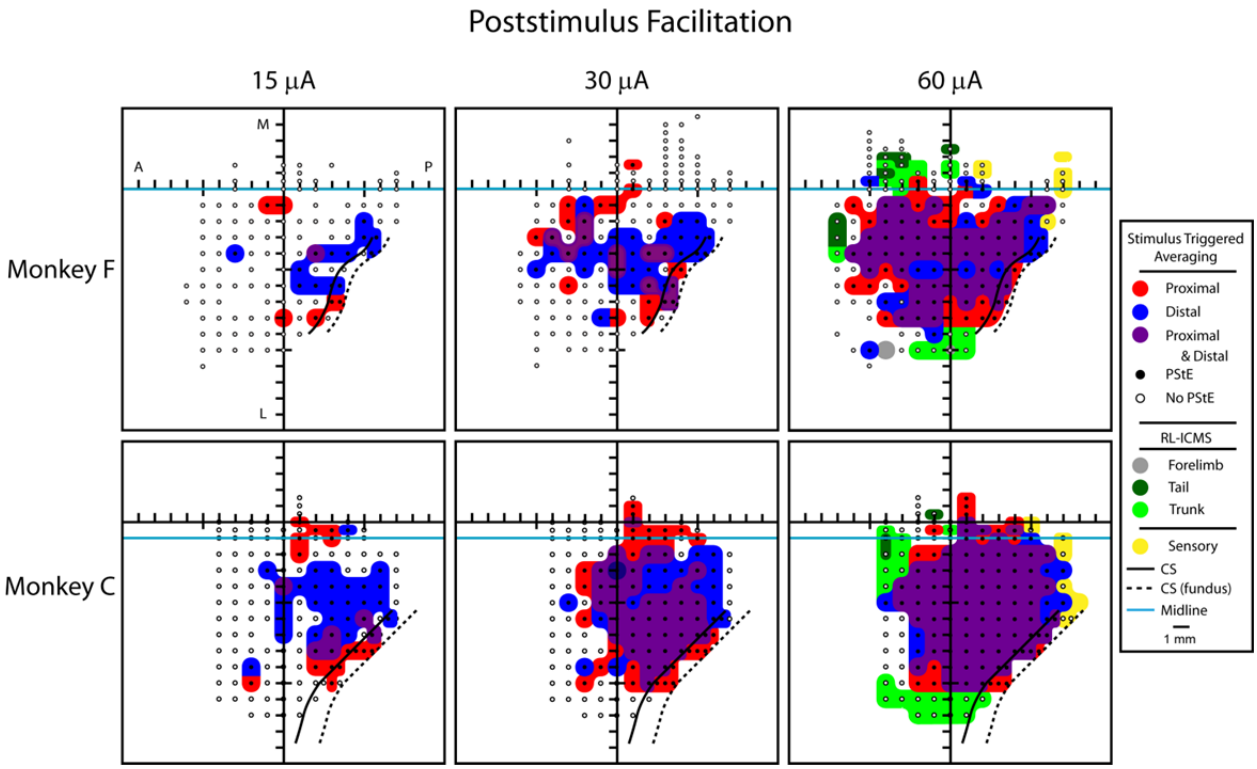
Poststimulus Facilitation
15 μA
30 μA
60 μA
Monkey F
Monkey C
M
L
A
P
Stimulus Triggered Averaging
Proximal
Distal
Proximal & Distal
PStE
No PStE
RL-ICMS
Forelimb
Tail
Trunk
Sensory
CS
CS (fundus)
Midline
1 mm

Figure 4. Maps showing the 2D representation of each of 19 hindlimb muscles in primary motor cortex after unfolding the medial wall and central sulcus. Maps are based on average magnitude (ppi) of PStF effects obtained at15 μA. Magnitude scales apply to the adjacent joint row. A) Monkey C. PERL is not included as the EMG leads to this muscle were compromised near the beginning of data collection. B) Monkey F. A map of PERL with an alternate magnitude scale is duplicated in the bottom right.

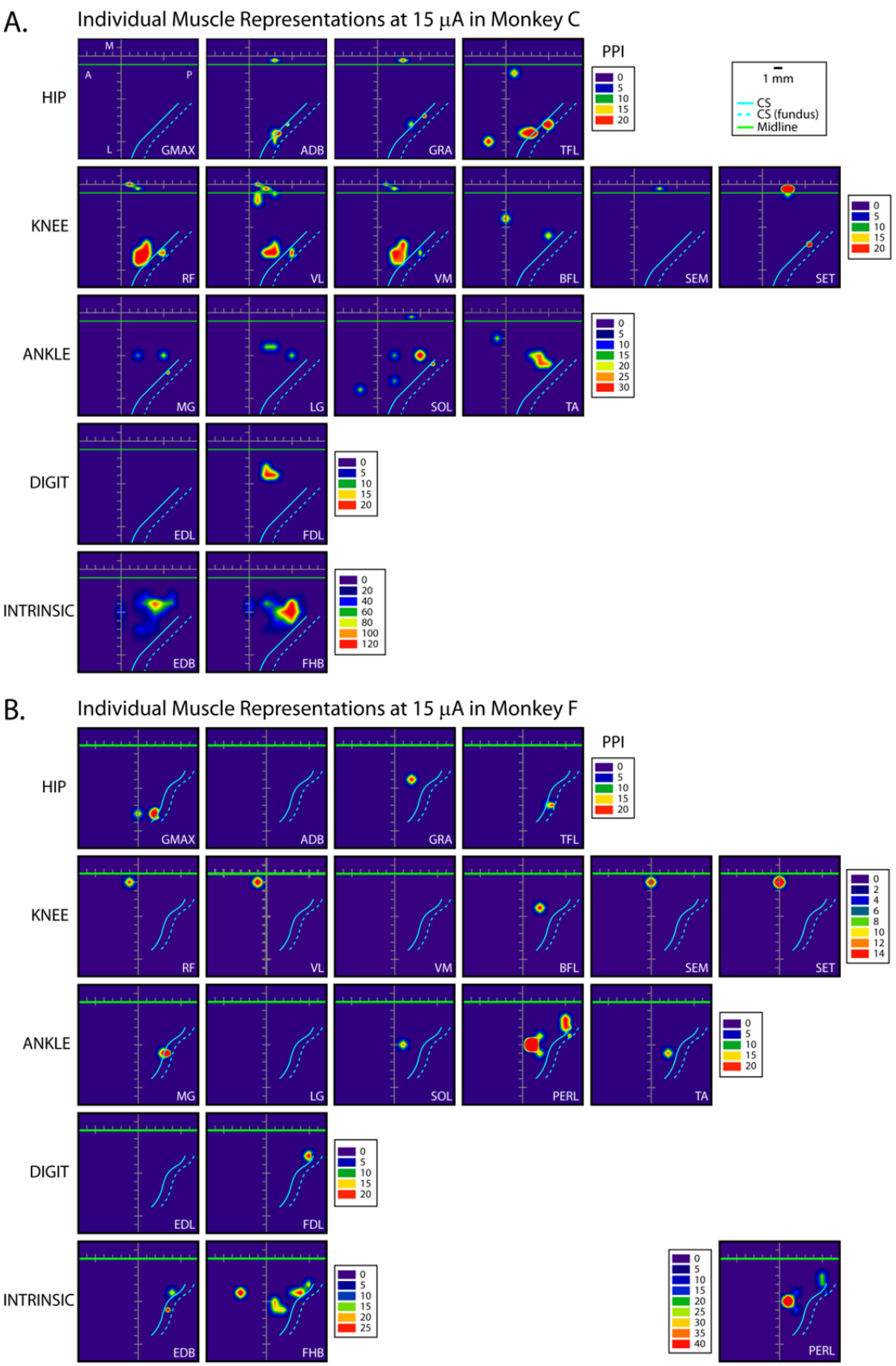
A.
Individual Muscle Representations at 15 μA in Monkey C
HIP
KNEE
ANKLE
DIGIT
INTRINSIC
M
A
P
L
GMAX
ADB
GRA
TFL
RF
VL
VM
BFL
SEM
SET
MG
LG
SOL
TA
EDL
FDL
EDB
FHB
PPI
0 5 10 15 20
1 mm
CS
CS (fundus)
Midline
0 5 10 15 20 25 30
0 20 40 60 80 100 120
B.
Individual Muscle Representations at 15 μA in Monkey F
HIP
KNEE
ANKLE
DIGIT
INTRINSIC
GMAX
ADB
GRA
TFL
RF
VL
VM
BFL
SEM
SET
MG
LG
SOL
PERL
TA
EDL
FDL
EDB
FHB
PPI
0 5 10 15 20
0 2 4 6 8 10 12 14
0 5 10 15 20 25 30 35 40

Figure 5. Same as Figure 4 only for maps obtained at 30 μA.

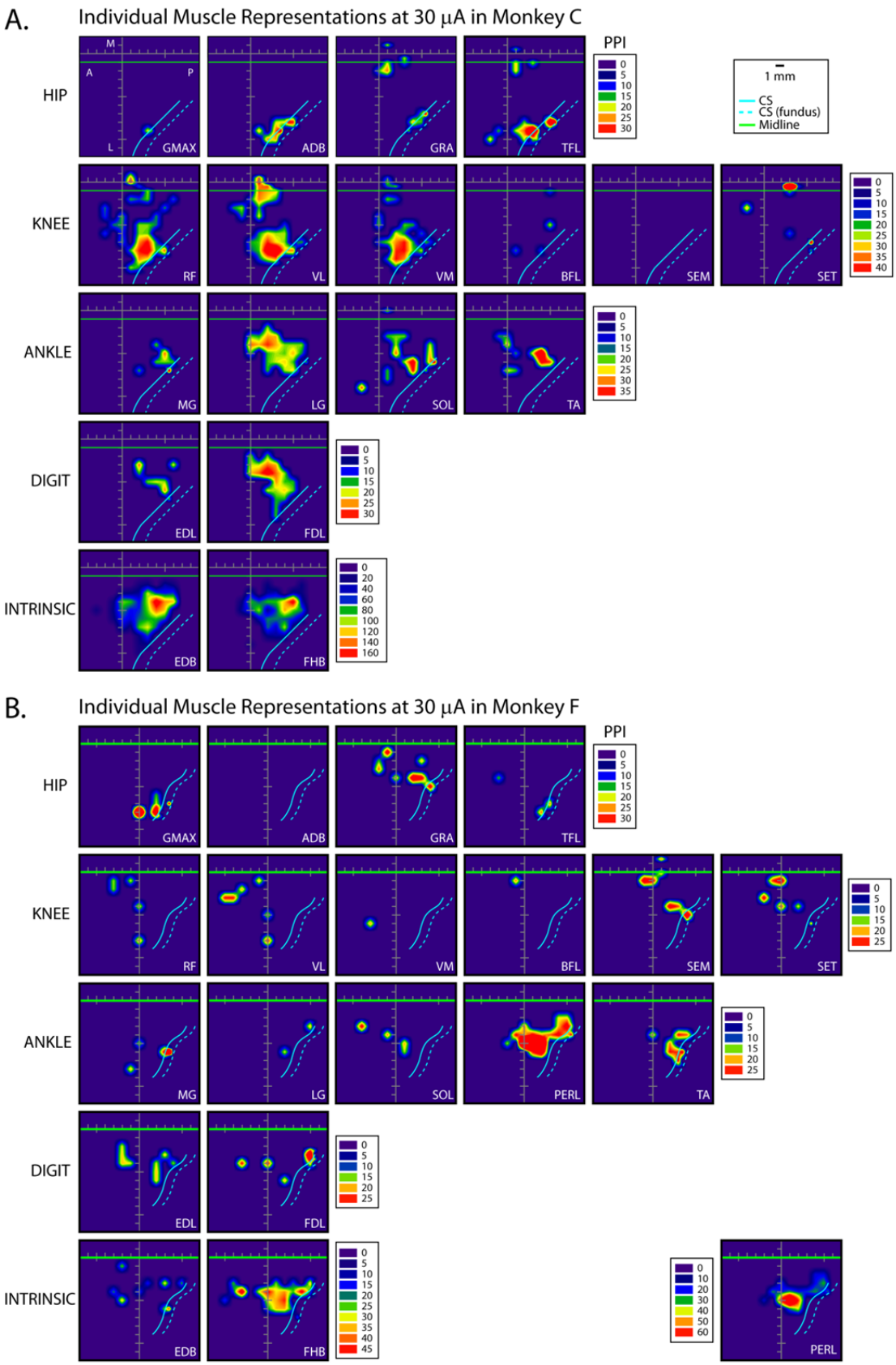
A.
Individual Muscle Representations at 30 µA in Monkey C
PPI
1 mm
CS
CS (fundus)
Midline
HIP
KNEE
ANKLE
DIGIT
INTRINSIC
M
A
P
L
GMAX
ADB
GRA
TFL
RF
VL
VM
BFL
SEM
SET
MG
LG
SOL
TA
EDL
FDL
EDB
FHB
B.
Individual Muscle Representations at 30 µA in Monkey F
PERL

Figure 6. Same as Figure 4 only for maps obtained at 60 μA. A) Monkey C. Maps of BFL, SEM and LG with alternate magnitude scales are duplicated in the bottom right. B) Monkey F. Maps of VL and PERL with alternate magnitude scales are duplicated in the bottom right.

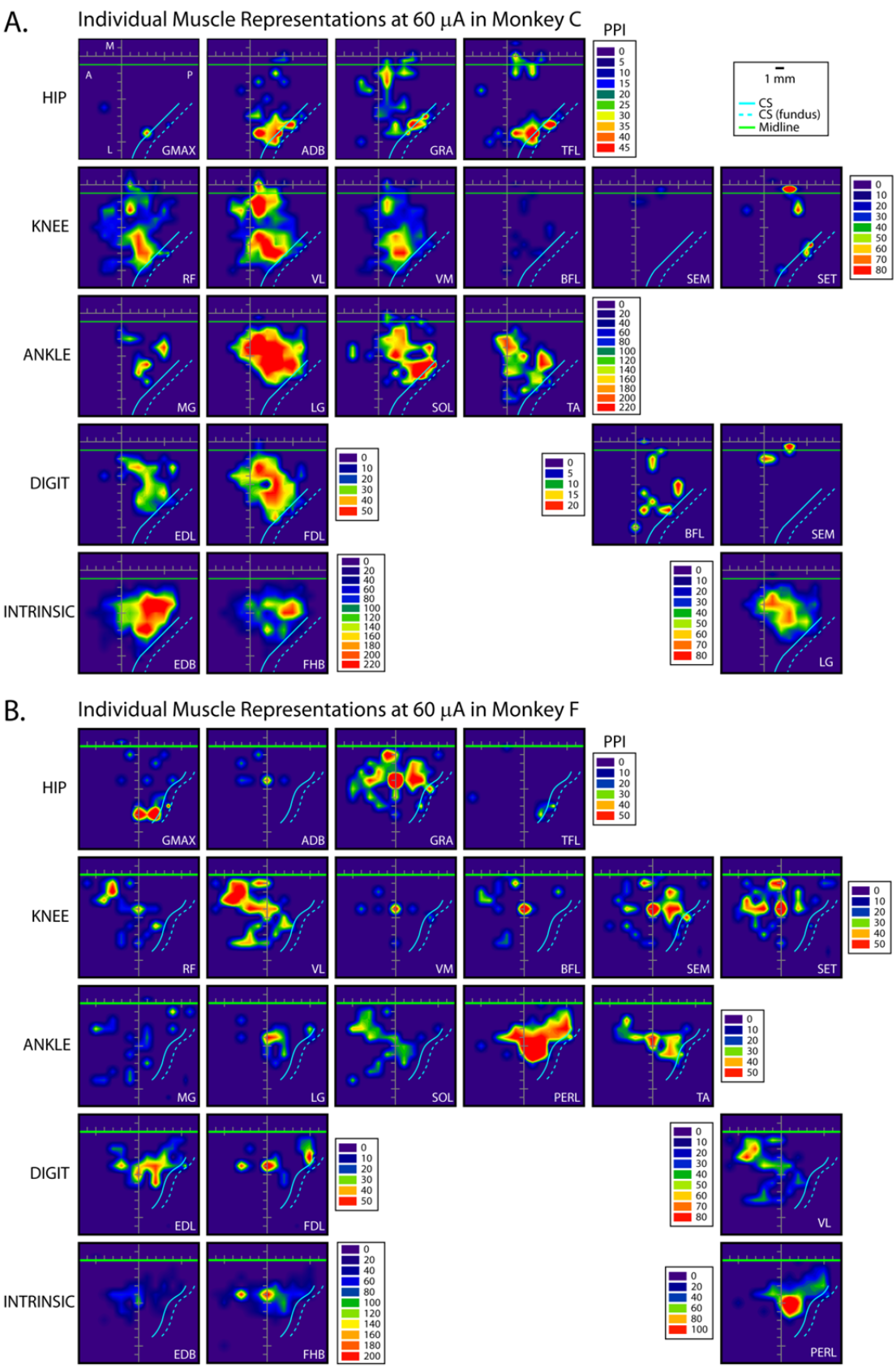
A.
Individual Muscle Representations at 60 μA in Monkey C
PPI
HIP
KNEE
ANKLE
DIGIT
INTRINSIC
M
A
P
L
GMAX
ADB
GRA
TFL
1 mm
CS
CS (fundus)
Midline
RF
VL
VM
BFL
SEM
SET
MG
LG
SOL
TA
EDL
FDL
EDB
FHB
B.
Individual Muscle Representations at 60 μA in Monkey F
PERL

Figure 7. Maps of hindlimb M1 flexor and extensor muscle representation at 15, 30 and 60 μA in monkeys F and C, represented in 2D after unfolding the medial wall and central sulcus. For mapping, an effect in only one muscle was sufficient to identify the site as extensor or flexor. To be categorized as extensor-flexor cofacilitation an effect had to be present in at least one extensor muscle and one flexor muscle.

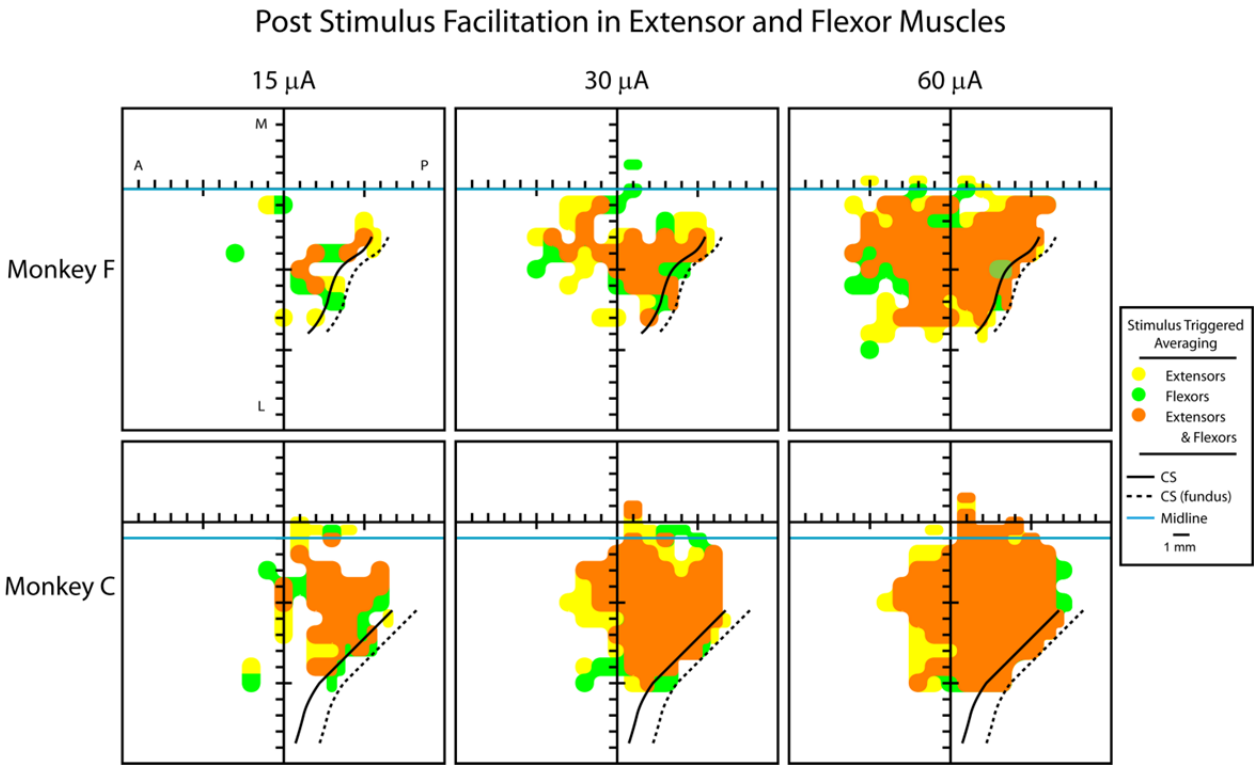
Post Stimulus Facilitation in Extensor and Flexor Muscles
15 μA
30 μA
60 μA
Monkey F
Monkey C
M
A
P
L
Stimulus Triggered Averaging
Extensors
Flexors
Extensors & Flexors
CS
CS (fundus)
Midline
1 mm

Figure 8. Maps of hindlimb M1 extensor and flexor muscle representation at 15, 30 and 60 μA in monkeys F and C color coded for the magnitude of effects. Maps are represented in 2D after unfolding the medial wall and central sulcus. Maps are based on average magnitude (ppi) of PStF effects at each joint. A common magnitude scale for the 5 joints is positioned at the left. The intrinsic muscles are mapped a second time using a different magnitude scale on the right. A: anterior. P: posterior. M: medial. L: lateral.

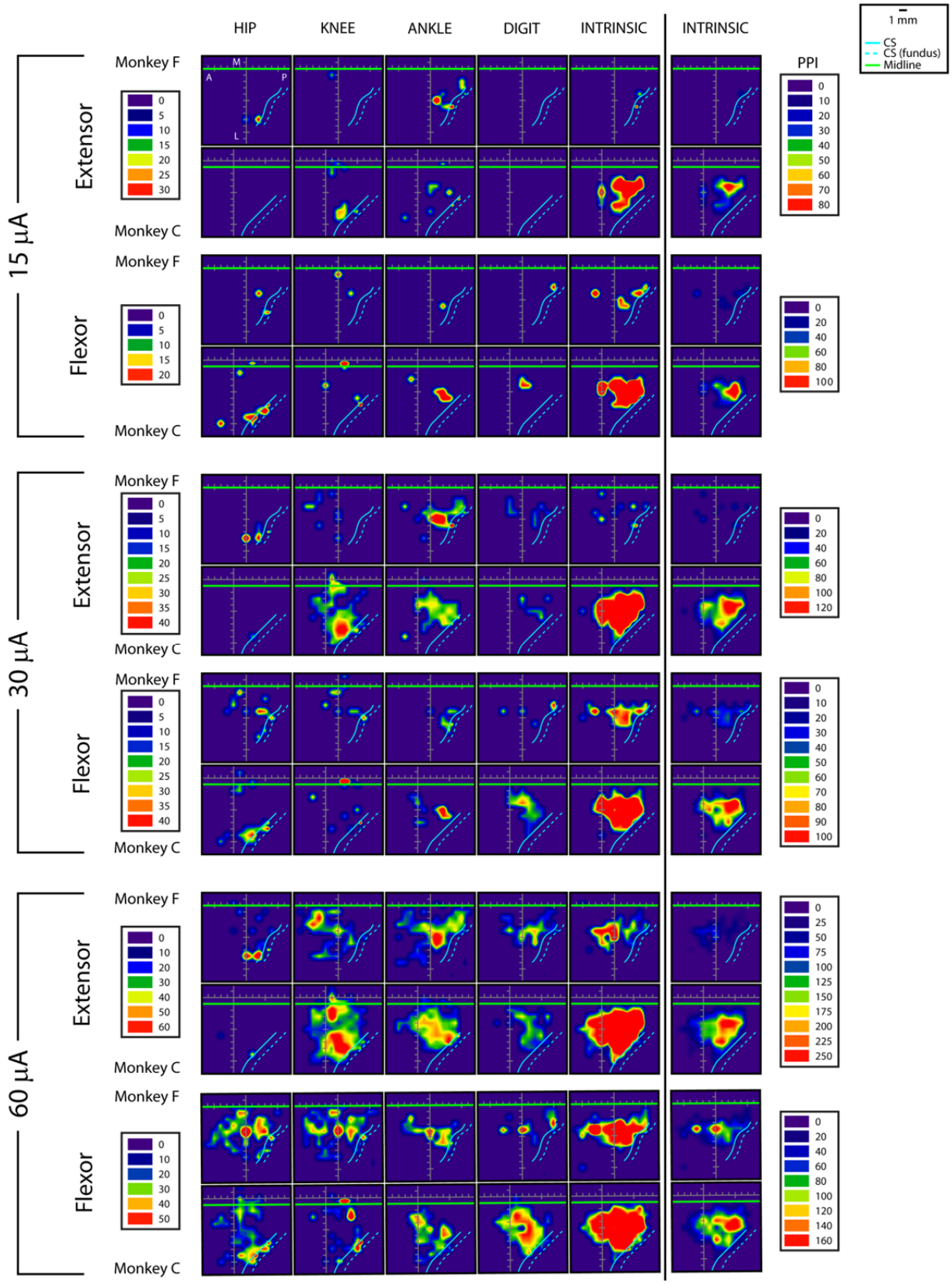
HIP
KNEE
ANKLE
DIGIT
INTRINSIC
INTRINSIC
PPI
1 mm
CS
CS (fundus)
Midline
15 µA
30 µA
60 µA
Extensor
Flexor
Monkey F
Monkey C
M
A
P
L

Figure 9. Maps of inhibitory output effects from primary motor cortex in monkeys F and C, represented in 2D after unfolding the medial wall and central sulcus. Maps are based on pure PStS effects at 15, 30 and 60 μA. Cortical areas producing only proximal muscle suppression, distal muscle suppression or proximal-distal muscle co-suppression are distinguished by color (red, blue, purple respectively). For mapping, an effect in only one muscle was sufficient to identify the site as distal or proximal. To be categorized as proximal-distal co-suppression an effect had to be present in at least one distal muscle and one proximal muscle. Light blue line: midline, above the light blue line represents the bank of the medial wall. Solid black curved line: central sulcus. Dotted black curved line: fundus of the central sulcus. A: anterior. P: posterior. M: medial. L: lateral.

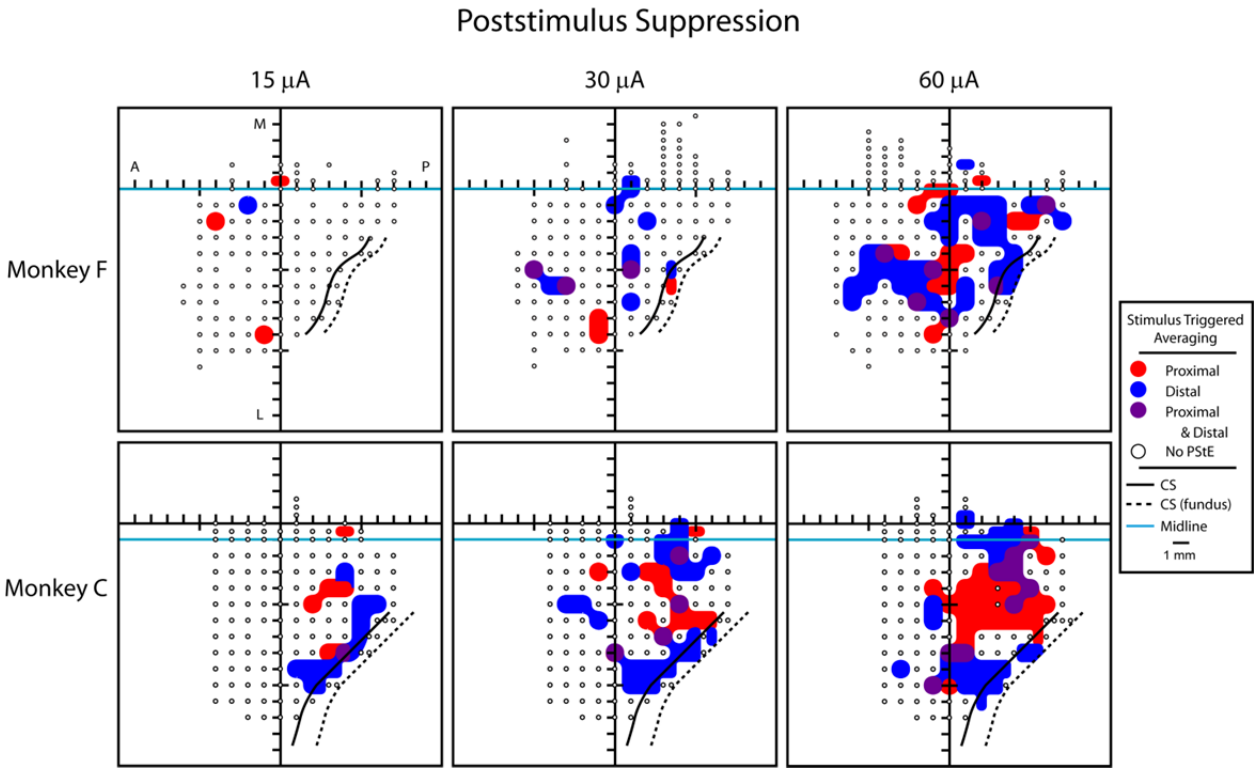
Poststimulus Suppression
15 µA
30 µA
60 µA
Monkey F
Monkey C
M
L
A
P
Stimulus Triggered Averaging
Proximal
Distal
Proximal & Distal
No PStE
CS
CS (fundus)
Midline
1 mm

Figure 10. Maps of forelimb muscle representation in primary motor cortex of two monkeys (D and M), represented in 2D after unfolding the central sulcus. 15 μA maps from Park et al. (2001). 60 μA maps are extrapolated from the 15 μA maps. Stimulation sites in each zone (proximal, distal, proximal-distal cofacilitation) were spaced at 1 mm intervals on the surface of the cortex and 0.5 mm intervals in the bank of the central sulcus. Extrapolation was based on estimating that physical spread of excitatory current from a 60 μA stimulus would have a radius of 447 μm based on a minimal *k* value of 300 μA/mm^2. This is computed from the expression:

$$r = \sqrt{i/k}$$

where *r* is the radius of the cortical volume containing the directly activated cells, *i* is the stimulus current, and *k* is the proportionality constant (Stoney et al. 1968; Ranck 1975; Cheney and Fetz 1985). The 60 μA maps were constructed by determining which muscle representations (proximal, distal or proximal-distal cofacilitation) in the 15 μA maps were contacted when a circle of 447 μm corresponding to 60 μA was applied at each stimulus site in the map.

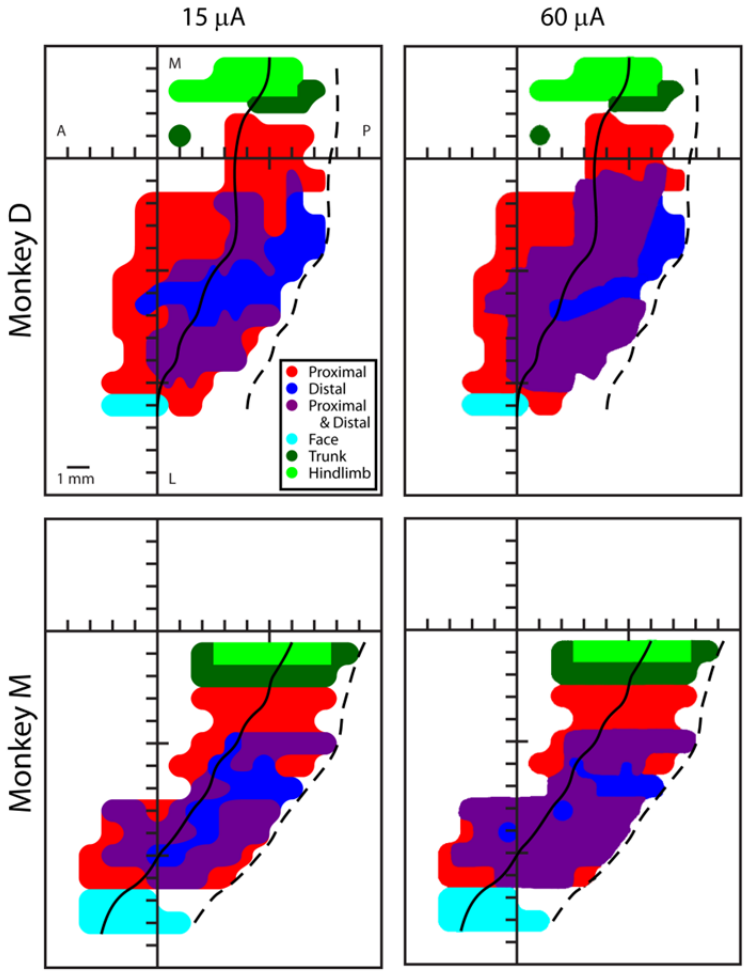
15 µA
60 µA
Monkey D
Monkey M
M
A
P
L
1 mm
Proximal
Distal
Proximal & Distal
Face
Trunk
Hindlimb

Figure 11. Possible models of corticospinal organization. Red: corticospinal neurons projecting to proximal muscle motoneurons. Yellow: corticospinal neurons projecting to proximal and distal muscle motoneurons. Blue: corticospinal neurons projecting to distal muscle motoneurons. P: motoneurons projecting to proximal muscles. D: motoneurons projecting to distal muscles. P+D: motoneurons projecting to both proximal and distal muscles.

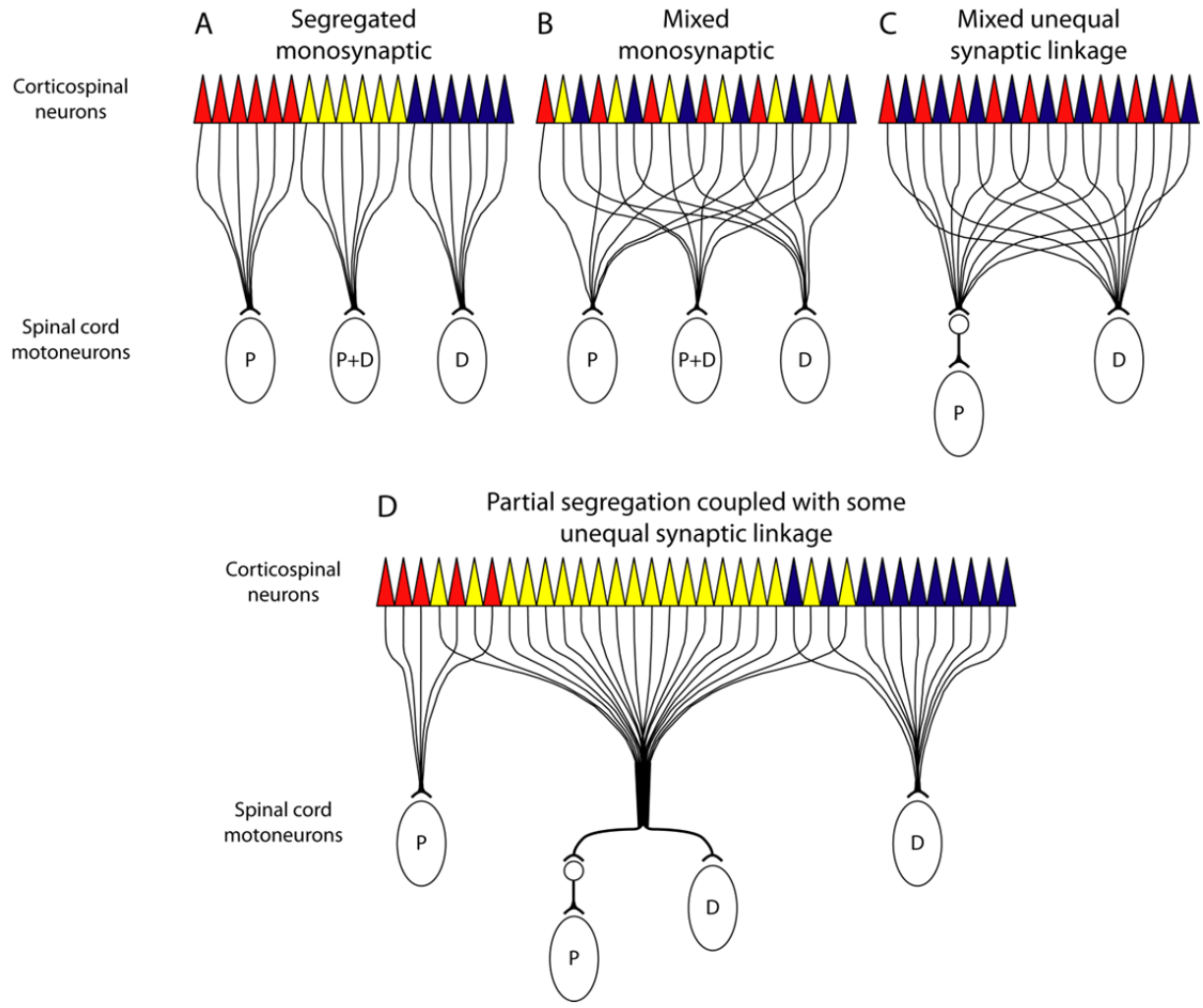
A
Segregated
monosynaptic
B
Mixed
monosynaptic
C
Mixed unequal
synaptic linkage
Corticospinal
neurons
Spinal cord
motoneurons
P
P+D
D
P
P+D
D
P
D
D
Partial segregation coupled with some
unequal synaptic linkage
Corticospinal
neurons
Spinal cord
motoneurons
P
D
D
P
D

CHAPTER 4

PROPERTIES OF PRIMARY MOTOR CORTEX OUTPUT TO HINDLIMB MUSCLES IN THE PRIMATE

INTRODUCTION

The cortical control of the hindlimb is a relatively unexplored territory when compared to the extensive studies of the forelimb, especially in the primate. The forelimb has been investigated using a variety of anatomical and electrophysiological techniques including stimulus triggered averaging (StTA), spike triggered averaging (SpTA), intracortical microstimulation (ICMS), intracellular recording and retrograde tracing (Asanuma et al., 1978; Asanuma and Rosén, 1972; Baker et al., 1998; Graziano et al., 2005; Luppino et al., 1991; McKiernan et al., 1998; Park et al., 2001, 2004; Plautz et al., 2001; Schieber and Rivlis, 2005). These studies have demonstrated important findings concerning the somatotopic organization of forelimb M1, anatomical projections to and from forelimb M1, neuron density and output properties of M1 to forelimb muscles. There are fewer studies of the cortical control of the hindlimb in the primate and less has been resolved.

Hindlimb studies in the cat have shown modulation of cortical neurons during treadmill locomotion and intense cortical activity related to trajectory modification (Drew et al., 2002; Widajewicz et al., 1994). In humans, transcranial magnetic stimulation (TMS) studies have shown facilitation and suppression effects in hindlimb motor evoked potentials (Bawa et al., 2002; Brouwer and Ashby, 1990, 1992; Thomas and Gorassini, 2005). More recent studies have investigated the use of TMS as therapy for spinal cord injury, stroke and other neurological orders affecting locomotion and gait, (Benito Penalva et al., 2010; Jayaram and Stinear, 2008; Mori et al., 2009; Perez et al., 2004).

In the primate, monosynaptic linkages have been observed between corticospinal neurons and motoneurons in both the forelimb and the hindlimb (Asanuma et al., 1979; Clough et al., 1968; Edgley et al., 1997; Jankowska et al., 1975; Lemon, 1990; Muir and Porter, 1973; Phillips and Porter, 1964; Preston et al., 1967; Preston and Whitlock, 1961; Shapovalov, 1975; Shapovalov and Kurchavyi, 1974). Single unit recordings in hindlimb M1 reported neurons related to flexion and extension (Neafsey, 1980; Sahrmann et al., 1984). Retrograde tracer and ICMS studies have confirmed the location of hindlimb M1

medial to forelimb M1 in the precentral cortex and extending into the bank of the central sulcus and the bank of the medial wall (Hatanaka et al., 2001; He et al., 1993; Luppino et al., 1991; Wise and Tanji, 1981). And recently, Ma and He (2010) monitored neuronal spikes in hindlimb M1 in relation to three contralateral and three ipsilateral hindlimb muscles in behaving monkeys. We developed a method to chronically implant EMG electrodes in large numbers of hindlimb muscles (Hudson et al., 2010). In this study, we computed stimulus triggered averages (StTA) of electromyographic (EMG) activity for 19 muscles of the hindlimb while the monkey performed a push-pull task (Hudson et al., 2010). The sign, latency and magnitude of poststimulus output effects were determined for each M1 site stimulated. The techniques are similar to a previous study in the forelimb (Park et al., 2004) allowing direct comparison of M1 output properties to hindlimb and forelimb muscles.

MATERIALS AND METHODS

Behavioral task

Data were collected from the left primary motor cortex of two male rhesus macaques (*Macaca mulatta*, ~10 kg, 6-7 years old). The stimulus triggered averaging (StTA) dataset analyzed for this paper is the same as that used in Chapter 3: Representation of Hindlimb Muscles in Primary Motor Cortex. Both monkeys were trained to perform a hindlimb push-pull task engaging both proximal and distal muscles in reliable and stereotyped patterns of activation (Hudson et al., 2010). Within a sound-attenuating chamber, the monkey was seated in a custom primate chair with both arms and the left leg restrained. With the right foot, the monkey gripped the manipulandum (horizontal post) and extended the leg until the target zone was achieved. After a hold period of 500 ms in the target zone, the monkey flexed the leg pulling the manipulandum to a second target zone. An applesauce reward was given following a second hold period of 500 ms. Visual and auditory cues guided the behavioral task.

MRI

The monkey's head was placed in an MRI-compatible stereotaxic apparatus and structural MRIs in the sagittal, coronal and horizontal planes were obtained using a Siemens Allegra 3T system. A 3-dimensional reconstruction of each monkey's brain was produced using CARET software (Computerized Anatomical Reconstruction and Editing Tool Kit).

Surgical procedures

Upon completion of training, each monkey was implanted with a titanium cortical recording chamber (30 mm inside diameter) centered at anterior 13.5 mm, lateral 0 mm and 0° angle to the midsagittal plane (Paxinos et al., 2000). Pairs of insulated, multi-stranded stainless steel wire (Cooner Wire, AS632) were implanted during an aseptic surgical procedure (Hudson et. al., 2010) to record EMG activity from 19 muscles of the hindlimb. Briefly, pairs of wires were tunneled subcutaneously to their

target muscles from either four external connector modules (ITT Canon) affixed to the upper arm with elastic medical adhesive tape (arm-mounted subcutaneous implant, monkey F) or an external circular connector (Amphenol) affixed to the skull using dental acrylic (cranial-mounted subcutaneous implant, monkey C). Each muscle was tested for proper placement of electrode pairs by stimulating through the electrodes with brief stimulus trains (biphasic pulse, 0.2 ms/phase, ~50 Hz) while observing the evoked movements. Wires were removed and reinserted if proper placement was not confirmed.

EMGs were recorded from four hip muscles: gluteus maximus (GMAX), adductor brevis (ADB), gracilis (GRA) and tensor fascia latae (TFL); six knee muscles: rectus femoris (RF), vastus lateralis (VL), vastus medialis (VM), biceps femoris (BFL), semimembranosus (SEM) and semitendonosus (SET); five ankle muscles: peroneus longus (PERL), medial gastrocnemius (MG), lateral gastrocnemius (LG), soleus (SOL) and tibialis anterior (TA); two digit muscles: extensor digitorum longus (EDL) and flexor digitorum longus (FDL); and two intrinsic foot muscles: extensor digitorum brevis (EDB) and flexor hallucis brevis (FHB). In monkey C, the EMG leads to PERL were compromised shortly after the implant. As a result, PERL was not included in the data set for monkey C.

All procedures were in accordance with the standards outlined by the *Guide for the Care and Use of Laboratory Animals* published by the National Institutes of Health and the U.S. Department of Health and Human Services. All surgeries were performed in an Association for Assessment and Accreditation of Laboratory Animal Care (AAALAC) accredited facility using full aseptic procedures. Postoperative analgesics (buprenorphine, 0.01 mg/kg) were administered for five days. Wound edges were inspected daily and treated with topical antibiotic and Betadine (10% povidone-iodine) when necessary.

Data collection

EMG activity, cortical activity and task-related signals were simultaneously monitored. Glass and mylar-insulated platinum-iridium electrodes (0.5-1.5 MΩ impedances, Frederick Haer) were used to record cortical unit activity and for stimulation. The electrode was positioned in the recording chamber

using a custom-built x-y positioner and advanced using a manual hydraulic microdrive (Frederick Haer). Electrode penetrations were systematically made at 1 mm intervals in the precentral cortex of the left hemisphere. Data were collected from layer V sites in the cortex, as determined by depth from first cortical activity and nature and size of neuronal spikes. Data were collected from layer V sites in the banks of the medial wall and central sulcus at 0.5 mm intervals over the extent of the electrode track.

At each layer V site, StTAs (15, 30 and 60 μA at 15 Hz) of EMG activity were computed for 19 muscles of the hindlimb as the monkey performed the hindlimb push-pull task. Individual stimuli were symmetrical biphasic pulses, 0.2 ms negative pulse followed by a 0.2 ms positive pulse, applied throughout all phases of the task. EMGs were filtered generally at 30 Hz to 1 kHz, digitized at 4 kHz and full-wave rectified. StTAs consisted of at least 500 trigger events and were compiled over an 80 ms epoch, 20 ms pre-trigger and 60 ms post-trigger. Segments of EMG activity associated with each stimulus were evaluated and accepted for averaging only when the average of all EMG data points over the entire 80 ms epoch was ≥ 5% of full-scale input (McKiernan et al., 1998) to prevent averaging periods where EMG activity was minimal or non-existent.

EMG-triggered averages were computed to evaluate cross-talk between muscles (Cheney and Fetz, 1980). Averages of EMG activity were compiled for each muscle using one muscle's EMG activity as a trigger and repeated using all 19 muscles as triggers. If the ratio between the test and trigger muscles exceeded the ratio of their cross-talk peaks by a factor of 2 or more, a muscle was considered to have an unacceptable level of cross-talk (Buys et al., 1986). No muscle in this study showed significant cross-talk.

Data analysis

Poststimulus facilitation (PStF) and suppression (PStS) effects were computer measured as described by Mewes and Cheney (1991). Each average was compiled over an 80 ms epoch, 20 ms pre-trigger and 60 ms post-trigger. A poststimulus effect (PStE) was defined as a peak or trough of EMG

activity that rose or fell from baseline EMG activity and maintained a level of activity exceeding two standard deviations of baseline for a period equal to or greater than 0.75 ms. Baseline EMG activity was measured as the 12 ms period preceding the onset of the effect, initially determined by visual inspection. Baseline statistics were then used to determine the onset of the effect as the point where the envelope of the record exceeded two standard deviations of baseline. The magnitude of PStEs was expressed as the peak percentage increase (+ppi) or peak percentage decrease (-ppi) in EMG activity above (PStF) or below (PStS) baseline. Only PStF effects with a ppi $\geq$ 15 and PStS effects with a ppi $\leq$ -15 were included in data analysis (Figure 1) to ensure PStEs were significant.

Unfolding the cortex

A 2-dimensional representation of layer V of the cortex in the medial wall of the hemisphere, the anterior bank of the central sulcus and the surface cortex required flattening and unfolding the curvature of the cortex. This process has been described in detail by Park et al. (2001). Briefly, the cortex was unfolded and 2-dimensional maps were generated based on known architectural landmarks, MRI images, observations during the cortical chamber implant surgery, electrode track x-y coordinates, electrode penetration depth and properties of recorded neurons.

RESULTS

Dataset

Table 1 summarizes the data collected from the left M1 in two male rhesus macaques. 312 electrode tracks were made (monkey F, 170; monkey C, 142). Stimulus triggered averages (15, 30 and 60 μA, 15 Hz) of rectified EMG activity were collected from 19 hindlimb muscles of the hip, knee, ankle, digit and intrinsic foot. Only data from layer V sites were analyzed. RL-ICMS (15-60 μA, 200 Hz, 500 ms) was performed at 133 sites to identify output effects (movements or EMG responses) when no poststimulus effects were obtained. The presence or absence of sensory responses was tested at 65 sites primarily to aid in identifying the border of somatosensory cortex. Figure 2 shows the location of electrode penetrations in the hindlimb representation of both monkey cortices.

Data were collected at three stimulus intensities: 15, 30 and 60 μA. Not all sites with PStEs at 30 and 60 μA had PStEs at 15 μA (Figure 3). Only the data from sites with PStEs at all three stimulus intensities were used to analyze the relationship between stimulus intensity and the latency and magnitude of effects. Data from all sites were used to analyze the distribution of effects. Table 2 summarizes the mean onset latencies and magnitudes of PStEs for muscles at different joints (A, sites with PStEs present at all stimulus intensities; B, all data).

Components of PStEs

Figure 1 shows examples of PStEs obtained in hindlimb muscles using a 15 Hz stimulation rate and an 80 ms analysis period. Similar data for forelimb muscles was presented by Park et al. (2001). Both hindlimb and forelimb have primary short latency, short duration facilitation and suppression effects. However, a striking difference between averages from hindlimb and forelimb muscles at 15 Hz is the presence of a large oscillation in the baseline EMG level in averages of hindlimb muscles. The oscillation is not dependent on the presence of a primary PStF effect as it was commonly found in the

absence of any primary effect (Figure 1, Baseline Oscillation). Using a slower stimulation rate of 5 Hz and a longer analysis period of 250 ms, we found most StTAs from hindlimb M1 contain a long latency, broad suppression that is not prominent in StTAs from forelimb M1. Figure 4 shows StTAs at 5 Hz for 13 muscles that had effects from one site in hindlimb M1 cortex. Several muscles show a short latency, short duration facilitation peak. This primary facilitation peak is comparable to the PStF observed from forelimb M1, although weaker. All muscles, however, show a considerably longer latency, broad suppression effect. The onset of the suppression is 20-23 ms later than the onset of the PStF and the duration can be nearly 50 ms. In comparison, primary PStS effects in hindlimb M1 have an onset latency that is only about 2-7 ms longer than the onset latency of PStF in the same muscles (Table 2). The broad suppression is usually followed by a broad and weaker facilitation. At 15 Hz, the interstimulus interval interacts with these longer latency effects which become reinforced and appear as an oscillation of the baseline of the stimulus triggered average.

Latency and magnitude

At 15 μA, the mean PStF onset latency was 15.5 ± 2.4 ms compared with a mean PStS onset latency of 17.0 ± 1.5 ms. As stimulus intensity increased from 30 to 60 μA, there was no significant change in the mean PStF onset latency. Overall, mean PStF onset latency increased from the more proximal joints to the more distal joints. There were no significant differences between the PStF onset latencies of the distal joints (ankle, digit and intrinsic foot) at any stimulus intensity. At 15 μA, all other comparisons of PStF onset latencies between joints were significant ($p < 0.05$, 1-way ANOVA). At 30 and 60 μA, the remaining comparisons between joints were significant except for knee versus hip and knee versus digit ($p < 0.05$, 1-way ANOVA). The dataset for mean onset latency of PStS effects was too small for meaningful statistical comparisons (Table 2A)

Figure 5 shows the distribution of PStF onset latencies for muscles acting at different joints of the hindlimb at 15, 30 and 60 μA. The distributions at each joint are all unimodal, although the hip does have

the suggestion of bimodality at 60 μA. The intrinsic muscles have the narrowest distribution at all stimulus intensities. The bimodal appearance of the distributions for all muscles, at each stimulus intensity, can be attributed to different conduction latencies at different joints.

At 15 μA, the mean PStF magnitude, expressed in peak percent increase (ppi) above baseline, was 30.4 ± 23.3 compared with -18.5 ± 2.8 for PStS. The mean PStF magnitude increased significantly as the stimulus intensity increased ($p<0.001$, 1-way ANOVA). Overall, the magnitude of PStF was strongest in intrinsic muscles than muscles at other joints and the differences were statistically significant in all cases except intrinsic versus ankle and intrinsic versus digit at 15 μA ($p<0.01$, 1-way ANOVA) and intrinsic versus digit at 30 μA ($p<0.001$, 1-way ANOVA). At 60 μA, the magnitude of PStF was strongest in intrinsic muscles compared to all other joints ($p<0.05$) (Table 2A).

Figure 6 shows the distribution of PStF magnitude for muscles acting at different joints of the hindlimb at 15, 30 and 60 μA. Similar trends are seen at all stimulus intensities. At all joints, the weakest effects are the most common, as evidenced by the skewed distributions. All joints, except the intrinsic joint, have a narrow range of magnitudes focused heavily toward weak effects. The maximum PStF magnitude at each stimulus intensity was from the intrinsic muscles (149.1, FHB, 15 μA; 187.6, EDB, 30 μA; 352.8, EDB, 60 μA).

Figure 7 shows there is a consistent trend among muscles at all joints for shorter PStF onset latencies to be associated with stronger magnitudes. This association was statistically significant at the hip, ankle and digit joints at 60 μA ($p < 0.05$, 1-way ANOVA).

Distribution of PStEs

Figure 8, A and B, show the distributions of PStF and PStS effects in hip, knee, ankle, digit and intrinsic foot muscles at 15, 30 and 60 μA. Of 144 PStF effects at 15 μA, 60% were in distal muscles including 19% in ankle, 3% in digit and 38% in intrinsic foot muscles. Forty percent of PStF effects were

in proximal muscles including 14% in hip and 26% in knee muscles. Inhibitory effects showed a similar trend. Of 27 PStS effects at 15 μA, 67% were in distal muscles including 48% in ankle, 0% in digit and 19% in intrinsic foot muscles. Thirty-three percent of PStS effects were in proximal muscles including 11% in hip and 22% in knee muscles. A similar trend was seen at 30 and 60 μA.

The difference in number of muscles recorded at each joint (4 hip, 6 knee, 5 ankle, 2 digit and 2 intrinsic foot muscles) may have skewed the distribution of effects. Figure 8, C and D, show the distributions of PStF and PStS effects at each joint after normalizing for the number of muscles sampled. After normalizing, it becomes clear that PStF effects are most common in intrinsic muscles at all stimulus intensities. There were fewer suppression effects in the knee muscles than other joints, especially at 30 and 60 μA.

Overall, PStF was more common in extensor muscles than flexor muscles at all stimulus intensities (Figure 9). Certain trends were clear at all stimulus intensities. At the knee joint, facilitation of the extensors dominated while at the hip joint, the flexors were more commonly facilitated. The most prominent number of effects was in the intrinsic muscles, with flexors and extensors equally facilitated. The smaller number of PStS effects limited interpretation of suppression effects in flexors and extensors. At 15 μA, 53% of all PStF effects were in extensor muscles (GMAX, RF, VL, VM, PERL, LG, MG, SOL, EDL or EDB) and 47% were in flexor muscles (GRA, ADB, TFL, BFL, SEM, SET, TA, FDL or FHB). At 30 and 60 μA, PStF was still predominantly in extensor muscles (58% extensors, 42% flexors).

Figure 10 shows the distribution of PStF and PStS effects observed in each of the 19 hindlimb muscles sampled at 15, 30 and 60 μA. Overall, there were more PStF effects than PStS effects at each stimulus intensity and at all joints. The differentiation of the hip and knee flexors and extensors supports what was evident in Figure 9 with extensor effects dominating at the knee and flexor effects dominating at the hip. PStS was more common in SOL than any other muscle at 15 and 30 μA. At 60 μA, the number of PStS effects in TFL is similar to SOL.

DISCUSSION

This study analyzes the cortical output from M1 to 19 muscles of the hindlimb in terms of the latency, magnitude and distribution of poststimulus facilitation and suppression effects. A similar study of the forelimb was based on stimulus triggered averaging at 15 μA stimulus (Park et al., 2004). It was evident in early data collection for the present study that there were far fewer PStEs in hindlimb at 15 μA than the forelimb. Consequently, StTAs were performed using three stimulus intensities (15, 30 and 60 μA). Several significant results were found. First, PStF was far more common than PStS at all joints. Second, as might be predicted, we found the onset latency of PStF increased from proximal to distal joints. Third, PStF magnitude increased significantly with stimulus intensity. Overall, the intrinsic muscles had the strongest PStF magnitudes. Fourth, PStF effects are the most common in intrinsic muscles and more common in extensors than flexors.

Comparison to hindlimb and forelimb M1 properties

Table 3 compares the key components of hindlimb and forelimb M1 output based on StTA data at 15 μA. The most striking difference between hindlimb and forelimb M1 is the number of PStEs. While forelimb M1 has 1398 PStF and 679 PStS effects, hindlimb M1 has only 144 PStF and 27 PStS effects. Even at 60 μA, there are only 1136 PStF and 175 PStS effects. The magnitudes of PStF effects are also strikingly different. At 15 μA in the hindlimb, the strongest PStF effects are in the intrinsic muscles. The same is true of forelimb, but the effects in the intrinsic hand muscles are twice as strong as the PStF effects in the intrinsic foot muscles. While the PStF effects in the other joints of the hindlimb are similar in magnitude, the PStF effects in forelimb clearly increase in strength from proximal to distal joints. The mean onset latency of PStF in the hindlimb was 6.3 ms longer than the forelimb. This reflects the increased conduction distance of the hindlimb corticospinal neurons. However, we cannot rule out a difference in synaptic linkage compared to the forelimb as another contributing factor to the longer latency. As was discussed in Chapter 3, the organization of hindlimb M1 supports a model involving

both monosynaptic and polysynaptic linkages to both proximal and distal motoneurons. There are also interesting differences between hindlimb and forelimb M1 in the distribution of effects. Overall, most PStF effects are in the distal muscles of both hindlimb and forelimb. However, nearly all the distal PStF effects are in the intrinsic foot muscles of the hindlimb compared to the similar distribution of forelimb distal PStF effects to digit and intrinsic hand muscles.

Implications for the differential control of intrinsic foot muscles

PStF is most common and strongest in the intrinsic foot muscles at all stimulus intensities. Interestingly, there are no significant differences in magnitude of PStF between muscles of the other joints at each stimulus intensity. However, at each stimulus intensity, there were no significant differences between the PStF onset latencies of intrinsic muscles compared to the other distal joints. This suggests that there may be a differential control of the intrinsic foot muscles that may lie in the strength of the synapses rather than the number of synapses in the linkage.

Table 1. Summary of data collected

	Monkey F			Monkey C			Total		
Electrode tracks	170			142			312		
RL-ICMS sites*	83			50			133		
Sensory test	24			41			65		
	15 μA	30 μA	60 μA	15 μA	30 μA	60 μA	15 μA	30 μA	60 μA
Sites stimulated	130	163	180	152	152	164	282	315	344
StTA records (all)	2470	3097	3420	2692	2692	2908	5162	5789	6328
Layer V sites	117	150	167	142	142	150	259	292	317
StTA records (layer V)	2223	2850	3173	2524	2524	2670	4747	5374	5843
Sites yielding PStEs	23	54	101	51	89	104	74	143	205
Sites yielding PStF	19	50	93	46	83	101	65	133	194
Sites yielding PStS	4	14	51	17	38	55	21	52	106
PStEs obtained	35	146	521	136	388	790	171	534	1311
PStF effects	31	127	445	113	331	691	144	458	1136
PStS effects	4	19	76	23	57	99	27	76	175

* 500 ms train, 200 Hz, 15-60 μA. For testing sites outside the hindlimb representation
Table is reproduced from Chapter 3: Representation of hindlimb muscles in primary motor cortex.

Table 2. Latency and magnitude of PStEs

A. Effects present at 15, 30 and 60 μA

PStF

	Onset Latency, ms						Magnitude, %					
	15 μA		30 μA		60 μA		15 μA		30 μA		60 μA	
Joint	*n*	Mean	*n*	Mean	*n*	Mean	*n*	Mean	*n*	Mean	*n*	Mean
Hip	19	12.5 ± 1.8	19	12.5 ± 1.8	19	12.6 ± 2.3	19	23.2 ± 7.4	19	35.8 ± 14.7	19	56.7 ± 24.3
Knee	33	13.8 ± 1.4	33	13.4 ± 1.5	33	13.4 ± 1.6	33	22.9 ± 12.0	33	38.7 ± 22.8	33	62.5 ± 37.7
Ankle	19	16.9 ± 2.6	19	16.7 ± 2.5	19	16.4 ± 2.9	19	25.3 ± 16.5	19	34.5 ± 22.8	19	57.7 ± 44.0
Digit	4	16.0 ± 1.0	4	15.4 ± 1.0	4	15.5 ± 0.8	4	20.7 ± 4.2	4	34.2 ± 10.2	4	48.5 ± 12.0
Intrinsic	53	17.2 ± 0.8	53	17.2 ± 1.0	53	16.9 ± 0.7	53	40.3 ± 30.8	53	72.5 ± 37.7	53	135.9 ± 71.2
Total	128	15.5 ± 2.4	128	15.4 ± 2.5	128	15.3 ± 2.4	128	30.4 ± 23.3	128	51.5 ± 33.6	128	90.9 ± 65.2

PStS

	Onset Latency, ms						Magnitude, %					
	15 μA		30 μA		60 μA		15 μA		30 μA		60 μA	
Joint	*n*	Mean	*n*	Mean	*n*	Mean	*n*	Mean	*n*	Mean	*n*	Mean
Hip	1	15.0	1	15.0	1	15.0	1	-23.8	1	-22.1	1	-21.0
Knee	0	---	0	---	0	---	0	---	0	---	0	---
Ankle	6	17.3 ± 1.3	6	17.5 ± 1.3	6	17.5 ± 1.1	6	-17.6 ± 1.7	6	-24.3 ± 7.7	6	-32.3 ± 9.4
Digit	0	---	0	---	0	---	0	---	0	---	0	---
Intrinsic	0	---	0	---	0	---	0	---	0	---	0	---
Total	7	17.0 ± 1.5	7	17.2 ± 1.5	7	17.2 ± 1.4	7	-18.5 ± 2.8	7	-24.0 ± 7.1	7	-30.6 ± 9.6

B. All effects

PStF

	Onset Latency, ms						Magnitude, %					
	15 μA		30 μA		60 μA		15 μA		30 μA		60 μA	
Joint	*n*	Mean	*n*	Mean	*n*	Mean	*n*	Mean	*n*	Mean	*n*	Mean
Hip	21	12.7 ± 1.9	58	13.2 ± 2.6	173	13.3 ± 2.0	21	23.0 ± 7.1	58	26.4 ± 11.9	173	30.7 ± 20.3
Knee	37	14.0 ± 1.7	144	13.9 ± 1.5	384	14.0 ± 1.8	37	22.2 ± 11.5	144	25.9 ± 13.9	384	34.9 ± 21.8
Ankle	28	17.6 ± 3.1	99	16.1 ± 2.3	255	16.0 ± 2.6	28	25.7 ± 14.8	99	26.2 ± 14.0	255	32.8 ± 20.1
Digit	4	16.0 ± 1.0	44	15.4 ± 1.3	120	15.2 ± 1.5	4	20.7 ± 4.2	44	20.7 ± 6.2	120	29.3 ± 11.8
Intrinsic	54	17.2 ± 0.8	113	17.3 ± 1.5	204	17.1 ± 1.2	54	40.0 ± 30.6	113	50.6 ± 35.3	204	70.0 ± 60.7
Total	144	15.8 ± 2.6	458	15.3 ± 2.4	1136	15.0 ± 2.3	144	29.6 ± 22.3	458	31.6 ± 23.5	1136	39.6 ± 34.5

PStS

	Onset Latency, ms						Magnitude, %					
	15 μA		30 μA		60 μA		15 μA		30 μA		60 μA	
Joint	*n*	Mean	*n*	Mean	*n*	Mean	*n*	Mean	*n*	Mean	*n*	Mean
Hip	3	20.0 ± 4.4	11	17.4 ± 2.5	50	16.1 ± 3.2	3	-19.1 ± 4.1	11	-18.0 ± 3.1	50	-20.4 ± 4.4
Knee	6	16.8 ± 1.6	10	17.4 ± 4.0	15	16.7 ± 2.5	6	-19.7 ± 10.1	10	-19.4 ± 4.6	15	-25.3 ± 7.7
Ankle	13	20.1 ± 3.7	30	18.8 ± 2.8	59	19.9 ± 2.9	13	-18.9 ± 3.5	30	-21.3 ± 6.3	59	-22.6 ± 6.3
Digit	0	---	4	18.1 ± 1.1	19	17.5 ± 1.0	0	---	4	-20.2 ± 2.8	19	-19.3 ± 3.0
Intrinsic	5	21.4 ± 1.2	21	20.9 ± 2.1	32	21.2 ± 2.5	5	-17.4 ± 1.6	21	-19.7 ± 4.7	32	-20.3 ± 4.9
Total	27	19.6 ± 3.4	76	19.0 ± 3.0	175	18.5 ± 3.4	27	-18.8 ± 5.2	76	-20.1 ± 5.2	175	-21.4 ± 5.6

Values are mean ± SD. %, peak percent increase above baseline. PStE, poststimulus effect. PStF, poststimulus facilitation. PStS, poststimulus suppression.

Table 3. Comparison of M1 hindlimb and forelimb StTA (15 μA) data.

	Hindlimb	Forelimb †
Magnitude of PStF		
Hip/Shoulder	23.0 ± 7.1 (21)	24.1 ± 10.5 (159)
Knee/Elbow	22.2 ± 11.5 (37)	34.6 ± 22.5 (405)
Ankle/Wrist	25.7 ± 14.8 (28)	70.4 ± 79.6 (349)
Digit	20.7 ± 4.2 (4)	77.0 ± 96.4 (350)
Intrinsic Foot/Hand	40.0 ± 30.6 (54)	82.1 ± 69.8 (135)
Onset Latency of PStF		
Hip/Shoulder	12.7 ± 1.9 (21)	9.5 ± 2.3 (159)
Knee/Elbow	14.0 ± 1.7 (37)	9.6 ± 1.8 (405)
Ankle/Wrist	17.6 ± 3.1 (28)	8.8 ± 1.4 (349)
Digit	16.0 ± 1.0 (4)	8.9 ± 1.3 (350)
Intrinsic Foot/Hand	17.2 ± 0.8 (54)	10.1 ± 0.9 (135)
Distribution of PStF by joint*, %		
Hip/Shoulder	11 (21)	11 (159)
Knee/Elbow	13 (37)	19 (405)
Ankle/Wrist	13 (28)	24 (349)
Digit	4 (4)	24 (350)
Intrinsic Foot/Hand	58 (54)	23 (135)
Distribution of PStS by joint*, %		
Hip/Shoulder	11 (3)	15 (109)
Knee/Elbow	14 (6)	20 (199)
Ankle/Wrist	40 (13)	24 (166)
Digit	0 (0)	21 (147)
Intrinsic Foot/Hand	35 (5)	20 (58)

Parentheses give number of observations. Magnitude expressed as mean ± SD.
*, data normalized by number of recorded muscles. †, data adapted from Park et al., 2004.

Figure 1. Types of effects observed in stimulus triggered averages of hindlimb muscle EMG activity. Facilitation and suppression peaks are outlined in the red box. Column on left: magnitude of the primary poststimulus facilitation (PStF) or poststimulus suppression (PStS) measured as peak percent increase above baseline EMG value just before the onset of the effect. Stimulation at 60 μA and 15 Hz repetition rate.

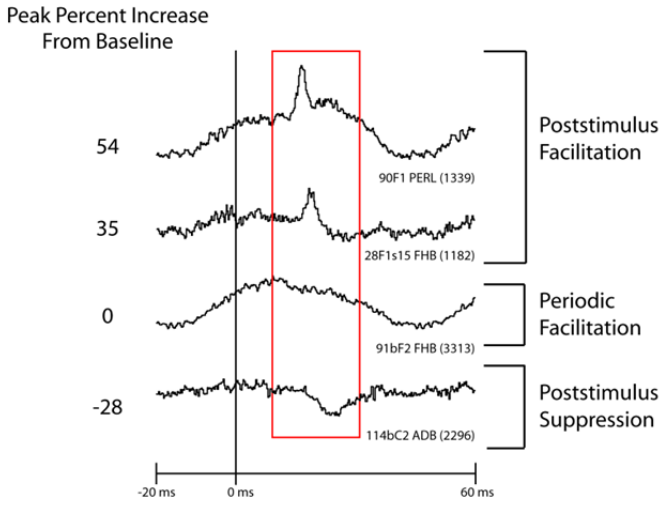
Peak Percent Increase
From Baseline
54
35
0
-28
90F1 PERL (1339)
28F1s15 FHB (1182)
91bF2 FHB (3313)
114bC2 ADB (2296)
-20 ms
0 ms
60 ms
Poststimulus
Facilitation
Periodic
Facilitation
Poststimulus
Suppression

Figure 2. Maps of hindlimb primary motor cortex organization in two monkeys (F and C), represented in two dimensions after unfolding the medial wall and central sulcus. Maps of hindlimb muscles were based on PStF effects at 15, 30 and 60 μA. If no effects were obtained with stimulus triggered averaging at 60 μA, RL-ICMS was used to evoke movements at joints whose muscles were not implanted with EMG electrodes. RL-ICMS was performed at 15, 30 and 60 μA and for clarity evoked movements for all stimulus intensities are represented in the 60 μA column. Cutaneous responses of cortical neurons were used to identify boundaries with sensory areas. Cortical areas producing hindlimb muscle facilitation are represented in blue. Black dots are sites that produced a poststimulus effect; open circles are sites that did not produce poststimulus effects in the hindlimb muscles tested but were tested with RL-ICMS. For mapping, an effect in only one muscle was considered sufficient to identify the site as hindlimb. Light blue line: midline, above the light blue line represents the bank of the medial wall of the hemisphere. Solid black curved line: central sulcus. Dotted black curved line: fundus of the central sulcus. A: anterior. P: posterior. M: medial. L: lateral.

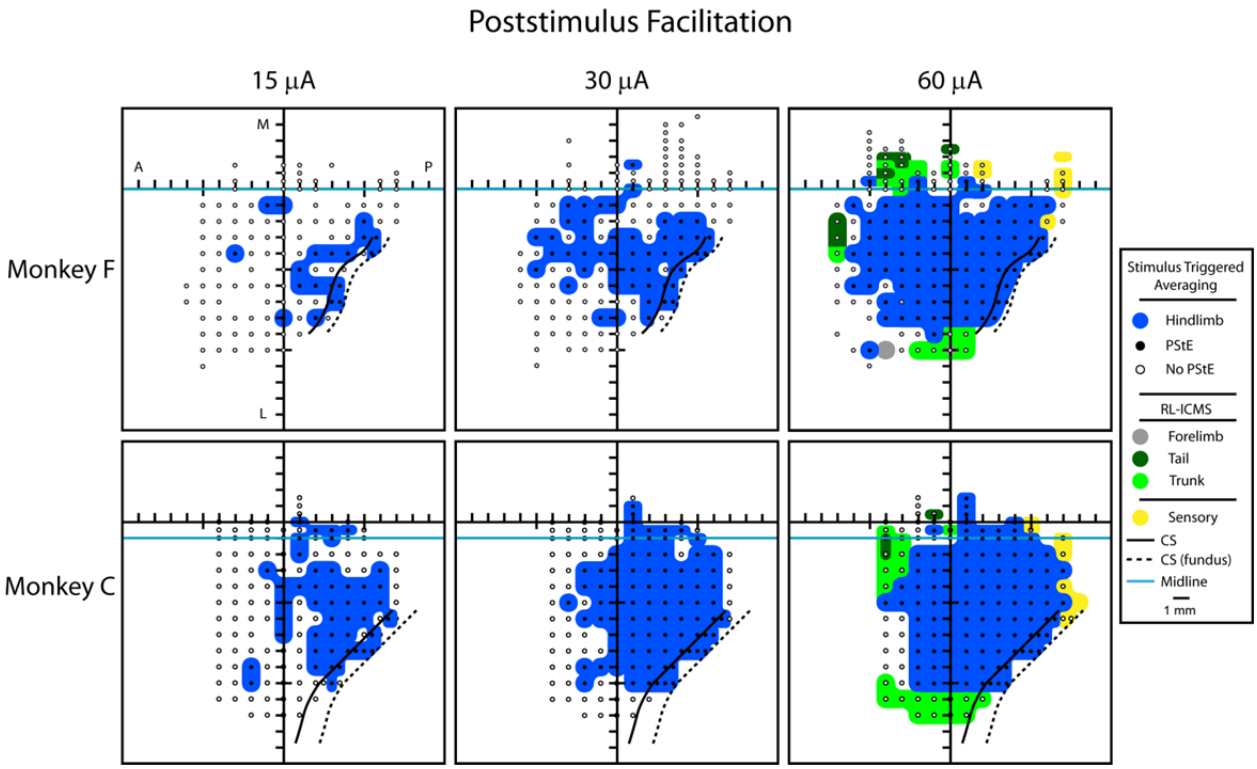
Poststimulus Facilitation
15 µA
30 µA
60 µA
Monkey F
Monkey C
M
L
A
P
Stimulus Triggered Averaging
Hindlimb
PStE
No PStE
RL-ICMS
Forelimb
Tail
Trunk
Sensory
CS
CS (fundus)
Midline
1 mm

Figure 3. Stimulus triggered averages (StTA) of 19 muscles of the hindlimb at 15, 30 and 60 μA from one site in hindlimb M1. Stimulus occurs at time 0. Range of trigger events listed at bottom of each stimulus column. GMAX, gluteus maximus; ADB, adductor brevis; GRA, gracilis; TFL, tensor fascia latae; RF, rectus femoris; VL, vastus lateralis; VM, vastus medialis; BFL, biceps femoris; SEM, semimembranosus; SET, semitendonosus; PERL, peroneus longus; MG, medial gastrocnemius; LG, lateral gastrocnemius; SOL, soleus; TA, tibialis anterior; EDL, extensor digitorum longus; FDL, flexor digitorum longus; EDB, extensor digitorum brevis; FHB, flexor hallucis brevis.

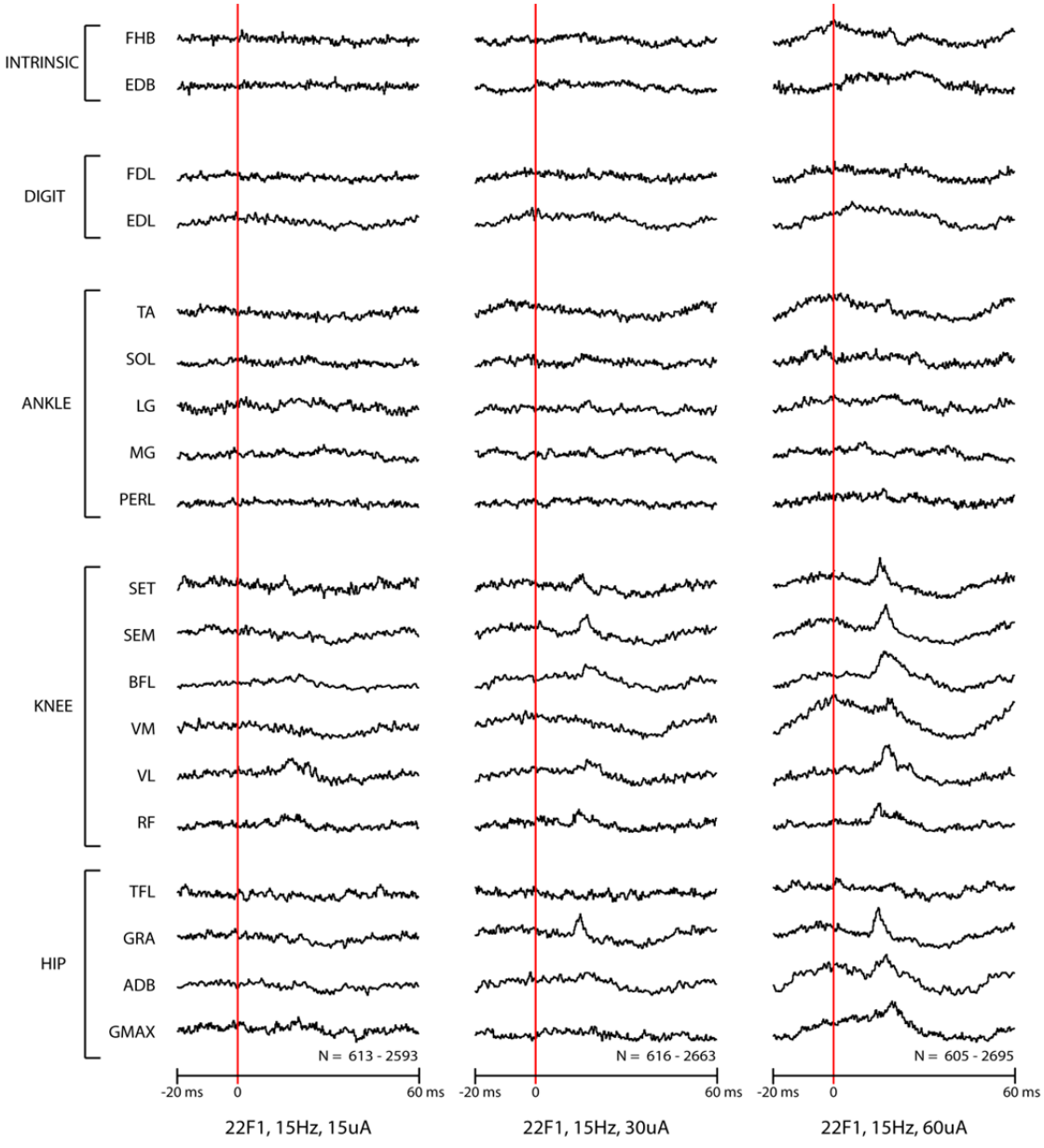
INTRINSIC
FHB
EDB
DIGIT
FDL
EDL
ANKLE
TA
SOL
LG
MG
PERL
KNEE
SET
SEM
BFL
VM
VL
RF
HIP
TFL
GRA
ADB
GMAX
N = 613 - 2593
N = 616 - 2663
N = 605 - 2695
-20 ms
0
60 ms
22F1, 15Hz, 15uA
22F1, 15Hz, 30uA
22F1, 15Hz, 60uA

Figure 4. Typical poststimulus effects from one site in M1 hindlimb cortex. All muscles with significant effects are shown and include hip to intrinsic foot muscles. Note the primary short latency, short duration facilitation in most muscles and the much longer latency broad inhibition in all muscles. Stimulation at 60 μA and 5 Hz repetition rate. Muscle abbreviations are the same as in Figure 3.

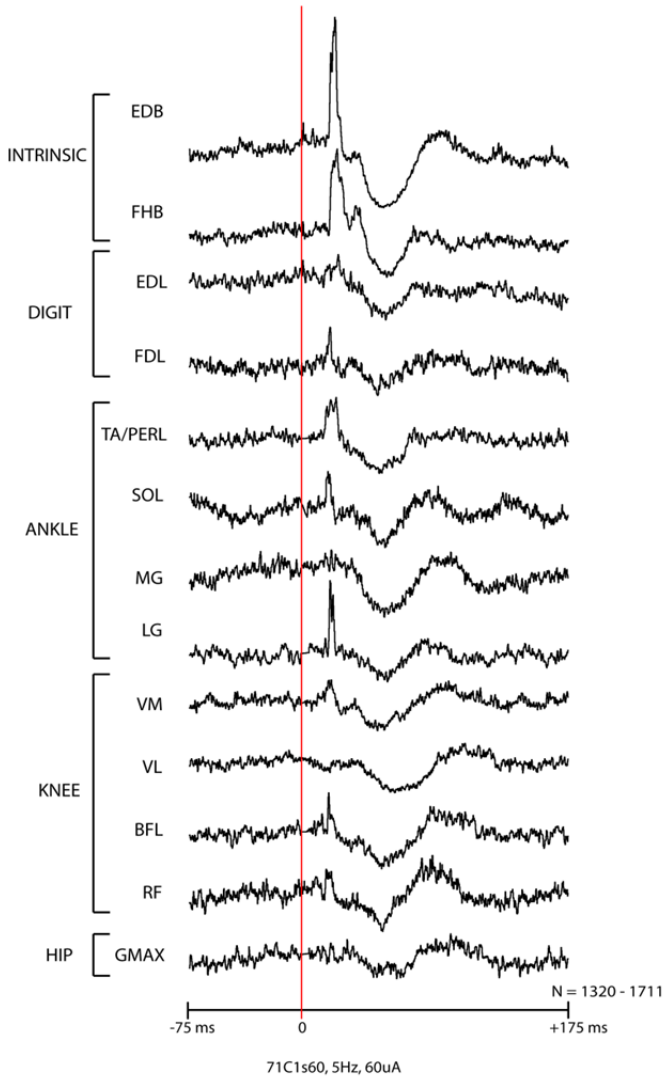
INTRINSIC
EDB
FHB
DIGIT
EDL
FDL
ANKLE
TA/PERL
SOL
MG
LG
KNEE
VM
VL
BFL
RF
HIP
GMAX
N = 1320 - 1711
-75 ms
0
+175 ms
71C1s60, 5Hz, 60uA

Figure 5. Distribution of PStF onset latencies for muscles at the hip, knee, ankle, digit and intrinsic foot joints at 15, 30 and 60 μA stimuli. The values given in parentheses for each graph represent the mean ± SD of the onset latency of the PStF.

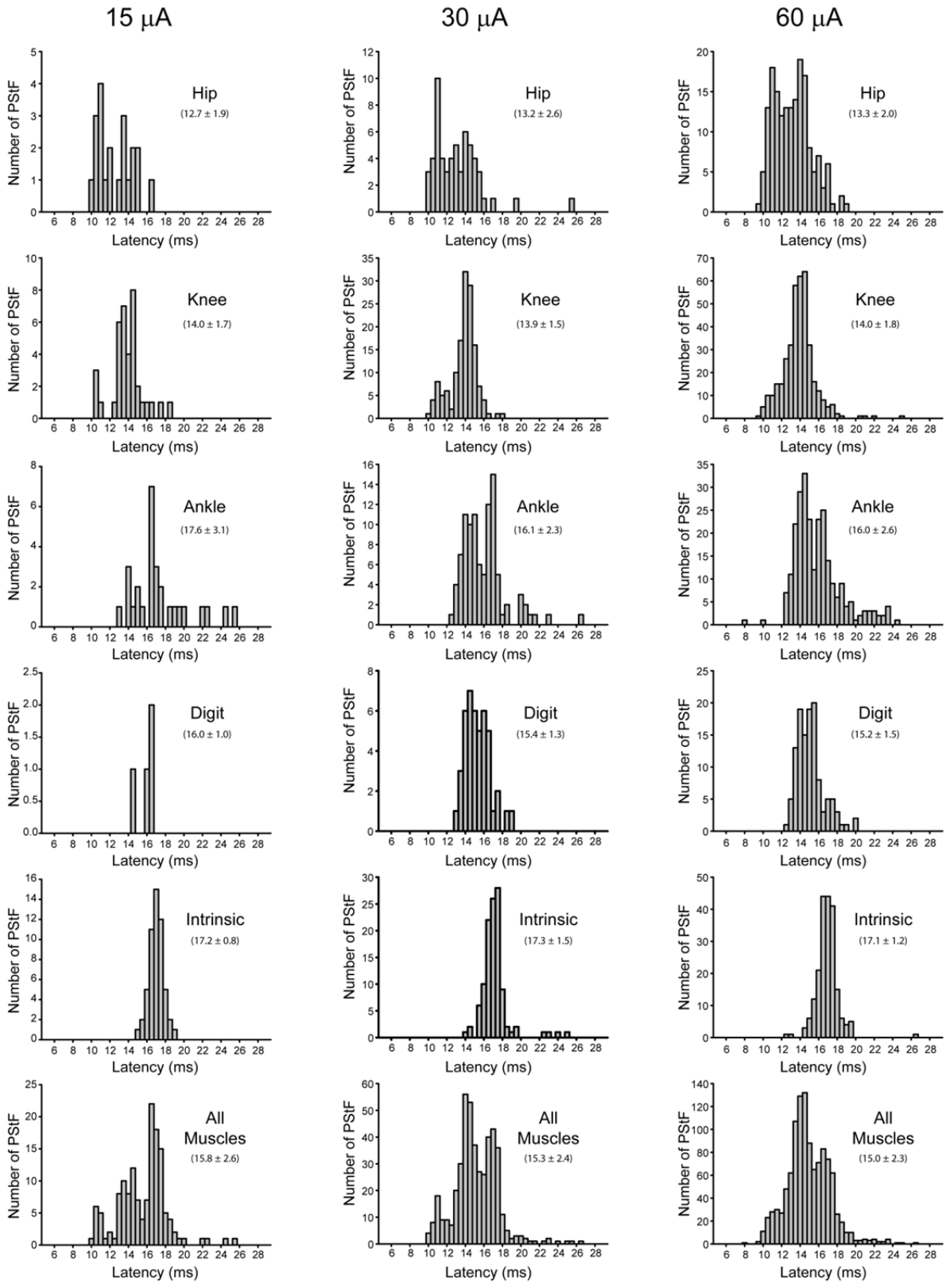
15 μA
30 μA
60 μA
Hip
(12.7 ± 1.9)
(13.2 ± 2.6)
(13.3 ± 2.0)
Knee
(14.0 ± 1.7)
(13.9 ± 1.5)
(14.0 ± 1.8)
Ankle
(17.6 ± 3.1)
(16.1 ± 2.3)
(16.0 ± 2.6)
Digit
(16.0 ± 1.0)
(15.4 ± 1.3)
(15.2 ± 1.5)
Intrinsic
(17.2 ± 0.8)
(17.3 ± 1.5)
(17.1 ± 1.2)
All Muscles
(15.8 ± 2.6)
(15.3 ± 2.4)
(15.0 ± 2.3)
Number of PStF
Latency (ms)

Figure 6. Distribution of PStF magnitudes for muscles at the hip, knee, ankle, digit and intrinsic foot joints at 15, 30 and 60 μA stimuli. The magnitudes are expressed as peak percent increase (ppi) above baseline. The values given in parentheses for each group represent the mean ± SD of the magnitude of the PStF.

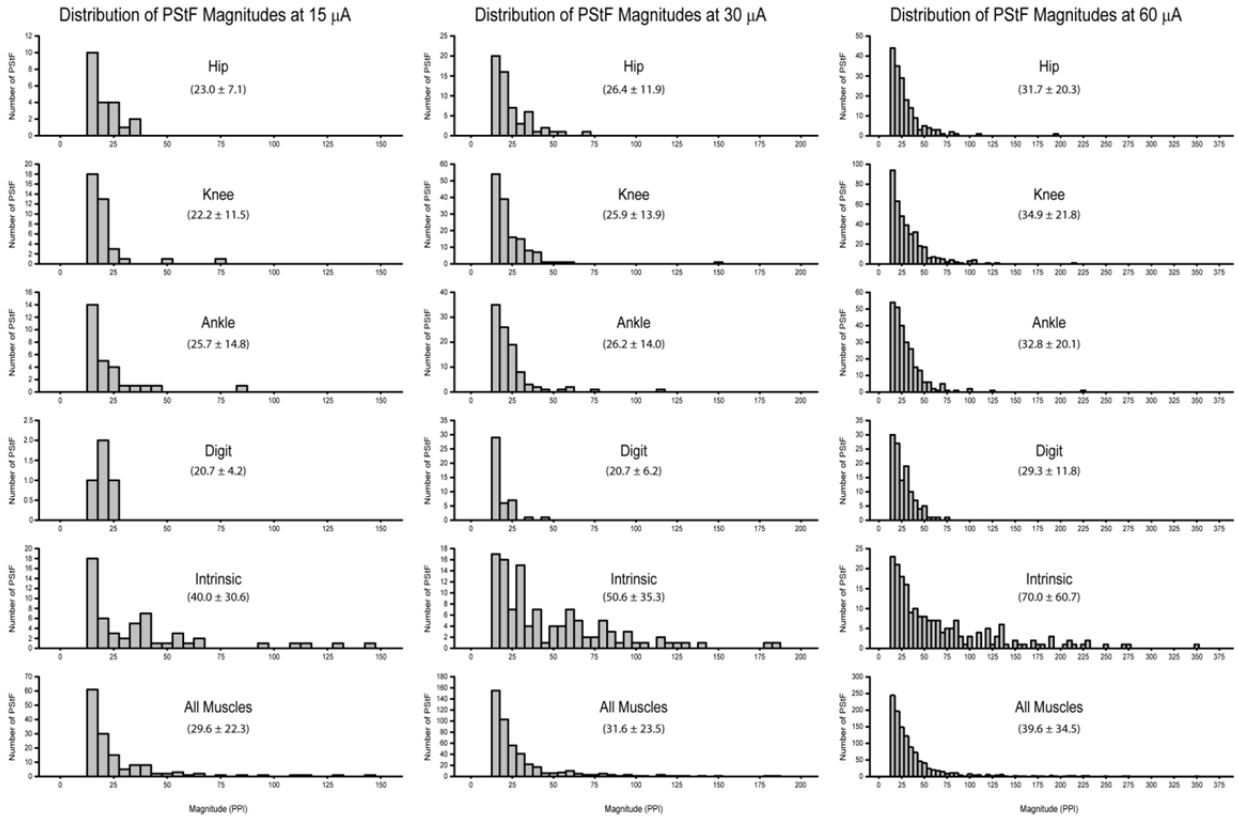
Distribution of PStF Magnitudes at 15 μA
Distribution of PStF Magnitudes at 30 μA
Distribution of PStF Magnitudes at 60 μA
Hip
(23.0 ± 7.1)
Hip
(26.4 ± 11.9)
Hip
(31.7 ± 20.3)
Knee
(22.2 ± 11.5)
Knee
(25.9 ± 13.9)
Knee
(34.9 ± 21.8)
Ankle
(25.7 ± 14.8)
Ankle
(26.2 ± 14.0)
Ankle
(32.8 ± 20.1)
Digit
(20.7 ± 4.2)
Digit
(20.7 ± 6.2)
Digit
(29.3 ± 11.8)
Intrinsic
(40.0 ± 30.6)
Intrinsic
(50.6 ± 35.3)
Intrinsic
(70.0 ± 60.7)
All Muscles
(29.6 ± 22.3)
All Muscles
(31.6 ± 23.5)
All Muscles
(39.6 ± 34.5)
Number of PStF
Magnitude (PPI)

Figure 7. Relationship between onset latency and magnitude of PStFs for hip, knee, ankle, digit and intrinsic foot muscles at 60 μA. Linear regression analysis was performed. Correlation coefficients (r) and P values for a non-zero relationship are given.

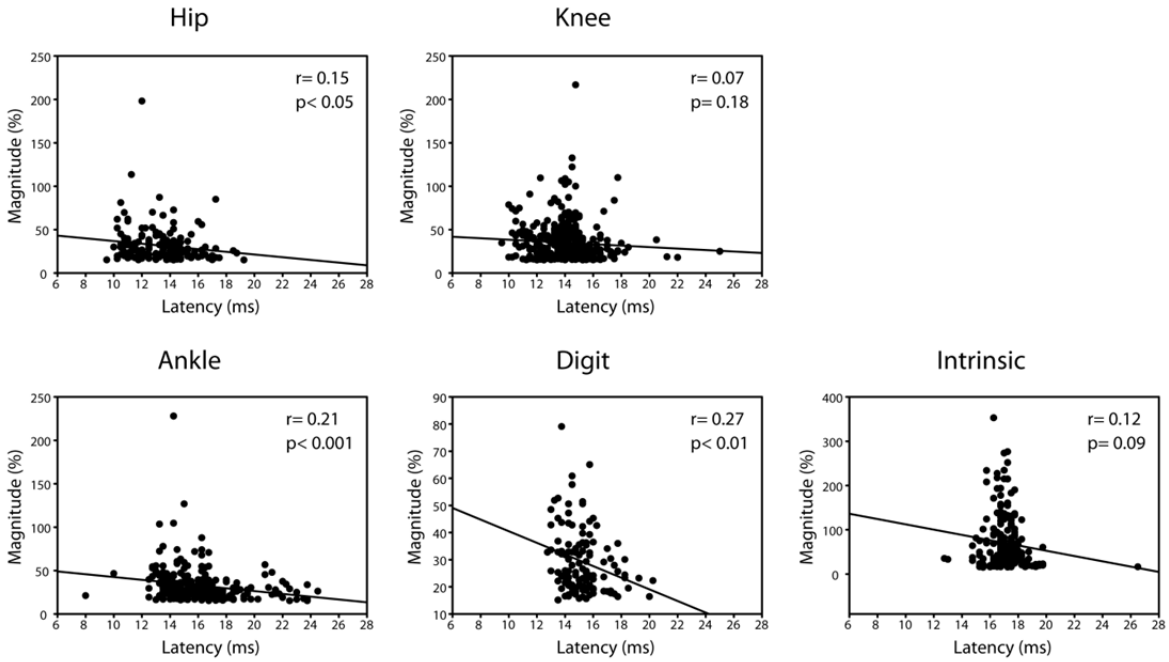
Hip
r= 0.15
p< 0.05
Knee
r= 0.07
p= 0.18
Ankle
r= 0.21
p< 0.001
Digit
r= 0.27
p< 0.01
Intrinsic
r= 0.12
p= 0.09
Magnitude (%)
Latency (ms)

Figure 8. Distribution of PStF (A) and PStS (B) in hip, knee, ankle, digit and intrinsic foot muscles at 15, 30 and 60 μA stimuli. Distribution of PStF (C) and PStS (D) after normalizing for the number of recorded muscles at each joint (dividing the total number of effects obtained by the number of muscles recorded at each joint).

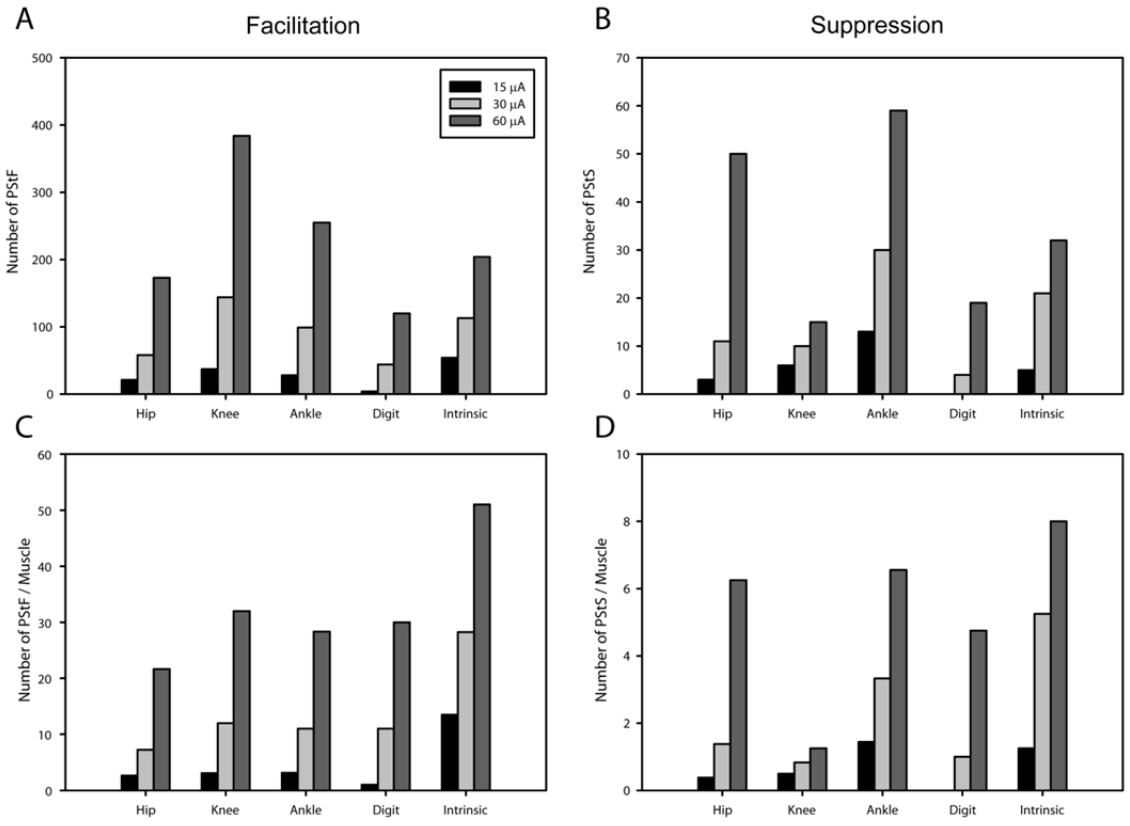
A
Facilitation
B
Suppression
15 µA
30 µA
60 µA
Number of PStF
Number of PStS
C
D
Number of PStF / Muscle
Number of PStS / Muscle
Hip
Knee
Ankle
Digit
Intrinsic

Figure 9. Distribution of PStF (A) and PStS (B) in extensor and flexor muscles of the hip, knee, ankle, digit and intrinsic foot joints at 15, 30 and 60 μA stimuli. Distribution of PStF (C) and PStS (D) after normalizing for the number of recorded muscles at each joint.

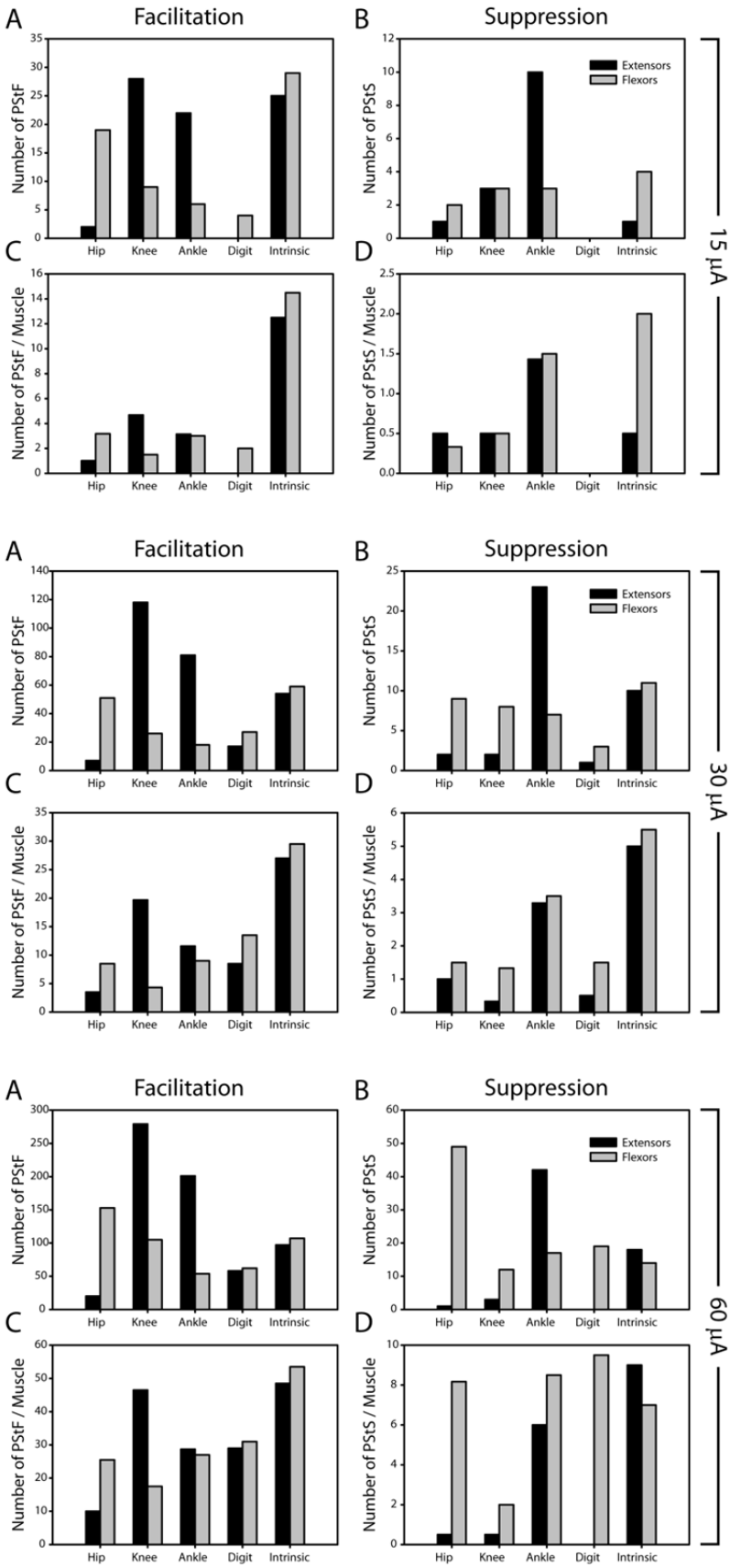
A
Facilitation
B
Suppression
Extensors
Flexors
Number of PStF
Number of PStS
C
D
Number of PStF / Muscle
Number of PStS / Muscle
Hip
Knee
Ankle
Digit
Intrinsic
15 µA
30 µA
60 µA

Figure 10. Distribution of PStF (right) and PStS (left) effects obtained from 19 muscles of the hindlimb. Dotted lines separate muscles belonging to different joints. Muscle abbreviations are the same as in Figure 3.

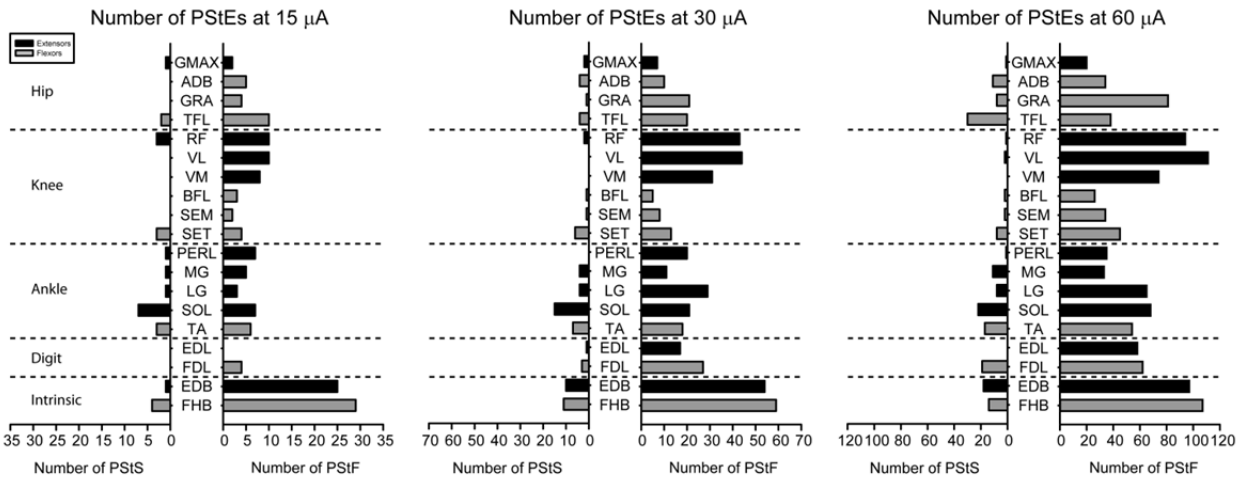
Number of PStEs at 15 μA
Number of PStEs at 30 μA
Number of PStEs at 60 μA
Extensors
Flexors
Hip
Knee
Ankle
Digit
Intrinsic
GMAX
ADB
GRA
TFL
RF
VL
VM
BFL
SEM
SET
PERL
MG
LG
SOL
TA
EDL
FDL
EDB
FHB
35 30 25 20 15 10 5 0
0 5 10 15 20 25 30 35
70 60 50 40 30 20 10 0
0 10 20 30 40 50 60 70
120 100 80 60 40 20 0
0 20 40 60 80 100 120
Number of PStS
Number of PStF

CHAPTER 5

CORTICAL OUTPUT TO FAST AND SLOW MUSCLES OF THE ANKLE

INTRODUCTION

The existence of fast and slow motor units has long been established (Andersen and Sears, 1964). It is well known that the ankle extensor, soleus, consists exclusively of slow motor units while tibialis anterior, an ankle flexor, consists largely of fast motor units. Medial and lateral gastrocnemius are mixed but with a predominance of fast motor units (Burke, 1967; Burke et al., 1970, 1971, 1974). The differential cortical control of these exclusively or predominantly fast and slow muscles has been the subject of many studies in cats, primates and humans yielding conflicting results.

Monosynaptic linkages have been established between corticospinal neurons and hindlimb motoneurons in primates (Asanuma et al., 1979; Edgley et al., 1997; Jankowska et al., 1975; Muir and Porter, 1973; Preston and Whitlock, 1963; Shapovalov and Kurchavyi, 1974). Preston and Whitlock (1963) and Uemura and Preston (1965), studying monosynaptic reflex conditioning in the "pyramidal" monkey preparation, reported corticospinal output to slow muscle (soleus) motoneurons was predominantly inhibitory while output to motoneurons of fast muscles (gastrocnemius and tibialis anterior) was excitatory. Kawai (1982), in the "pyramidal" cat preparation, demonstrated largely excitatory post synaptic potentials (EPSPs) to fast motoneurons and inhibitory post synaptic potentials (IPSPs) to slow motoneurons. Jankowska (1975) reported EPSPs in soleus were half as strong as EPSPs in tibialis anterior in the monkey.

Transcranial magnetic stimulation (TMS) and electrical stimulation (TES) have been used in numerous human subject studies yielding varied results. It has been established from these studies that TMS produces clear, short latency facilitation in tibialis anterior (Bawa et al., 2002; Brouwer and Ashby, 1990, 1992; Brouwer and Qiao, 1995; Ertekin et al., 1995; Valls-Solé et al., 1994). Some studies have shown that facilitation of soleus from TMS or electrical stimulation of the cortex is either weak or non-existent (Ashby and Advani, 1990; Brouwer and Ashby, 1990, 1992; Brouwer and Qiao, 1995; Cowan et

al., 1986). In contrast, other studies have shown that TMS produces short latency facilitation in soleus (Bawa et al., 2002; Valls-Solé et al., 1994).

Despite several studies in animals and humans, the cortical control of fast and slow muscles of the ankle remains controversial. The goal of this study was to investigate the cortical control of fast and slow muscles of the ankle in the rhesus macaque using stimulus triggered averages (StTA) of EMG activity recorded from tibialis anterior (TA), medial and lateral gastrocnemius (MG and LG), and soleus (SOL) muscles during a hindlimb push-pull task. These methods provide a more sensitive and higher resolution approach to delineating cortical motor output effects than the methods applied in previous studies.

MATERIALS AND METHODS

Behavioral task

Data were collected from the left primary motor cortex (M1) of two male rhesus macaques (*Macaca mulatta*, ~10 kg, 6-7 years old). The monkeys were trained to perform a hindlimb push-pull task engaging both proximal and distal muscles in reliable and stereotyped patterns of activation (Hudson et al., 2010). Seated in a custom primate chair within a sound-attenuating chamber, both arms and the left leg were restrained. With the right foot, the monkey gripped the manipulandum (horizontal post) and extended the leg until the target zone was achieved. After a hold period of 500 ms in the target zone, the monkey flexed the leg pulling the manipulandum to a second target zone. Following a second hold period of 500 ms, the monkey was given an applesauce reward. The behavioral task was guided by visual and auditory cues.

MRI

The monkey's head was placed in an MRI-compatible stereotaxic apparatus and structural MRIs in the sagittal, coronal and horizontal planes were obtained using a Siemens Allegra 3T system. A 3-dimensional reconstruction of each monkey's brain was produced using CARET software (Computerized Anatomical Reconstruction and Editing Tool Kit).

Surgical procedures

Upon completion of training, each monkey was implanted with a titanium cortical recording chamber (30 mm inside diameter) centered at anterior 13.5 mm, lateral 0 mm and 0° angle to the midsagittal plane (Paxinos et al. 2000). EMG activity was recorded from 19 muscles of the hindlimb using pairs of insulated, multi-stranded stainless steel wire (Cooner Wire, AS632) implanted during an aseptic surgical procedure (Hudson et. al, 2010). Briefly, pairs of wires were tunneled subcutaneously to their target muscles from either an external circular connector (Amphenol) affixed to the skull using

dental acrylic and titanium screws (cranial-mounted subcutaneous implant, monkey C) or four external connector modules (ITT Canon) affixed to the upper arm with elastic medical adhesive tape (arm-mounted subcutaneous implant, monkey F). Proper placement of electrode pairs in each muscle was tested by stimulating through the electrodes with brief stimulus trains (biphasic pulse, 0.2 ms/phase, ~50 Hz) while observing appropriate evoked movements. Wires were removed and reinserted if proper placement was not confirmed. Similar stimulation tests were performed at various times after implantation to confirm electrode location. Within weeks of implantation, loops of extra wire length tucked into a subcutaneous pocket in the back becomes embedded in connective tissue rigidly anchoring the electrodes in place.

EMGs were recorded from four hip muscles: gracilis (GRA), adductor brevis (ADB), gluteus maximus (GMAX) and tensor fascia latae (TFL); six knee muscles: biceps femoris (BFL), semimembranosus (SEM), semitendonosus (SET), rectus femoris (RF), vastus lateralis (VL) and vastus medialis (VM); five ankle muscles: tibialis anterior (TA), peroneus longus (PERL), medial gastrocnemius (MG), lateral gastrocnemius (LG) and soleus (SOL); two digit muscles: flexor digitorum longus (FDL) and extensor digitorum longus (EDL); and two intrinsic foot muscles: flexor hallucis brevis (FHB) and extensor digitorum brevis (EDB). In monkey C, the EMG leads to PERL were compromised shortly after the implant and were excluded. In this paper, only data from the ankle muscles TA, SOL, MG and LG are reported.

All procedures were in accordance with the standards outlined by the *Guide for the Care and Use of Laboratory Animals* published by the U.S. Department of Health and Human Services and the National Institutes of Health. All surgeries were performed in an Association for Assessment and Accreditation of Laboratory Animal Care (AAALAC) accredited facility using full aseptic procedures. Postoperative analgesics (buprenorphine, 0.01 mg/kg) were administered for five days. Wound edges were inspected daily and treated with Betadine (10% povidone-iodine) and topical antibiotic when necessary.

Data collection

EMG activity, cortical activity and task-related signals were simultaneously monitored. Glass and mylar-insulated platinum-iridium electrodes (0.5-1.5 MΩ impedances, Frederick Haer) were used to record cortical unit activity and for stimulation. The electrode was positioned in the recording chamber using a custom-built x-y positioner and advanced using a manual hydraulic microdrive (Frederick Haer). Electrode penetrations were systematically made at 1 mm intervals in the precentral cortex of the left hemisphere. Data were collected from sites in layer V of the cortex, as determined by depth from first cortical activity and size and nature of neuronal spikes. Data were collected from layer V sites in the bank of the medial wall and central sulcus at 0.5 mm intervals over the extent of the electrode track.

At each layer V site, StTAs (15, 30 and 60 μA at 15 Hz) of EMG activity were computed for 19 muscles of the hindlimb as the monkey performed the push-pull task. Individual stimuli were symmetrical biphasic pulses, 0.2 ms negative pulse followed by a 0.2 ms positive pulse, applied throughout all phases of the task. EMGs were generally filtered at 30 Hz to 1 kHz, digitized at 4 kHz and full-wave rectified. StTAs were compiled over an 80 ms epoch, 20 ms pre-trigger and 60 ms post-trigger, and consisted of at least 500 trigger events. To prevent averaging periods where EMG activity was minimal or non-existent, segments of EMG activity associated with each stimulus were evaluated and accepted for averaging only when the average of all EMG data points over the entire 80 ms epoch was ≥ 5% of full-scale input (McKiernan et al., 1998).

Cross-talk between muscles was evaluated by computing EMG-triggered averages (Cheney and Fetz, 1980). Averages of EMG activity were compiled for each muscle using one muscle's EMG activity as a trigger and repeated using all 19 muscles as triggers. If the ratio of the cross-talk peak in the test versus trigger muscle exceeded the ratio of their poststimulus effects by a factor of 2 or more, a muscle was considered to have an unacceptable level of cross-talk (Buys et al., 1986). No muscle in this study showed significant cross-talk using this criterion.

Data analysis

At each stimulation site, stimulus triggered averages were obtained from all 19 muscles. This study focuses only on data from the ankle muscles TA, SOL, MG and LG. Poststimulus facilitation (PStF) and suppression (PStS) effects were computer measured as described by Mewes and Cheney (1991). Each average consisted of an 80 ms epoch, 20 ms pre-trigger and 60 ms post-trigger. A poststimulus effect (PStE) was defined as a peak or trough of EMG activity that rose or fell from baseline and maintained a level exceeding two standard deviations of baseline for a period equal to or greater than 0.75 ms. Baseline EMG activity was measured as the 12 ms period preceding the onset of the effect initially determined by visual inspection. Baseline statistics were then used to determine the onset of the effect as the point where the envelope of the record exceeded two standard deviations of baseline. The magnitude of PStEs was expressed as the peak percentage increase (+ppi) or peak percentage decrease (-ppi) in EMG activity above (PStF) or below (PStS) baseline. To avoid skewing of the data and conclusions from very weak effects, only PStF effects with a ppi ≥ 15 and PStS effects with a ppi ≤ -15 were included in analysis (Figure 1).

Unfolding the cortex

A two-dimensional representation of cortical layer V of the cortex in the medial wall of the hemisphere, the anterior bank of the central sulcus and the surface cortex required flattening and unfolding the curvature of the cortex. This process has been described in detail by Park et al. (2001). Briefly, the cortex was unfolded and 2-dimensional maps were generated based on known architectural landmarks, observations during the cortical chamber implant surgery, MRI images, electrode track x-y coordinates, electrode penetration depth and properties of recorded neurons.

RESULTS

Dataset

Table 1 summarizes the data collected from the left M1 cortex in two rhesus macaques. A total of 312 electrode tracks were made (monkey F, 170; monkey C, 142). At 15 μA, stimulus triggered averaging of EMG activity from 4 ankle muscles was performed at 259 layer V sites (292 sites, 30 μA; 317 sites, 60 μA). Twenty-seven layer V sites yielded poststimulus effects (PStEs) at 15 μA, 73 at 30 μA and 134 at 60 μA. Both PStF and PStS were observed for all ankle muscles. Figure 2 shows the EMG activity of TA, MG, LG and SOL throughout different phases of the hindlimb task. The extensors (MG, LG and SOL) all showed a similar pattern of modulation with the strongest activity during the extension (push) phase of the task but continuing at a lower level through the hold phase of extension and also during leg flexion (pull). The flexor muscle (TA) showed a more focused pattern with activity confined primarily to the flexion (pull and hold) phase of the task.

Data were collected at three stimulus intensities: 15, 30 and 60 μA. Not all sites with PStEs at 30 and 60 μA had PStEs at 15 μA. Only the data from sites with PStEs at all three stimulus intensities were used to analyze the relationship between stimulus intensity and the latency and magnitude of effects. Data from all sites were used to analyze the distribution of effects. Table 2 summarizes the mean onset latencies and magnitudes of PStEs in ankle muscles (A, sites with PStEs present at all stimulus intensities; B, all data).

Muscle representation

Figure 3 shows the representation of each muscle, based on PStF effects, in M1 of both monkeys. All muscles were represented in both monkeys. There was massive overlap in the territories for each muscle, not only of the extensors (MG, LG and SOL) but also of the flexor muscle, TA. While monkey F had considerably fewer effects than monkey C, the same trend was apparent in both monkeys.

Latency and magnitude

At 15 μA, the average PStF onset latency across all ankle muscles was 18.5 ± 3.0 ms compared with an average PStS onset latency of 19.9 ± 3.8 ms (Table 2B). The latency difference increased to 2.2 ms at 30 μA and 3.7 ms at 60 μA, with the PStS onset latency significantly longer than PStF latency at both 30 and 60 μA ($p=0.001$, 1-way ANOVA). The dataset limited to effects present at all three intensities (Table 2A) was too small in many cases to make meaningful statistical comparisons.

Figure 4 shows the distribution of PStF onset latencies for the ankle muscles at 15, 30 and 60 μA. There was a similar distribution of latencies among all muscles, although TA had a clear suggestion of bimodality that was not present in the distributions for other muscles. The minimum onset latency decreased with intensity although the decrease from 30 to 60 μA was small. Regardless of muscle, the minimum latency was approximately 12-13 ms (30 and 60 μA). The only exceptions were two effects in MG at 60 μA that were 8 and 10 ms.

At 15 μA, the overall mean PStF magnitude, expressed as peak percent increase (ppi) above baseline, was 24.4 ± 8.7 compared with -19.0 ± 3.6 for PStS (Table 2B). None of the differences in mean PStF magnitudes between muscles were statistically significant ($p>0.29$, 1-way ANOVA). This was true for all stimulus intensities. The mean PStF magnitude across all muscles increased linearly as stimulus intensity increased from 15 to 60 μA (Table 2A). The magnitude changes from 30 to 60 μA were statistically significant when all muscles were lumped together ($p<0.05$, 1-way ANOVA) and were also significant for LG individually ($p<0.05$, 1-way ANOVA). The dataset for magnitude of PStS effects was too small for statistical comparisons (Table 2A). There was a similar distribution of magnitudes of PStF among all muscles with a consistent trend toward skewing of the distributions toward effects with the weakest magnitudes (Figure 5).

Distribution of PStEs

Figure 6 shows the distribution of PStF and PStS effects observed in each of the ankle muscles sampled at 15, 30 and 60 μA. Both PStF and PStS effects were observed in each muscle at each stimulus intensity. Overall, PStF was more common than PStS in TA, LG and MG. PStS was most common in SOL, especially at 15 μA and this trend persisted at higher stimulus intensities. Both monkeys displayed these trends.

DISCUSSION

Early studies in the primate and more recent studies in human subjects have yielded conflicting results regarding the motor cortex's role in the control of slow muscles such as soleus. While it was established that the motor cortex has an excitatory effect on fast muscles, the cortical control of the slow muscle, soleus, was not clear. In this study, we investigated the cortical control of fast (TA, MG and LG) and slow (SOL) muscles of the ankle using stimulus triggered averaging of EMG activity. With this method, microstimuli are superimposed on a background of EMG activity associated with task performance. The effects of single stimuli are subthreshold for overt EMG responses but the evoked EPSPs and IPSPs in motoneurons have an influence on the firing probability of motoneurons that can be revealed with signal averaging over thousands of stimuli. This yields a highly sensitive method capable of revealing both excitatory and inhibitory effects.

Poststimulus facilitation was observed in all muscles and was as common in the slow muscle, soleus, as in the fast muscles. The mean onset latencies of PStF effects were similar among the fast and slow muscles. The mean magnitudes of PStF effects were also similar among the fast and slow muscles. The distributions of PStF magnitudes were similar among all muscles, demonstrating a consistent trend of the weakest magnitudes being the most common. Poststimulus suppression was observed in all muscles; however, it was more common in the slow muscle, soleus, than the fast muscles, especially at lower stimulus intensities.

The question arises as to why early studies in the primate and some studies in human subjects did not find similar results. The early studies of Preston and Whitlock (1963) and Uemura and Preston (1965) used the "pyramidal" preparation monkey which involves lesioning the brainstem sparing only the pyramidal tract, while the monkeys in our study were awake, with an intact nervous system, and performing a trained motor behavioral task. In human subjects, Bawa et al. (2002) found that a higher stimulus intensity was needed to elicit a short latency facilitation in soleus compared to tibialis anterior.

Moreover, Valls-Solé et al., (1994) found that TMS effects in soleus were difficult to elicit unless the subjects were standing on their toes which would produce a large excitability increase in soleus motoneurons. Reports of weak or non-existent soleus excitation may have been due to low stimulus intensities (Brouwer and Qiao, 1995). In this study, we used three stimulus intensities and found the number of suppression and facilitation effects in soleus to be similar at lower intensities. At higher intensities, facilitation of soleus was more common than suppression.

Based on our results, there can be no doubt that the motor cortex, in primates, has a powerful excitatory effect on soleus motoneurons. The motor cortex also has an inhibitory effect on soleus and the inhibitory effects are more prominent in the slow muscle, soleus, than the fast muscles. Overall, our results support the findings of recent TMS studies in human subjects demonstrating short latency facilitation of both fast and slow muscles of the ankle (Bawa et al., 2002; Valls-Solé et al., 1994).

Table 1. Summary of data collected

	Monkey F			Monkey C			Total		
Electrode tracks	170			142			312		
	15 μA	30 μA	60 μA	15 μA	30 μA	60 μA	15 μA	30 μA	60 μA
Layer V sites stimulated	117	150	167	142	142	150	259	292	317
Sites yielding PStEs (total)	23	54	101	51	89	104	74	143	205
Sites yielding PStEs (ankle)	4	17	55	23	56	79	27	73	134
Sites yielding PStF (ankle)	4	15	47	14	35	66	18	50	113
Sites yielding PStS (ankle)	0	2	11	11	22	29	11	24	40
PStEs obtained (ankle)	4	20	99	29	89	179	33	109	278
PStF effects	4	18	84	17	61	136	21	79	220
PStS effects	0	2	15	12	28	43	12	30	58

PStE, poststimulus effec; PStF, poststimulus facilitation; PStS, poststimulus suppression.

Table 2. Latency and magnitude of PStEs

A. Effects present at 15, 30 and 60 μA

PStF

	Onset Latency, ms						Magnitude, %					
	15 μA		30 μA		60 μA		15 μA		30 μA		60 μA	
Muscle	*n*	Mean	*n*	Mean	*n*	Mean	*n*	Mean	*n*	Mean	*n*	Mean
TA	5	19.5 ± 2.9	5	18.8 ± 3.0	5	19.2 ± 3.0	5	24.5 ± 4.3	5	34.8 ± 15.8	5	41.9 ± 5.6
SOL	3	17.9 ± 2.0	3	17.8 ± 2.0	3	18.2 ± 2.3	3	24.2 ± 10.9	3	31.9 ± 11.7	3	57.3 ± 30.1
LG	3	16.3 ± 0.9	3	16.9 ± 0.1	3	15.9 ± 1.0	3	19.0 ± 0.7	3	29.5 ± 4.3	3	51.0 ± 14.4
MG	1	17.5	1	17.8	1	17.0	1	20.8	1	31.8	1	27.8
Total	12	18.1 ± 2.4	12	18.0 ± 2.2	12	17.9 ± 2.5	12	22.8 ± 5.9	12	32.5 ± 11.1	12	46.8 ± 17.1

PStS

	Onset Latency, ms						Magnitude, %					
	15 μA		30 μA		60 μA		15 μA		30 μA		60 μA	
Muscle	*n*	Mean	*n*	Mean	*n*	Mean	*n*	Mean	*n*	Mean	*n*	Mean
TA	0	---	0	---	0	---	0	---	0	---	0	---
SOL	5	17.2 ± 1.4	5	17.5 ± 1.4	5	17.5 ± 1.2	5	-18.0 ± 1.6	5	-25.9 ± 7.4	5	-33.5 ± 9.9
LG	1	17.8	1	17.8	1	17.8	1	-15.7	1	-16.3	1	-26.0
MG	0	---	0	---	0	---	0	---	0	---	0	---
Total	6	17.3 ± 1.3	6	17.5 ± 1.3	6	17.5 ± 1.1	6	-17.6 ± 1.7	6	-24.3 ± 7.7	6	-32.3 ± 9.4

B. All effects

PStF

	Onset Latency, ms						Magnitude, %					
	15 μA		30 μA		60 μA		15 μA		30 μA		60 μA	
Muscle	*n*	Mean	*n*	Mean	*n*	Mean	*n*	Mean	*n*	Mean	*n*	Mean
TA	6	20.3 ± 3.3	18	16.3 ± 3.2	54	17.3 ± 3.9	6	23.7 ± 4.3	18	26.2 ± 10.0	54	29.9 ± 10.5
SOL	7	19.3 ± 3.1	21	16.9 ± 1.9	68	16.6 ± 2.0	7	24.6 ± 10.9	21	25.6 ± 8.2	68	30.9 ± 14.7
LG	3	16.3 ± 0.9	29	16.2 ± 1.1	65	15.6 ± 1.3	3	19.0 ± 0.7	29	21.8 ± 4.8	65	33.4 ± 16.3
MG	5	16.5 ± 1.4	11	17.6 ± 3.4	33	15.8 ± 2.4	5	28.2 ± 11.6	11	28.9 ± 18.8	33	24.2 ± 8.6
Total	21	18.5 ± 3.0	79	16.6 ± 2.3	220	16.3 ± 2.6	21	24.4 ± 8.7	79	24.8 ± 9.9	220	30.4 ± 13.8

PStS

	Onset Latency, ms						Magnitude, %					
	15 μA		30 μA		60 μA		15 μA		30 μA		60 μA	
Muscle	*n*	Mean	*n*	Mean	*n*	Mean	*n*	Mean	*n*	Mean	*n*	Mean
TA	3	24.9 ± 1.1	7	21.9 ± 3.3	17	23.2 ± 2.8	3	-19.9 ± 3.6	7	-17.8 ± 2.2	17	-22.2 ± 5.5
SOL	7	18.6 ± 3.1	15	17.6 ± 2.1	22	18.3 ± 1.4	7	-19.4 ± 3.8	15	-24.3 ± 7.6	22	-24.2 ± 7.8
LG	1	17.8	4	18.6 ± 0.8	8	19.0 ± 0.8	1	-15.7	4	-19.3 ± 3.5	8	-22.2 ± 5.2
MG	1	16.8	4	18.3 ± 2.1	11	19.0 ± 2.4	1	-16.6	4	-18.3 ± 2.4	11	-20.3 ± 5.1
Total	12	19.9 ± 3.8	30	18.8 ± 2.8	58	20.0 ± 2.9	12	-19.0 ± 3.6	30	-21.3 ± 6.3	58	-22.6 ± 6.4

Values are mean ± SD. %, peak percent increase above baseline. PStE, poststimulus effect. PStF, poststimulus facilitation. PStS, poststimulus suppression.

Figure 1. Types of effects observed in stimulus triggered averages of ankle muscle EMG activity. Column on left: magnitude of the primary poststimulus facilitation (PStF) or poststimulus suppression (PStS) measured as peak percent increase above baseline EMG value just before the onset of the effect. Stimulation at 60 μA and 15 Hz repetition rate.

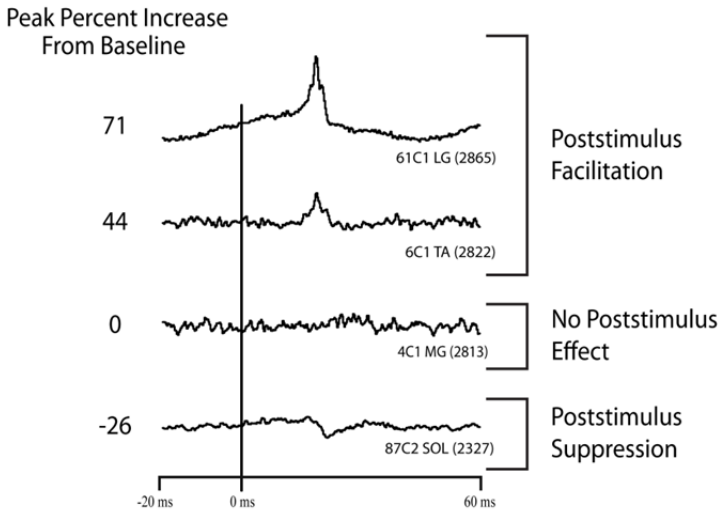
Peak Percent Increase
From Baseline
71
61C1 LG (2865)
44
6C1 TA (2822)
0
4C1 MG (2813)
-26
87C2 SOL (2327)
-20 ms
0 ms
60 ms
Poststimulus
Facilitation
No Poststimulus
Effect
Poststimulus
Suppression

Figure 2. A. Hindlimb push-pull task. The monkey is seated in a custom-built primate chair with both arms and the left leg restrained. The monkey gripped the push-pull device's manipulandum (horizontal post) with the right foot and pushed it to a target zone. After a hold period of 500 ms in the target zone, the monkey pulled the manipulandum to a second target zone and held for 500 ms. Upon successful completion of each push-pull trial, the monkey was given an applesauce reward. The behavioral task was guided by visual and auditory cues. B. EMG records of ankle muscles during two phases of the hindlimb push-pull task. TA, tibialis anterior; MG, medial gastrocnemius; LG, lateral gastrocnemius; SOL, soleus. Figure adapted from Chapter 2 and Hudson et al. (2010).

A.

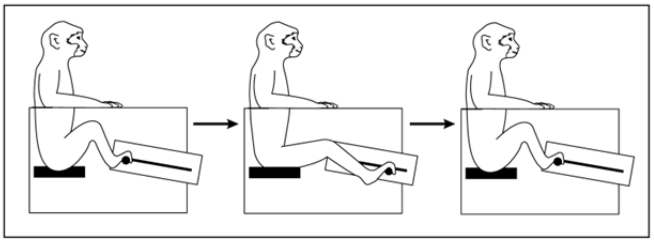

B.

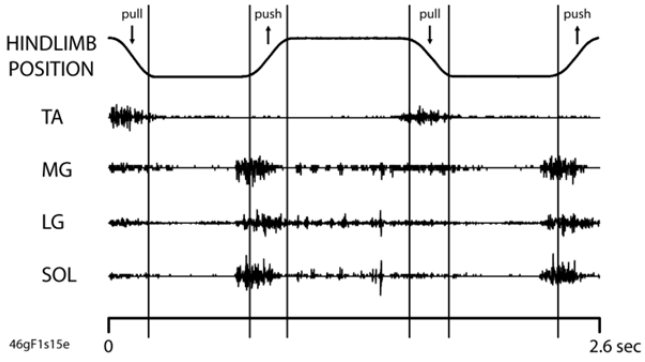
pull
push
pull
push
HINDLIMB POSITION
TA
MG
LG
SOL
46gF1s15e
0
2.6 sec

Figure 3. Maps of individual ankle muscle representations in hindlimb primary motor cortex in two monkeys (F and C), represented in two dimensions after unfolding the medial wall and central sulcus. Maps of hindlimb muscles were based on PStF effects at 15, 30 and 60 μA. Light blue line: midline, above the light blue line represents the bank of the medial wall of the hemisphere. Solid black curved line: central sulcus. Dotted black curved line: fundus of the central sulcus. A: anterior. P: posterior. M: medial. L: lateral. Muscle abbreviations are the same as in Figure 2.

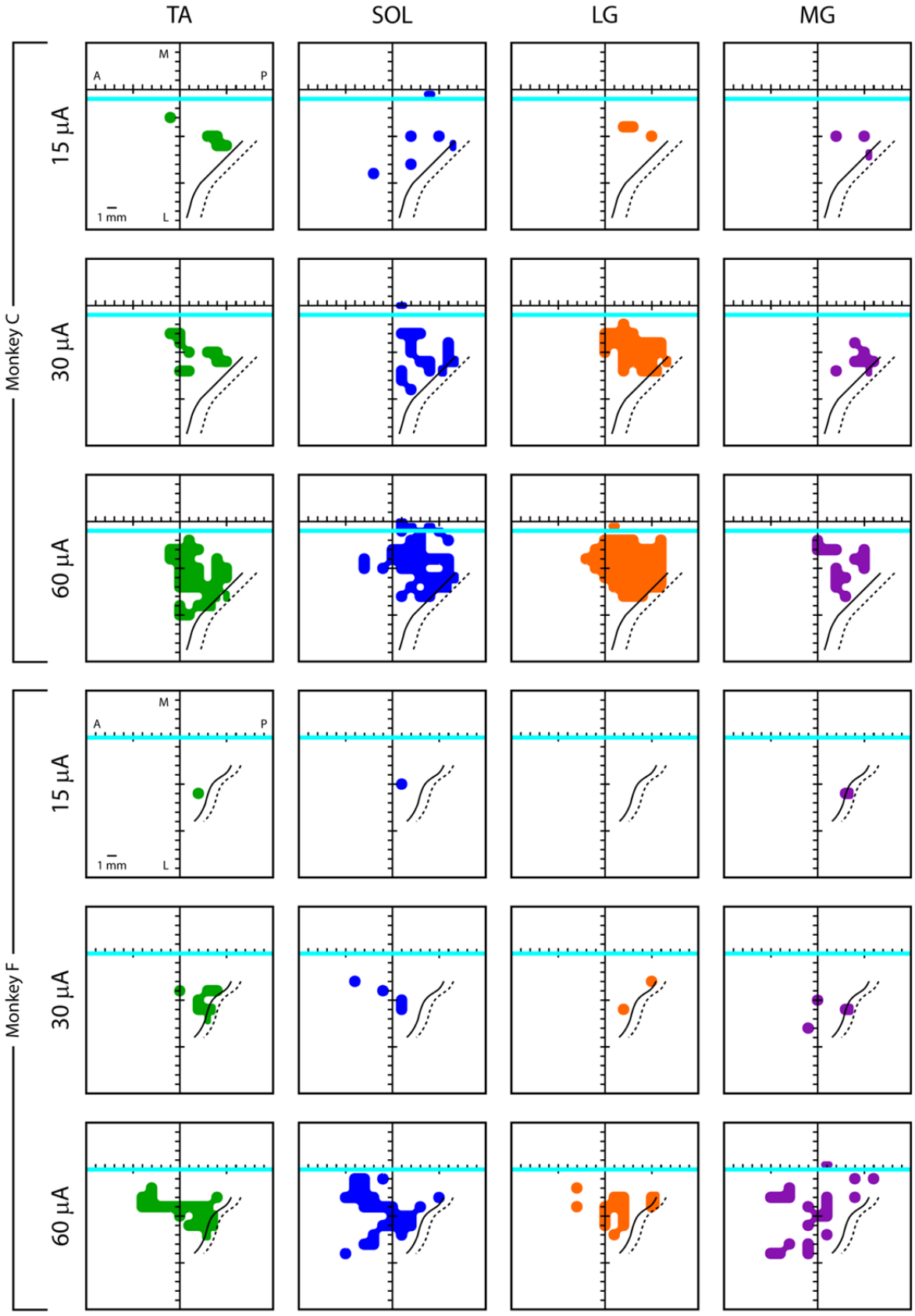
TA
SOL
LG
MG
Monkey C
Monkey F
15 µA
30 µA
60 µA
M
A
P
L
1 mm

Figure 4. Distribution of PStF onset latencies for ankle muscles at 15, 30 and 60 μA stimuli. The values given in parentheses for each graph represent the mean ± SD of the onset latency of the PStF. Muscle abbreviations are the same as in Figure 2.

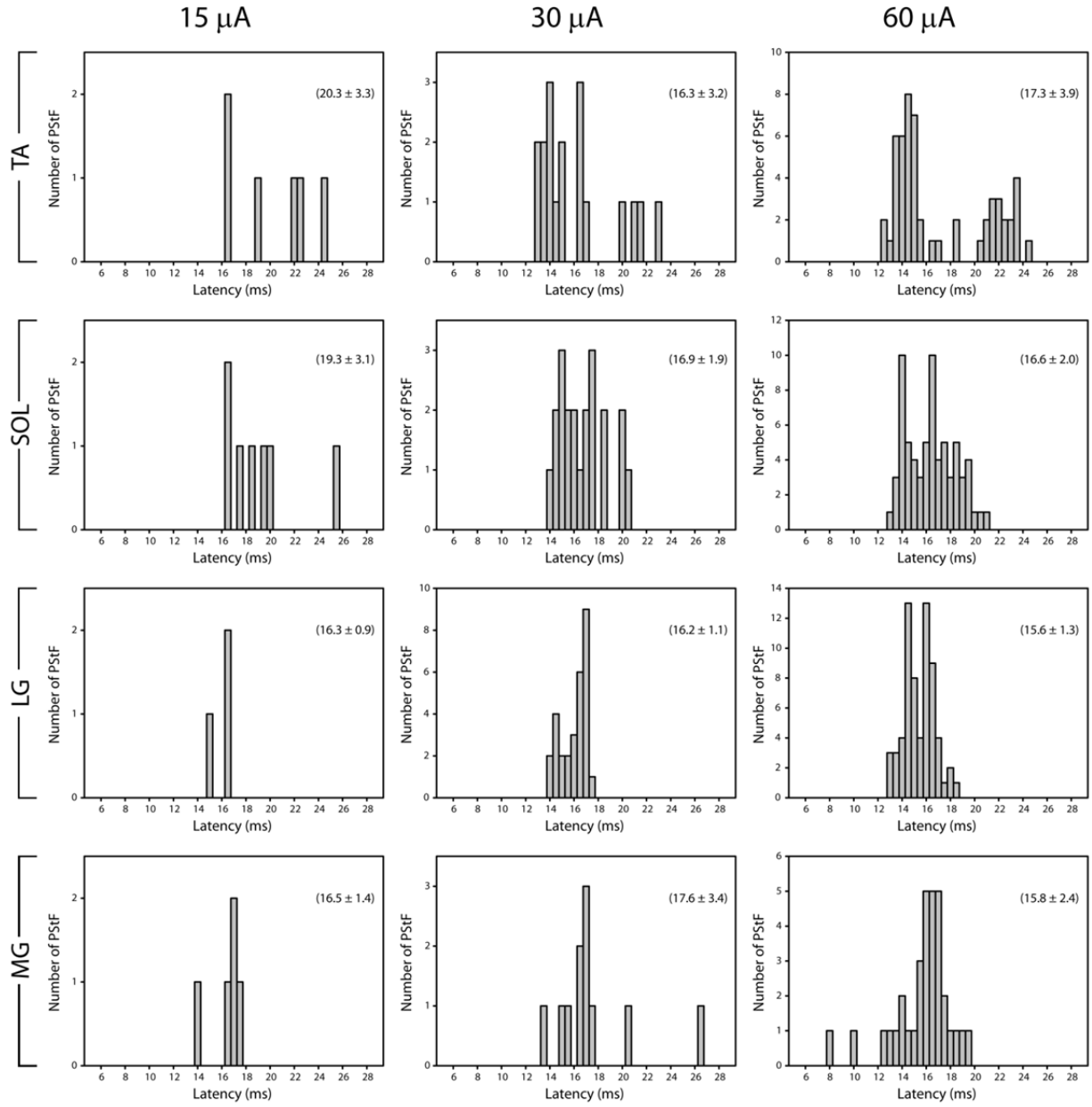
15 μA
30 μA
60 μA
TA
SOL
LG
MG
Number of PStF
Latency (ms)
(20.3 ± 3.3)
(16.3 ± 3.2)
(17.3 ± 3.9)
(19.3 ± 3.1)
(16.9 ± 1.9)
(16.6 ± 2.0)
(16.3 ± 0.9)
(16.2 ± 1.1)
(15.6 ± 1.3)
(16.5 ± 1.4)
(17.6 ± 3.4)
(15.8 ± 2.4)

Figure 5. Distribution of PStF magnitudes for ankle muscles at 15, 30 and 60 μA stimuli. The magnitudes are expressed as peak percent increase (ppi) above baseline. The values given in parentheses for each graph represent the mean ± SD of the magnitude of the PStF. Muscle abbreviations are the same as in Figure 2.

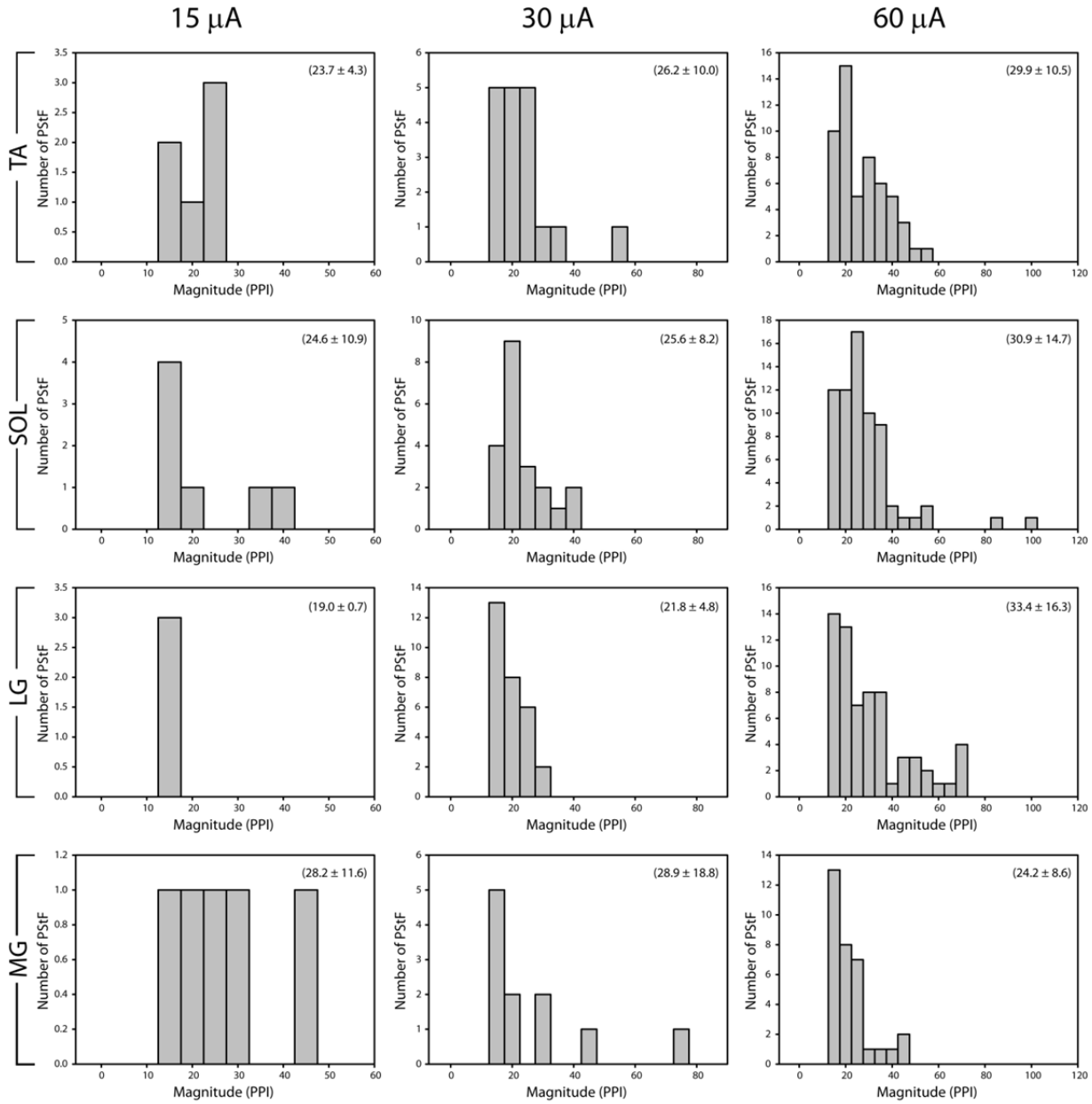
15 μA
30 μA
60 μA
TA
SOL
LG
MG
Number of PStF
Magnitude (PPI)
(23.7 ± 4.3)
(26.2 ± 10.0)
(29.9 ± 10.5)
(24.6 ± 10.9)
(25.6 ± 8.2)
(30.9 ± 14.7)
(19.0 ± 0.7)
(21.8 ± 4.8)
(33.4 ± 16.3)
(28.2 ± 11.6)
(28.9 ± 18.8)
(24.2 ± 8.6)

Figure 6. Distribution of PStF (right) and PStS (left) effects obtained from four ankle muscles of the hindlimb at 15, 30 and 60 μA stimuli. Grey bars: fast muscles. Black bars: slow muscle. Muscle abbreviations are the same as in Figure 2.

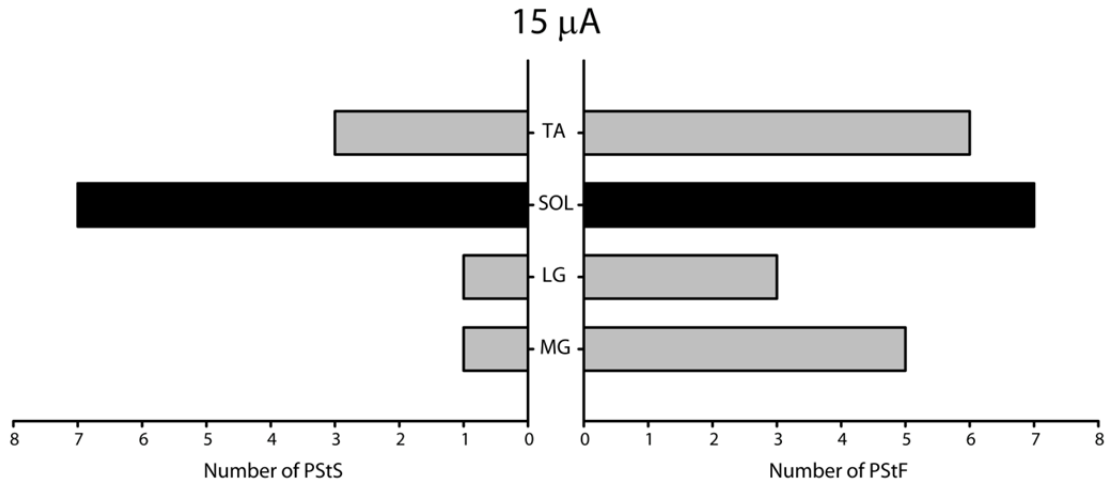
15 μA
TA
SOL
LG
MG
8 7 6 5 4 3 2 1 0
0 1 2 3 4 5 6 7 8
Number of PStS
Number of PStF

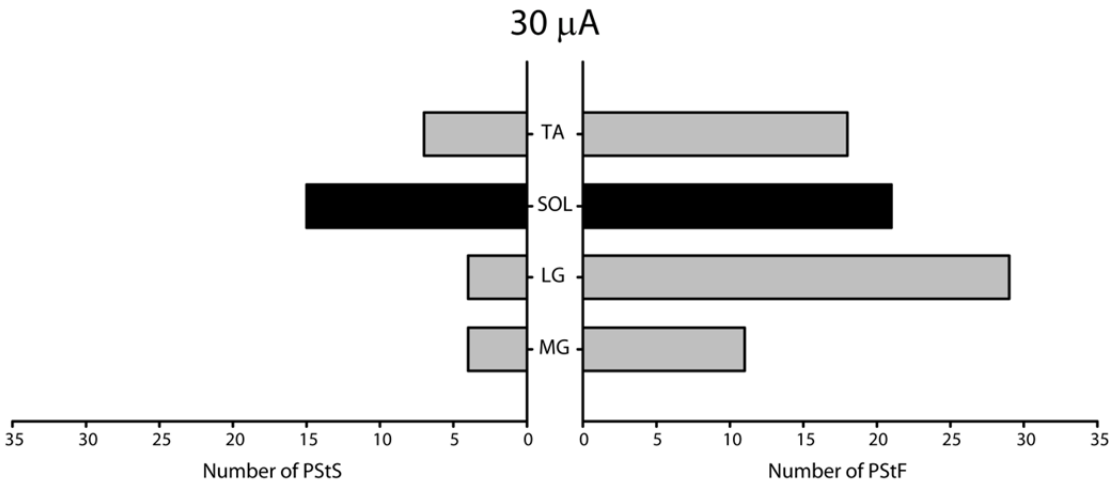
30 μA
TA
SOL
LG
MG
35 30 25 20 15 10 5 0
0 5 10 15 20 25 30 35
Number of PStS
Number of PStF

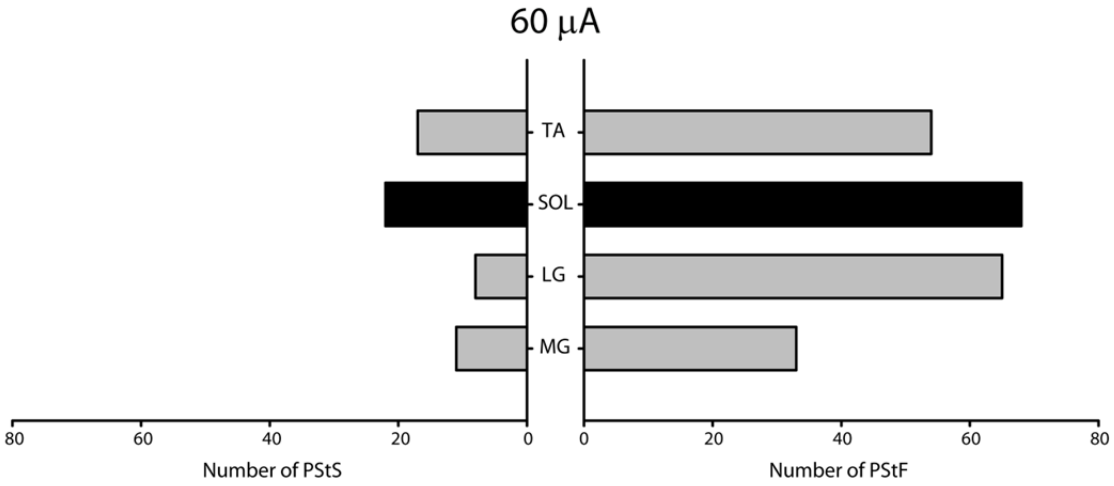
60 μA
TA
SOL
LG
MG
80 60 40 20 0
0 20 40 60 80
Number of PStS
Number of PStF

CHAPTER 6

CONCLUSION

To study corticospinal output to hindlimb muscles, we first needed to design both a behavioral task that could be easily learned by a monkey and a method to chronically implant EMG electrodes in large numbers of hindlimb muscles. We developed a hindlimb push-pull task that activated large numbers of proximal and distal hindlimb muscles in a reliable and stereotyped pattern. The monkey was required to grab a manipulandum, push and pull the manipulandum to target zones repeatedly, extending and flexing the hindlimb. The task was relatively easy for the monkey to learn in that each monkey was able to perform the task at a basic level after only a couple of months of training. However, proficiency at the task (i.e. continuous performance of the task for greater than two hours) took over a year of training for each monkey. Ideally, the behavioral task would replicate natural hindlimb movements, such as locomotion, but data recording methods necessitated a more rigid, controlled design. The goal of activating large numbers of hindlimb muscles, both proximal and distal as well as extensors and flexors, was achieved. However, the task design limited the activation of hip, digit and intrinsic foot muscles. A task that both required larger movements of the hip and more skilled movements of the foot and digits, such as the reach and prehension task used in forelimb studies (Belhaj-Saïf et al., 1998), would provide greater activation of the hip, digit and intrinsic foot muscles but would also require a much longer training period as well as new primate chair and head restraint designs.

We developed two chronic EMG implant methods that provide stable, long-term EMG recording from large numbers of muscles of the hindlimb in awake, behaving monkeys. Both the arm-mounted subcutaneous implant and the cranial-mounted subcutaneous implant are minimally invasive, have minimal risk of infection, are relatively non-traumatic and are capable of recording from large numbers of hindlimb muscles simultaneously for periods of many months to years. The manufacturer of the EMG wire used in this study now offers EMG wires with colored insulation (Cooner Wire, AS632) that would be a great asset in wire identification during surgery.

We investigated the organization of the hindlimb representation of primary motor cortex (M1) using stimulus triggered averaging (15, 30 and 60 μA; 15 Hz) of EMG activity recorded from 19 muscles

of the hindlimb. Consistent with previous hindlimb studies in which high frequency stimulation was used to elicit movements, we found a core distal muscle representation surrounded by a peripheral proximal muscle representation based on poststimulus facilitation effects (Hatanaka et al., 2001; Wise and Tanji, 1981). However, in our study the distal and proximal representations were separated by a large region of proximal-distal cofacilitation, similar to the forelimb maps of Park et al. (2001). The hindlimb maps at 15 μA differed greatly from those at 60 μA. At 15 μA, there was a large distal representation and a smaller, peripheral proximal representation. As the stimulus intensity was increased to 60 μA, both the proximal and distal representations decreased in size, while the proximal-distal cofacilitation region increased dramatically in size. The increase in the proximal-distal cofacilitation region cannot be explained by stimulus-current spread alone. Rather, we propose a cortical organization involving a partial segregation of proximal- and distal-specific corticospinal neurons coupled with unequal synaptic linkages to distal and proximal motoneurons in the spinal cord.

Next, we analyzed the cortical output from M1 to 19 muscles of the hindlimb in terms of the latency, magnitude and distribution of poststimulus facilitation (PStF) and suppression (PStS) effects from stimulus triggered averages (15, 30 and 60 μA; 15 Hz) of EMG activity recorded from 19 muscles of the hindlimb and found several noteworthy results. First, PStF was far more common than PStS at all joints. Second, PStF onset latency increased from proximal to distal joints as expected based on increased conduction distances. Third, PStF was strongest in the intrinsic muscles and magnitude declined the more proximal the muscle group. Fourth, PStF was most common in intrinsic muscles and more common in extensors than flexors. These results were compared to a similar study that analyzed stimulus triggered averages from 24 forelimb muscles using a 15 μA stimulus (Park et al., 2004). Several striking differences were found between hindlimb and forelimb effects. First, there were far fewer poststimulus effects (PStEs) in hindlimb muscles. At 15 μA, there were 171 PStEs in hindlimb compared to 2079 in forelimb reflecting a smaller cortical representation. While the strongest PStF effects were in the intrinsic muscles of both the hindlimb and the forelimb, the PStF in the intrinsic hand muscles was

twice as strong as PStF in the intrinsic foot muscles. The difference in PStF magnitude was even more striking for wrist and digit muscles compared to the analogous hindlimb muscles, ankle and digit. In the forelimb, PStF magnitude was consistently weaker the more proximal the muscle group. In the hindlimb, while PStF was strongest for intrinsic foot muscles, at all other joints, PStF was weak and essentially of equal strength. Interestingly, PStF in shoulder muscles was nearly equal to PStF in hip muscles suggesting a similar synaptic linkage to motoneurons of the most proximal muscles of each limb. The weakness of these effects suggests a sparse monosynaptic component or synapses located on the distal segments of motoneuron dendrites. Finally, there was a striking qualitative difference between stimulus triggered averages from hindlimb and forelimb muscles. Stimulus triggered averages compiled at a 5 Hz frequency from hindlimb M1 contained a long latency, broad suppression usually followed by a broad and weaker facilitation. At 15 Hz, these longer latency effects produced a prominent oscillation in the baseline of the stimulus triggered average which was rarely observed in averages of forelimb muscles.

How does this data translate to behavior? In comparison to forelimb, hindlimb movements are generally more stereotyped and involve the cofacilitation of muscles at different joints. Locomotion involves whole limb movement in coordinated cycles of activation and inhibition of agonist and antagonist muscle groups. Considering locomotion is one of the main actions of hindlimb movement, an organization of hindlimb M1 such that a large area facilitates both proximal and distal muscles is reasonable. However, at a low stimulus intensity (15 μA) there was a small proximal-distal cofacilitation area but a large distal only representation. This could be explained by differing synaptic linkages of corticospinal neurons projecting to proximal and distal muscle motoneurons as proposed in Figure 11 in Chapter 2: Representation of Hindlimb Muscles in Primary Motor Cortex. Monosynaptic connections to distal muscle motoneurons may be associated with skilled movements of the digits. This is reinforced by data on the magnitude of facilitation effects. We found that facilitation was most common and strongest in intrinsic foot muscles. This could reflect a monosynaptic pathway to intrinsic foot muscle motoneurons that does not exist for motoneurons projecting to other muscles. A more rigorous

investigation of the anatomical pathway from M1 to both proximal and distal hindlimb muscles would greatly add to our understanding of the functional organization of hindlimb M1.

Finally, we investigated the cortical control of the fast and slow muscles of the ankle. Conflicting results have been reported in primate and human studies concerning the role of motor cortex in the control of slow muscles. Some studies have found weak or non-existent facilitation of the slow muscle, soleus (Ashby and Advani, 1990; Brouwer and Ashby, 1990, 1992; Brouwer and Qiao, 1995; Cowan et al., 1986; Preston and Whitlock, 1963; Uemura and Preston, 1965). The rationale was that the slow muscle, soleus, is a postural muscle. Soleus actively maintains posture during phases of inactivity of the hindlimb. In order to initiate a movement of the hindlimb, soleus activity must be inhibited. However, other studies have reported short latency facilitation of soleus similar to that of the fast muscle, tibialis anterior (Bawa et al., 2002; Valls-Solé et al., 1994). Interestingly, while facilitation of soleus was just as strong as fast muscle facilitation in these studies, this was only true at higher stimulus intensities. The studies showing weak or non-existent soleus facilitation may have seen soleus facilitation if higher stimulus intensities were used. We computed stimulus triggered averaging of EMG activity (15, 30 and 60 μA; 15 Hz) in awake monkeys performing a behavioral task to investigate this issue. EMG activity was recorded from three fast (or mixed) ankle muscles (tibialis anterior, medial gastrocnemius and lateral gastrocnemius) and one slow ankle muscle (soleus) to investigate M1 output to these muscles. We found that poststimulus facilitation (PStF) was just as common and just as strong in the slow muscle, soleus, as the fast muscles and PStF onset latencies and magnitudes were similar in all muscles. Poststimulus suppression (PStS), however, was more common in soleus than the fast muscles, especially at lower stimulus intensities. Our results demonstrate that motor cortex is capable of powerful excitatory effects on soleus motoneurons, equal to those on fast muscles.

REFERENCES

Andersen P, Sears TA. The mechanical properties and innervation of fast and slow motor units in the intercostal muscles of the cat. J Physiol 173: 114-129, 1964.

Asanuma H, Hongo T, Jankowska E, Marcus S, Shinoda Y, Zarzecki P. Pattern of projections of individual pyramidal tract neurons to the spinal cord of the monkey. J Physiol (Paris) 74: 235-236, 1978.

Asanuma H, Rosén I. Topographical organization of cortical efferent zones projecting to distal forelimb muscles in the monkey. Exp Brain Res 14: 243-256, 1972.

Asanuma H, Sakata H. Functional organization of a cortical efferent system examined with focal depth stimulation in cats. J Neurophysiol 30: 35-54, 1967.

Asanuma H, Zarzecki P, Jankowska E, Hongo T, Marcus S. Projection of individual pyramidal tract neurons to lumbar motor nuclei of the monkey. Exp Brain Res 34: 73-89, 1979.

Ashby P, Advani A. Corticospinal control of soleus motoneurons in man. Can J Pharmacol 68: 1231-1235, 1990.

Baker SN, Oliver E, Lemon RN. An investigation of the intrinsic circuitry of the motor cortex of the monkey using intra-cortical microstimulation. Exp Brain Res 123: 397-411, 1998.

Barker AT, Jalinous R, Freeston IL. Noninvasive magnetic stimulation of the human motor cortex. Lancet 1: 1106-1107, 1985.

Bawa P, Chalmers GR, Stewart H, Eisen AA. Responses of ankle extensor and flexor motoneurons to transcranial magnetic stimulation. J Neurophysiol 88: 124-132, 2002.

Belhaj-Saïf A, Fourment A, Maton B. Adaptation of the precentral cortical command to elbow muscle fatigue. Exp Brain Res 111: 405-416, 1996.

Belhaj-Saïf A, Hill Karrer J, Cheney PD. Distribution and characteristics of poststimulus effects in proximal and distal forelimb muscles from red nucleus in the monkey. J Neurophysiol 79: 1777-1789, 1998.

Benito Penalva J, Opisso E, Medina J, Corrons M, Kumru H, Vidal J, Valls-Solé J. H reflex modulation by transcranial magnetic stimulation in spinal cord injury subjects after gait training with electromechanical systems. Spinal Cord. 48: 400-406, 2010.

Bretzner F, Drew T. Contribution of the motor cortex to the structure and the timing of hindlimb locomotion in the cat: a microstimulation study. J Neurophysiol 94: 657-672, 2005.

Brouwer B, Ashby P. Corticospinal projections to the lower limb motoneurons of man. Exp Brain Res 89: 649-654, 1992.

Brouwer B, Ashby P. Corticospinal projections to upper and lower limb spinal motoneurons in man. EEG and Clin Neurophysiol 76: 509-519, 1990.

Brouwer B, Qiao J. Characteristics and variability of lower limb motoneurons responses to transcranial magnetic stimulation. Electroencephalogr Clin Neurophysiol 97: 49-54, 1995.

Burke RE. Motor unit types of cat triceps surae muscle. J Physiol 193: 141-160, 1967.

Burke RE, Jankowska E, ten Bruggencate G. A comparison of peripheral and rubrospinal synaptic input to slow and fast twitch motor units of triceps surae. J Physiol 207: 709-732, 1970.

Burke RE, Levine DN, Zajac FE. Mammalian motor units: physiological-histochemical correlation in three types in cat gastrocnemius. Science 174: 709-712, 1971.

Burke RE, Tsairis P. The correlation of physiological properties with histochemical characteristics in single muscle units. Ann New York Acad Sci 228: 145-159, 1974.

Buys EJ, Lemon RN, Mantel GW, Muir RB. Selective facilitation of different hand muscles by single corticospinal neurons in the conscious monkey. J Physiol 381: 529 –549, 1986.

Cheney PD, Fetz EE. Comparable patterns of muscle facilitation evoked by individual corticomotoneuronal (CM) cells and by single intracortical microstimuli in primates: evidence for functional groups of CM cells. J Neurophysiol 53: 786-804, 1985.

Cheney PD, Fetz EE. Functional classes of primate corticomotoneuronal cells and their relation to active force. J Neurophysiol 44: 773–791, 1980.

Clough JFM, Kernell D, Phillips CG. The distribution of monosynaptic excitation from the pyramidal tract and from primary spindle afferents to motoneurones of the baboon's hand and forearm. J Physiol 198: 145-166, 1968.

Courtine G, Roy RR, Hodgson J, McKay H, Raven J, Zhong H, Yang H, Tuszynski MH, Edgerton VR. Kinematic and EMG determinants in quadrupedal locomotion of a non-human primate (Rhesus). J Neurophysiol 93: 3127-3145, 2005.

Cowan JM, Day BL, Marsden C, Rothwell JC. The effect of percutaneous motor cortex stimulation on H reflexes in muscles of the arm and leg in intact man. J Physiol (London) 377: 333-347, 1986.

Drew T. Motor cortical cell discharge during voluntary gait modification. Brain Res 457: 181-187, 1988.

Drew T, Jiang W, Widajewicz W. Contributions of the motor cortex to the control of the hindlimbs during locomotion in the cat. Brain Res Brain Res Rev 40: 178-191, 2002.

Edgley SA, Eyre JA, Lemon RN, Miller S. Comparison of activation of corticospinal neurons and spinal motor neurons by magnetic and electrical transcranial stimulation in the lumbosacral cord of the anaesthetized monkey. Brain 120: 839-853, 1997.

Ertekin C, Ertaş M, Efendi H, Larsson LE, Sirin H, Araç N, Toygar A, Demir Y. A stable late soleus EMG response elicited by cortical stimulation during voluntary ankle dorsiflexion. Electroenchepalogr Clin Neurophysiol 97: 275-283, 1995.

Ferrier D. Experiments in the brain of monkeys. Proc R Soc Lond B Biol Sci 23:409-430, 1875.

Fetz EE, Cheney PD. Postspike facilitation of forelimb muscle activity by primate corticomotoneuronal cells. J Neurophysiol 44: 751-772, 1980.

Fritsch G, Hitzig E. Uber die elektrische Erregbarkeit des Gross-hirns. Archs Anat Physiol Wiss Med 37:300-332. (Translation by Bonin, G von. The cerebral cortex. pp. 73-96. Thomas, Springfield, Illinois.)

Graziano MS, Aflalo TN, Cooke DF. Arm movements evoked by electrical stimulation in the motor cortex of monkeys. J Neurophysiol. 94: 4209-4023, 2005.

Graziano MS, Taylor CS, Moore T. Complex movements evoked by microstimulation of precentral cortex. Neuron 34: 841-851, 2002.

Hatanaka N, Nambu A, Yamashita A, Takada M, Tokuno H. Somatotopic arrangement and corticocortical inputs of the hindlimb region of the primary motor cortex in the macaque monkey. Neurosci Res 40: 9-22, 2001.

He SQ, Dum RP, Strick PL. Topographic organization of corticospinal projections from the frontal lobe: motor areas on the lateral surface of the hemisphere. J Neurosci 13: 952-980, 1993.

Hodgson JA, Wichayanuparp S, Recktenwald MR, Roy RR, McCall G, Day MK, Washburn D, Fanton JW, Kozlovskaya I, Edgerton VR. Circadian force and EMG activity in hindlimb muscles of rhesus monkeys. J Neurophysiol 86: 1430-1444, 2001.

Hoffer JA, Loeb GE, Marks WB, O'Donovan MJ, Pratt CA, Sugano N. Cat hindlimb motoneurons during locomotion. I. Destination, axonal conduction velocity, and recruitment threshold. J Neurophysiol 57: 510-529, 1987.

Hoffer JA, Caputi AA, Pose IE, Griffiths RI. Roles of muscle activity and load on the relationship between muscle spindle length and whole muscle length in the freely walking cat. Prog Brain Res 80: 75-85; discussion 57-60, 1989.

Howell AB, Straus WL. The Muscular System. In: Hartman CG, Straus WL, editors. The Anatomy of the Rhesus Monkey. Hafner Publishing Company: New York, 1971.

Hudson HM, Griffin DM, Belhaj-Saïf A, Lee SP, Cheney PD. Methods for chronic recording of EMG activity from large numbers of hindlimb muscles in awake rhesus macaques. J Neurosci Methods 189: 153-161, 2010.

Jankowska E, Padel Y, Tanaka R. Projections of pyramidal tract cells to alpha-motoneurones innervating hind-limb muscles in the monkey. J Physiol 249: 637-667, 1975.

Jayaram G, Stinear JW. Contralesional paired associative stimulation increases paretic lower limb motor excitability post-stroke. Exp Brain Res. 185: 563-570, 2008.

Kawai Y. [Motor cortex control of fast and slow motoneurons innervating forelimb muscles of the cat]. Nippon Seirigaku Zasshi 44: 587-599, 1982.

Kwan HC, MacKay WA, Murphy JT, Wong YC. Spatial organization of precentral cortex in awake primates. II. Motor outputs. J Neurophysiol 41: 1120-1131, 1978.

Lemon RN. Mapping the output functions of motor cortex. In: *Signal and Sense*, edited by Edelman GM, Gall WE, and Cowan WM. New York: Wiley-Liss, 1990, p. 315-355.

Loeb GE. Asymmetry of hindlimb muscle activity and cutaneous reflexes after tendon transfers in kittens. J Neurophysiol 82: 3392-3405, 1999.

Luppino G, Matelli M, Camarda RM, Gallese V, Rizzolatti G. Multiple representations of body movements in mesial area 6 and the adjacent cingulate cortex: an intracortical microstimulation study in the macaque monkey. J Comp Neurol 311: 463-482, 1991.

Ma C, He J. A method for investigating cortical control of stand and squat in conscious behavioral monkeys. J Neurosci Methods. 192: 1-6, 2010.

McKiernan BJ, Marcario JK, Karrer JH, Cheney PD. Corticomotoneuronal postspike effects in shoulder, elbow, wrist, digit, and intrinsic hand muscles during a reach and prehension task. J Neurophysiol 80: 1961–1980, 1998.

Merton PA, Morton HB. Stimulation of the cerebral cortex in the intact human subject. Nature 285: 227, 1980.

Mewes K, Cheney PD. Facilitation and suppression of wrist and digit muscles from single rubromotoneuronal cells in the awake monkey. J Neurophysiol 66: 1965–1977, 1991.

Miller LE, van Kan PL, Sinkjaer T, Andersen T, Harris GD, Houk JC. Correlation of primate red nucleus discharge with muscle activity during free-form arm movements. J Physiol 469: 213-243, 1993.

Mitz AR, Wise SP. The somatotopic organization of the supplementary motor area: intracortical microstimulation mapping. J Neurosci 7: 1010-1021, 1987.

Mori F, Koch G, Foti C, Bernardi G, Centonze D. The use of repetitive transcranial magnetic stimulation (rTMS) for the treatment of spasticity. Prog Brain Res. 175: 429-439, 2009.

Muir RB, Porter R. The effect of a preceding stimulus on temporal facilitation at corticomotoneuronal synapses. J Physiol 228: 749-63, 1973.

Neafsey EJ. Precentral cortical zones related to flexion and extension in two hindlimb movements in the monkey. Brain Res 198: 453-459, 1980.

Park MC, Belhaj-Saïf A, Cheney PD. Chronic recording of EMG activity from large numbers of forelimb muscles in awake macaque monkeys. J Neurosci Methods 96: 153-160, 2000.

Park MC, Belhaj-Saïf A, Cheney PD. Properties of primary motor cortex output to forelimb muscles in rhesus macaques. J Neurophysiol 92: 2968-2984, 2004.

Park MC, Belhaj-Saïf A, Gordon M, Cheney PD. Consistent features in the forelimb representation of primary motor cortex in rhesus macaques. J Neurosci 21: 2784 –2792, 2001.

Paxinos G, Huang XF, Toga AW. *The rhesus monkey brain in stereotaxic coordinates.* San Diego, CA: Academic Press, 2000, p. 163 p.

Penfield W, Boldrey E. Somatic motor and sensory representation in the cerebral cortex of man as studied by electrical stimulation. Brain 60: 389-443, 1937.

Perez MA, Lungholt BA, Nyborg K, Nielsen JB. Motor skill training induces changes in the excitability of the leg cortical area in healthy humans. Exp Brain Res. 159: 197-205, 2004.

Phillips CG, Porter R. The pyramidal projection to motoneurones of some muscle groups of the baboon's forelimb. In: *Progress in Brain Research. Physiology of Spinal Neurons*, edited by Eccles JC and Schade JP. Amsterdam: Elsevier, 1964, vol. 12, p. 222-224.

Plautz EJ, Milliken GW, Nudo RJ. Effects of repetitive motor training on movement representations in adult squirrel monkeys: role of use versus learning. Neurobiol Learn Mem. 74: 27-55, 2000.

Preston JB, Shende MC, Uemura K. The motor cortex-pyramidal system: patterns of facilitation and inhibition on motoneurons innervating limb musculature of cat and baboon and their possible adaptive

significance. In: *Neurophysiological Basis of Normal and Abnormal Motor Activities*, edited by Yahr MD and Purpura DP. New York: Raven, 1967, p. 61-72.

Preston JB, Whitlock DG. A comparison of motor cortex effects on slow and fast muscle innervations in the monkey. Exp Neurol 7: 327-41, 1963.

Prochazka A, Schofield P, Westerman RA, Ziccone SP. Reflexes in cat ankle muscles after landing from falls. J Physiol 272: 705-719, 1977.

Prochazka A, Trend P, Hulliger M, Vincent S. Ensemble proprioceptive activity in the cat step cycle: towards a representative look-up chart. Prog Brain Res 80: 61-74; discussion 57-60, 1989.

Ranck JB. Which elements are excited in electrical stimulation of mammalian central nervous system: a review. Brain Res 98: 417-440, 1975.

Rathelot JA, Strick PL. Muscle representation in the macaque motor cortex: an anatomical perspective. Proc Natl Acad Sci USA 103: 8257-8262, 2006.

Rathelot JA, Strick PL. Subdivisions of primary motor cortex based on cortico-motoneuronal cells. Proc Natl Acad Sci USA 106: 918-923, 2009.

Recktenwald MR, Hodgson JA, Roy RR, Riazanski S, McCall GE, Kozlovskaya I, Washburn DA, Fanton JW, Edgerton VR. Effects of spaceflight on rhesus quadrupedal locomotion after return to 1G. J Neurophysiol 81: 2451-2463, 1999.

Sahrmann SA, Clare MH, Montgomery EB, Landau WM. Motor cortical neuronal activity patterns in monkeys performing several force tasks at the ankle. Brain Res 310: 55-66, 1984.

Schieber MH, Rivlis G. A spectrum from pure post-spike effects to synchrony effects in spike-triggered averages of electromyographic activity during skilled finger movements. J Neurophysiol 94: 3325-3341, 2005.

Shapovalov AI. Neuronal organization and synaptic mechanisms of supraspinal motor control in vertebrates. Rev Physiol Biochem Pharmacol 72: 1-54, 1975.

Shapovalov AI, Kurchavyi GG. Effects of trans-membrane polarization and TEA injection on monosynaptic actions from motor cortex, red nucleus and group Ia afferents on lumbar motoneurons in the monkey. Brain Res 82: 49-67, 1974.

Stepniewska I, Preuss TM, Kaas JH. Architectonics, Somatotopic organization, and ipsilateral cortical connections of the primary motor area (M1) of owl monkeys. J Comp Neurol 330: 238-271, 1993.

Stoney Jr SD, Thompson WD, Asanuma H. Excitation of pyramidal tract cells by intracortical microstimulation: effective extent of stimulation current. J Neurophysiol 31: 659-669, 1968.

Thomas SL, Gorassini MA. Increases in corticospinal tract function by treadmill training after incomplete spinal cord injury. J Neurophysiol. 94: 2844-2855, 2005.

Uemura K, Preston JB. Comparison of motor cortex influences upon various hind-limb motoneurons in pyramidal cats and primates. J Neurophysiol 28: 398-412, 1965.

Valls-Solé J, Alvarez R, Tolosa ES. Responses of the soleus muscle to transcranial magnetic stimulation. Electroencephalogr Clin Neurophysiol 93: 421-427, 1994.

Widajewicz W, Kably B, Drew T. Motor cortical activity during voluntary gait modifications in the cat. II. Cells related to the hindlimbs. J Neurophysiol 72: 2070-2089, 1994.

Widener GL, Cheney PD. Effects on muscle activity from microstimuli applied to somatosensory and motor cortex during voluntary movement in the monkey. J Neurophysiol 77: 2446 –2465, 1997.

Wise SP, Tanji J. Supplementary and precentral motor cortex: contrast in responsiveness to peripheral input in the hindlimb area of the unanesthetized monkey. J Comp Neurol 195: 433-451, 1981.

Wolpaw JR, Herchenroder PA. Operant conditioning of H-reflex in freely moving monkeys. J Neurosci Methods 31: 145-152, 1990.

Woolsey CN. Organization of somatic sensory and motor areas of the cerebral cortex. In: Biological and biochemical basis of behavior. HF Harlow, CN Woolsey (eds). Madison: U of Wisconsin Press, 1958, p. 63-81.